

NAVAL POSTGRADUATE SCHOOL
Monterey, California



19980102 130

THESIS

**ANALYSIS OF POTENTIAL STRUCTURAL DESIGN
MODIFICATIONS FOR THE TAIL SECTION OF THE
RAH-66 COMANCHE HELICOPTER**

by

Vincent M. Tobin

June, 1997

Thesis Co-Advisors:

E. Roberts Wood
Donald A. Danielson
Joshua H. Gordis

Approved for public release; distribution is unlimited.

DTIC QUALITY INSPECTED 4

REPORT DOCUMENTATION PAGE

Form Approved OMB No. 0704-0188

Public reporting burden for this collection of information is estimated to average 1 hour per response, including the time for reviewing instruction, searching existing data sources, gathering and maintaining the data needed, and completing and reviewing the collection of information. Send comments regarding this burden estimate or any other aspect of this collection of information, including suggestions for reducing this burden, to Washington Headquarters Services, Directorate for Information Operations and Reports, 1215 Jefferson Davis Highway, Suite 1204, Arlington, VA 22202-4302, and to the Office of Management and Budget, Paperwork Reduction Project (0704-0188) Washington DC 20503.

1. AGENCY USE ONLY <i>(Leave blank)</i>	2. REPORT DATE June 1997	3. REPORT TYPE AND DATES COVERED Master's Thesis	
4. ANALYSIS OF POTENTIAL STRUCTURAL DESIGN MODIFICATIONS FOR THE TAIL SECTION OF THE RAH-66 COMANCHE HELICOPTER		5. FUNDING NUMBERS	
6. AUTHOR(S) Tobin, Vincent M.			
7. PERFORMING ORGANIZATION NAME(S) AND ADDRESS(ES) Naval Postgraduate School Monterey CA 93943-5000		8. PERFORMING ORGANIZATION REPORT NUMBER	
9. SPONSORING/MONITORING AGENCY NAME(S) AND ADDRESS(ES)		10. SPONSORING/MONITORING AGENCY REPORT NUMBER	
11. SUPPLEMENTARY NOTES The views expressed in this thesis are those of the author and do not reflect the official policy or position of the Department of Defense or the U.S. Government.			
12a. DISTRIBUTION/AVAILABILITY STATEMENT Approved for public release; distribution is unlimited.		12b. DISTRIBUTION CODE	
13. ABSTRACT <i>(maximum 200 words)</i> The Army RAH-66 Comanche Helicopter made its first flight in January of 1996. Its current structural configuration, however, does not meet The Army's requirements for radar signature. Structural configurations of the tailcone that meet radar cross-section requirements tend to lack sufficient structural stiffness due to the presence of Kevlar in place of graphite on the outer mold line. This thesis investigates potential structural design modifications to the Comanche tailcone that would move the design closer to meeting both its structural and radar signature requirements. Geometry modifications with baseline (current configuration) materials increased torsional stiffness by nine percent. Structural geometry modifications using radar signature-compliant materials reduced torsional stiffness by 10 percent. The geometry changes analyzed produce structural performance improvements insufficient to allow the use of radar-compliant materials without further geometry changes.			
14. SUBJECT TERMS: RAH-66 Comanche Helicopter, Comanche Tail Section, Structural Analysis, PATRAN Analysis, NASTRAN Analysis		15. NUMBER OF PAGES 117	
		16. PRICE CODE	
17. SECURITY CLASSIFICATION OF REPORT Unclassified	18. SECURITY CLASSIFICATION OF THIS PAGE Unclassified	19. SECURITY CLASSIFICATION OF ABSTRACT Unclassified	20. LIMITATION OF ABSTRACT UL

NSN 7540-01-280-5500

Standard Form 298 (Rev. 2-89)
Prescribed by ANSI Std. Z39-18 298-102

Approved for public release; distribution is unlimited.

**ANALYSIS OF POTENTIAL STRUCTURAL DESIGN MODIFICATIONS FOR
THE TAIL SECTION OF THE RAH-66 COMANCHE HELICOPTER**

Vincent M. Tobin
Major, United States Army
B.S., Bucknell University, 1985

Submitted in partial fulfillment
of the requirements for the degree of

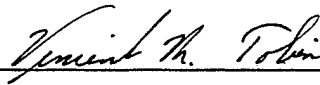
MASTER OF SCIENCE IN AERONAUTICAL ENGINEERING

from the

NAVAL POSTGRADUATE SCHOOL

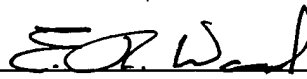
June 1997

Author:



Vincent M. Tobin

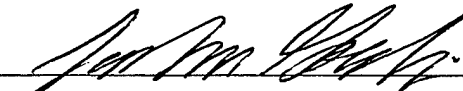
Approved by:



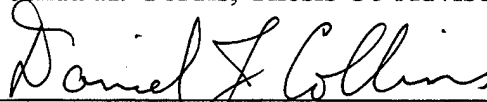
E. Roberts Wood, Thesis Co-Advisor



Donald A. Danielson, Thesis Co-Advisor



Joshua H. Gordis, Thesis Co-Advisor



Daniel J. Collins, Chairman

Department of Aeronautics and Astronautics

ABSTRACT

The Army RAH-66 Comanche Helicopter made its first flight in January of 1996. Its current structural configuration, however, does not meet the Army's requirements for radar signature. Structural configurations of the tailcone that meet radar cross-section requirements tend to lack sufficient structural stiffness due to the presence of Kevlar in place of graphite on the outer mold line. This thesis investigates potential structural design modifications to the Comanche tailcone that would move the design closer to meeting both its structural and radar signature requirements. Structural geometry modifications with baseline (current configuration) materials increased torsional stiffness by nine percent. Geometry modifications using radar signature-compliant materials reduced torsional stiffness by 10 percent. The geometry changes analyzed produce structural performance improvements insufficient to allow the use of radar-compliant materials without further geometry changes.

TABLE OF CONTENTS

I. INTRODUCTION	1
A. GENERAL	1
B. SCOPE	1
II. BACKGROUND	5
A. DESIGN CONSTRAINTS	5
B. FINITE ELEMENT THEORY	6
C. NASTRAN	9
D. PATRAN	10
III. RESEARCH METHODS	13
A. MODEL DEVELOPMENT	13
1. Baseline	13
2. Baseline with Kevlar Exterior Skin (Base-Kevlar)	21
3. Bulkhead Section Modified (Bulk-Mod)	22
4. Aft Tail Cone Modified (Cone-Mod)	28
5. Bulkhead Section and Aft Tail Cone Modified (Full-Mod)	29
6. Full-Mod with Kevlar Exterior Skin (Full-Kevlar)	30
B. LOAD CASES	30
IV. RESULTS AND ANALYSIS	33
V. CONCLUSIONS AND RECOMMENDATIONS	71
A. CONCLUSIONS	71
B. RECOMMENDATIONS	72
1. Aluminum Forward Tail Landing Gear Bay Bulkhead	72
2. Vertical Stabilizer Longerons	72
3. Tail Fan Gear Box Struts	73
4. Tail Landing Gear	73
5. Tail Configuration for Transportability	75
6. Dynamic Analysis	75
7. PATRAN Composite Modeling	76
APPENDIX A: MODIFICATIONS LISTING	77
APPENDIX B: MASS AND CENTER OF GRAVITY CHANGES	91
APPENDIX C: LIST OF PATRAN DATABASES	97
LIST OF REFERENCES	99
INITIAL DISTRIBUTION LIST	101

LIST OF FIGURES

FIGURE 1: US ARMY COMANCHE HELICOPTER.....	2
FIGURE 2: COMANCHE TAIL SECTION	3
FIGURE 3: PITCH ATTITUDE GROUND CLEARANCE REQUIREMENT	7
FIGURE 4: BASELINE TAIL CONE	15
FIGURE 5: BASELINE TAIL CONE, EXHAUST COVERS NOT DISPLAYED	16
FIGURE 6: EXHAUST COOLING SCHEMATIC	17
FIGURE 7: FORWARD TAIL LANDING GEAR BAY BULKHEAD, BASELINE MODEL.....	18
FIGURE 8: FTLGGB SECTION IN TAIL CONE	20
FIGURE 9: FRONT VIEW OF FTLGGB SECTION.....	21
FIGURE 10: BULK-MOD FTLGGB	23
FIGURE 11: AIRCRAFT SKIN ADDED FOR FTLGGB MODIFICATION.....	24
FIGURE 12: WATERLINE 3160 DECK.....	26
FIGURE 13: ADDED ELEMENTS, BULK-MOD	27
FIGURE 14: AFT TAIL CONE MODIFICATION (CONE-MOD).....	29
FIGURE 15: TORSION DISPLACEMENT OF BASELINE MODEL.....	35
FIGURE 16: TORSION STRAIN ENERGY DENSITY FRINGE OF BASELINE MODEL.....	36
FIGURE 17: HORIZONTAL DISPLACEMENT OF BASELINE MODEL	37
FIGURE 18: HORIZONTAL STRAIN ENERGY DENSITY FRINGE OF BASELINE MODEL.....	38
FIGURE 19: VERTICAL DISPLACEMENT OF BASELINE MODEL.....	39
FIGURE 20: VERTICAL STRAIN ENERGY DENSITY FRINGE OF BASELINE MODEL.....	40
FIGURE 21: TORSION DISPLACEMENT OF BASE-KEVLAR MODEL	41
FIGURE 22: TORSION STRAIN ENERGY DENSITY FRINGE OF BASE-KEVLAR MODEL.....	42
FIGURE 23: HORIZONTAL DISPLACEMENT OF BASE-KEVLAR MODEL.....	43
FIGURE 24: HORIZONTAL STRAIN ENERGY DENSITY FRINGE OF BASE-KEVLAR MODEL ...	44
FIGURE 25: VERTICAL DISPLACEMENT OF BASE-KEVLAR MODEL.....	45

FIGURE 26: VERTICAL STRAIN ENERGY DENSITY FRINGE OF BASE-KEVLAR MODEL.....	46
FIGURE 27: TORSION DISPLACEMENT OF BULK-MOD MODEL	47
FIGURE 28: TORSION STRAIN ENERGY DENSITY FRINGE OF BULK-MOD MODEL	48
FIGURE 29: HORIZONTAL DISPLACEMENT OF BULK-MOD MODEL	49
FIGURE 30: HORIZONTAL STRAIN ENERGY DENSITY FRINGE OF BULK-MOD MODEL	50
FIGURE 31: VERTICAL DISPLACEMENT OF BULK-MOD MODEL.....	51
FIGURE 32: VERTICAL STRAIN ENERGY DENSITY FRINGE OF BULK-MOD MODEL.....	52
FIGURE 33: TORSION DISPLACEMENT OF CONE-MOD MODEL.....	53
FIGURE 34: TORSION STRAIN ENERGY DENSITY FRINGE OF CONE-MOD MODEL.....	54
FIGURE 35: HORIZONTAL DISPLACEMENT OF CONE-MOD MODEL	55
FIGURE 36: HORIZONTAL STRAIN ENERGY DENSITY FRINGE OF CONE-MOD MODEL	56
FIGURE 37: VERTICAL DISPLACEMENT OF CONE-MOD MODEL	57
FIGURE 38: VERTICAL STRAIN ENERGY DENSITY FRINGE OF CONE-MOD MODEL	58
FIGURE 39: TORSION DISPLACEMENT OF FULL-MOD MODEL.....	59
FIGURE 40: TORSION STRAIN ENERGY DENSITY FRINGE OF FULL-MOD MODEL.....	60
FIGURE 41: HORIZONTAL DISPLACEMENT OF FULL-MOD MODEL.....	61
FIGURE 42: HORIZONTAL STRAIN ENERGY DENSITY FRINGE OF FULL-MOD MODEL.....	62
FIGURE 43: VERTICAL DISPLACEMENT OF FULL-MOD MODEL.....	63
FIGURE 44: VERTICAL STRAIN ENERGY DENSITY FRINGE OF FULL-MOD MODEL.....	64
FIGURE 45: TORSION DISPLACEMENT OF FULL-KEVLAR MODEL.....	65
FIGURE 46: TORSION STRAIN ENERGY DENSITY FRINGE OF FULL-KEVLAR MODEL	66
FIGURE 47: HORIZONTAL DISPLACEMENT OF FULL-KEVLAR MODEL.....	67
FIGURE 48: HORIZONTAL STRAIN ENERGY DENSITY FRINGE OF FULL-KEVLAR MODEL....	68
FIGURE 49: VERTICAL DISPLACEMENT OF FULL-KEVLAR MODEL.....	69
FIGURE 50: VERTICAL STRAIN ENERGY DENSITY FRINGE OF FULL-KEVLAR MODEL	70
FIGURE 51: PROPOSED STRUT CONFIGURATION SCHEMATIC.....	74

LIST OF TABLES

TABLE 1: MODEL STIFFNESSES IN SI UNITS.....	33
TABLE 2: MODEL STIFFNESSES IN ENGLISH UNITS.....	34
TABLE 3: MODEL STIFFNESSES NORMALIZED TO BASELINE VALUES.....	34

ACKNOWLEDGEMENTS

First and foremost I would like to thank my family for their support and patience during our time here at the Naval Postgraduate School and throughout my Army career.

Many thanks go to Professor E. Roberts Wood for his generous commitment of time and enthusiasm to all his students. He is the recipient of my utmost respect as one of the few civilian faculty members who seems to fully understand that the ultimate purpose of this institution is to enhance the war-fighting capability of the United States and our allies. His pragmatic mission focus is a true asset.

I would like to thank Professor Donald A. Danielson for his dedication to this thesis effort. I truly appreciate his encouragement, concern, and especially the countless hours of his time that he spent with me imparting his expertise.

I also thank Professor Joshua H. Gordis for his eager willingness to help. Special thanks go to Bob Tomaine and Mark Smith in the Comanche Program Office for their assistance and support of this effort.

Finally, I want to express my appreciation for the support that I received from Boeing engineers. Dave Peakes, Phil Lang, and Chris Strueven provided me with drawings, a NASTRAN database, and many other pieces of information that were critical to this effort.

I. INTRODUCTION

A. GENERAL

The RAH-66 Comanche is a twin-turbine, tandem-seat, armed reconnaissance helicopter. Its primary mission for the United States Army will be armed reconnaissance and light attack. It replaces the Army fleet of OH-58, OH-6 and AH-1 helicopters whose average age is near 30 years. The Comanche features such technology as a five-bladed bearingless main rotor, a triple-redundant fly-by-wire flight control system, the FANTAIL anti-torque system, and Low Observable (LO) technology to substantially reduce radar, infrared, acoustic and electronic signatures. The Comanche is currently scheduled to achieve Early Operational Capability (EOC) as early as 2003.

Team Comanche led by Boeing Defense and Space Group's Helicopter Division of Philadelphia, Pennsylvania and United Technologies' Sikorsky Aircraft of Stratford, Connecticut is currently developing the Comanche. The RAH-66 is the world's most advanced helicopter and is a focal point for many of the new technologies of the helicopter industry. A photograph of the Comanche is shown in Figure 1.

B. SCOPE

The two major contractor companies have divided responsibilities for design and fabrication. Sikorsky has structural design responsibility for the forward portion of the aircraft fuselage, while Boeing has responsibility for the aft section of the aircraft, including the tailcone, fan, shroud and vertical and horizontal stabilizers. Figure 2 shows the Boeing portion of the structure. The portion of the Boeing structure displayed in

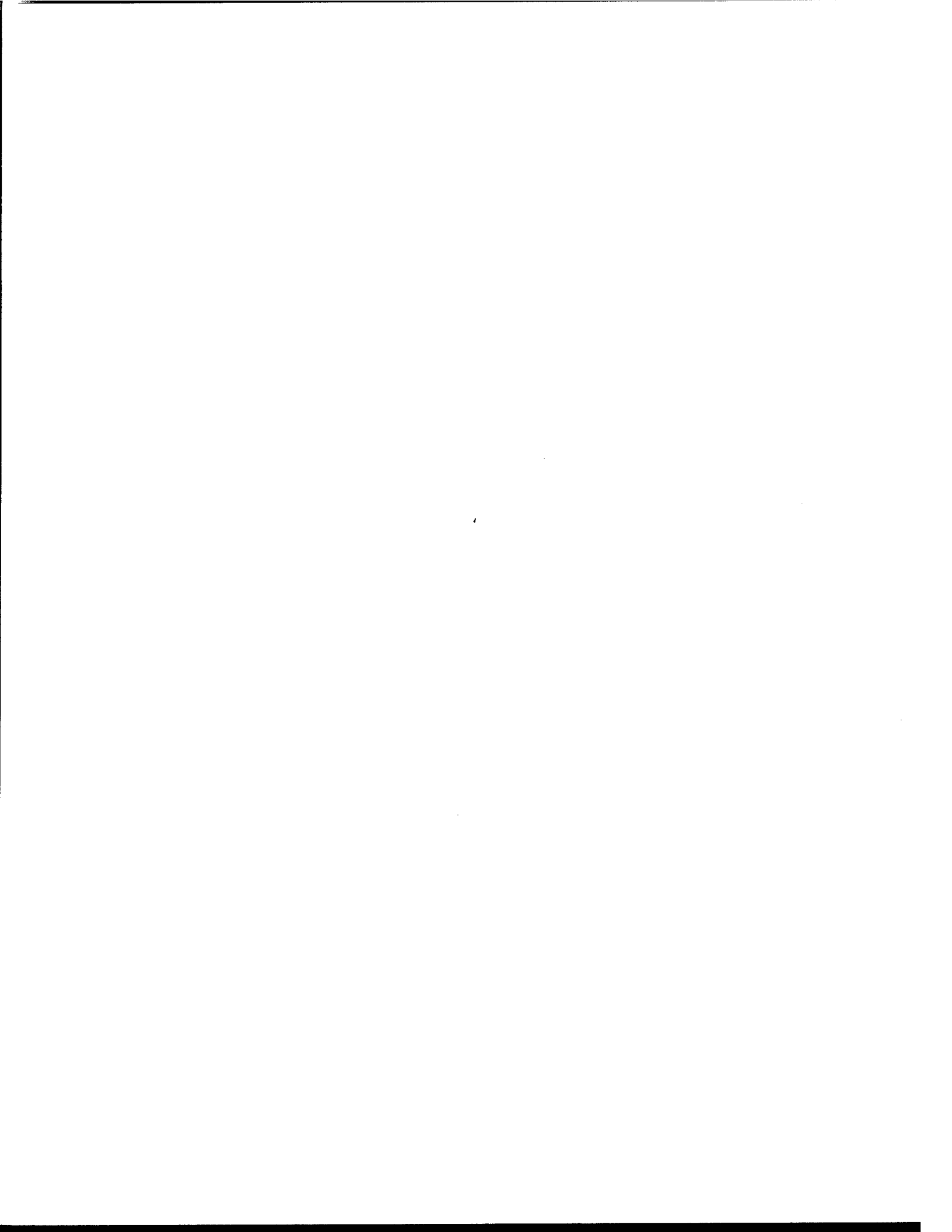


green will be referred to here as the tail cone. This is the portion of the structure that is of primary interest in this study. The aft portion of the structure, shown in pink has not been structurally modified. Therefore, this portion of the structure is not of interest here. All loads were applied at the aft end of the tail cone and hence the remaining aft structure (pink section) displaced as a rigid body for all analysis cases.



Figure 1: US Army Comanche Helicopter

The purpose of this research is to investigate structural design modifications that could potentially increase the tail section's torsional and bending stiffness. The research was conducted using a NASTRAN finite element model of the Comanche representing the aircraft structure at the time of its first flight in January of 1996. Boeing Helicopter Company provided the model of the "first flight" configuration to be used as a baseline. The model was then modified to represent structural design changes to be evaluated for potential bending and torsional stiffness increases.



While this research deals with static load cases, analysis of static cases is done strictly to provide insight into the likely dynamic implications of structural modifications. The goal of the designers is to produce design modifications that will optimize natural frequency placement without increasing gross weight and without increasing infrared and radar signatures. Typically, structural stiffening will raise natural frequencies provided there is no significant increase in weight associated with the stiffening [Ref. 1].

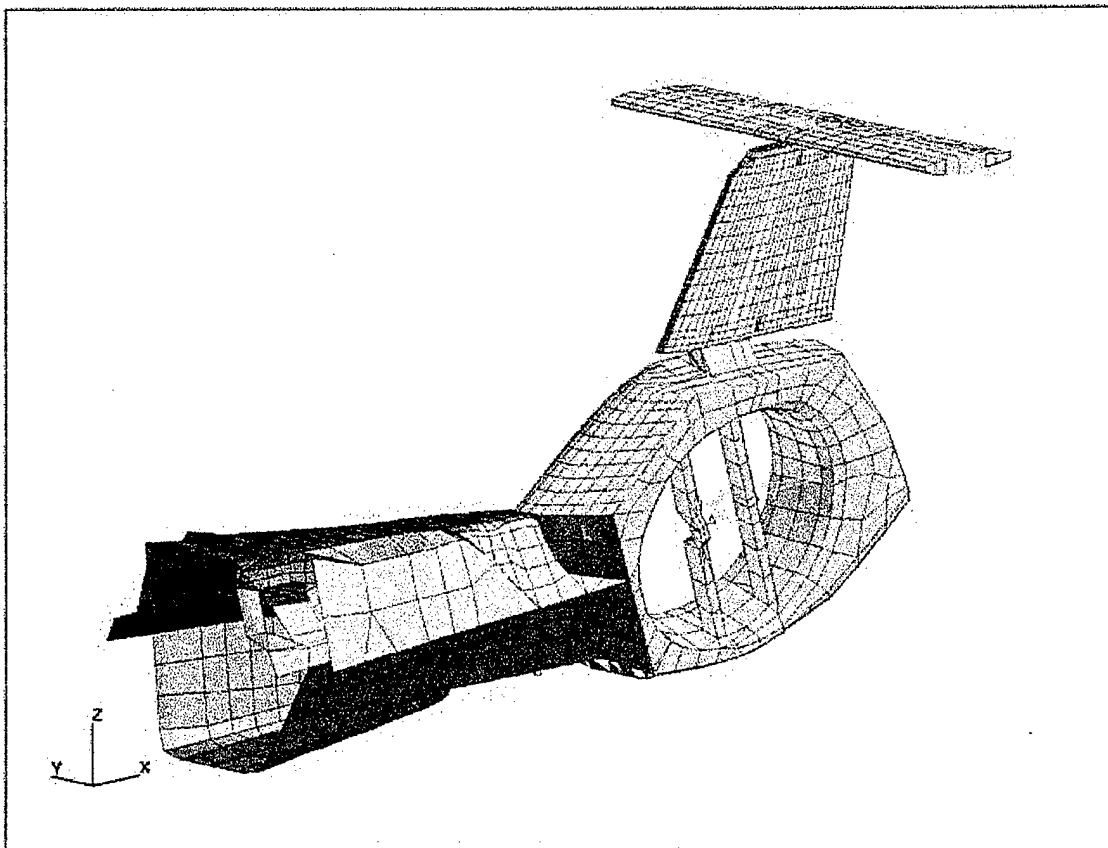


Figure 2: Comanche Tail Section

II. BACKGROUND

A. DESIGN CONSTRAINTS

The Army's performance requirements for the RAH-66 Comanche can be found in the Operational Requirements Document for the aircraft. What will be discussed here are those requirements having an impact on the structural design of the tail section, i.e., those requirements imposing constraints on design.

The assumption for this research is that the current design represents the aircraft's maximum allowable gross weight. Therefore, any structural modification that increases gross weight of the airframe must be offset by an equal weight reduction elsewhere. Obviously weight reduction while meeting other requirements is highly desirable. Also, because the Comanche's center of gravity is currently farther aft than optimum, a forward shift of the center of gravity would also be considered an improvement of the design. Forward shift of center of gravity would reduce gross weight because ballast currently required in the front end could be removed.

The Comanche must meet stringent infrared signature requirements. This involves elaborate structural attributes to shield hot engine components during operation and cooling of hot engine exhaust before ejecting it from the aircraft.

The aircraft must achieve a very low radar cross section to reduce the threat of radar-controlled weapons to the aircraft. Radar visibility for the Comanche will be orders of magnitude less than that for Army helicopters currently in the inventory. This stealth requirement imposes the need to retract the landing gear and even to retract the

gun when not in use. This requirement also limits the use of untreated graphite on the outer mold line (OML), the exterior skin of the aircraft, due to the reflective properties of graphite. It also requires more than an inch of shielding material, such as Nomex or similar core material, between the outer and inner mold lines of the bulk of the skin. The core material is necessary to absorb sufficient radar energy for adequate suppression of radar signature. Increasing the difficulty of structural design is the fact that structural performance and radar signature performance are typically competing requirements. Improvements in radar cross section are almost sure to negatively impact structural performance and vice versa.

A requirement for the tail landing gear that has significant structural impact is the need for the aircraft to contact the tail wheel to the landing surface before the lower tail fan shroud does at angles of up to 30 degrees between the aircraft datum line and the landing surface. For a level runway landing, this means that the aircraft could descend to the runway surface in as much as a 30 degree nose-high pitch attitude and initially contact the runway with the tail wheel. At pitch angles exceeding 30 degrees, the lower shroud structure would contact the ground prior to the tail wheel, potentially causing structural damage. See Figure 3 for an illustration of this requirement.

B. FINITE ELEMENT THEORY

This research uses two powerful software packages, NASTRAN and PATRAN, to analyze structural stiffness results based on geometry and material stiffness properties of a structural model of interest. The foundation of these software packages is the Finite

Element Method (FEM). The FEM provides the basis for algorithms that can efficiently analyze complex structures such as the tailcone of the Comanche.

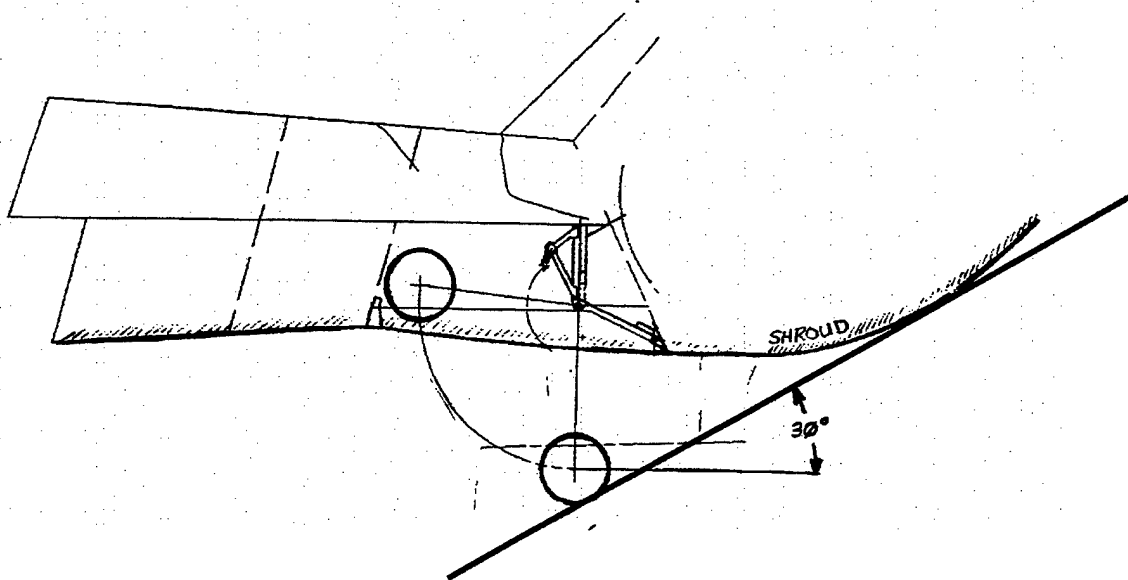


Figure 3: Pitch Attitude Ground Clearance Requirement

Modern aerospace structures such as the Comanche are comprised of many structural elements which include longitudinal spars, frames, bulkheads, composite panels, stiffeners, and others. For analysis purposes, these individual structural components can usually be idealized using beam bending theory, torsion theory, plate theory or shear flow methods. However, analysis of structures that represent the compounding of these individual components is very difficult. The presence of discontinuities such as thickness and cross-sectional variation, cutouts, and joints adds to the difficulty. [Ref. 2]

The large number of members makes exact solutions based on solving the governing differential equations impractical if not impossible. The need, then, is for a general procedure that accounts for the complicating factors noted above and provides a systematic, easily implemented procedure that lends itself to use of a digital computer.

The Finite Element Stiffness Method was developed in the late 1950s to fill this need. The finite element method views a complete structure as the conglomeration of a finite number of discrete base elements such as beams, shear webs, panels, and rods. The deformation response of each of these elements is relatively easily determined as compared with the structure taken as a whole. The finite element method provides a mathematical model based on the discretization of a complete structure into elements.

[Ref. 3]

The elements of the complete structure can be analyzed separately for equilibrium. The elements are then tied back together with compatibility requirements imposed on displacements and equilibrium requirements on forces. Elements are joined at nodes. Nodal forces and displacements must be unique regardless of how many elements are joined at that node. The node represents a single point on the structure and that point cannot occupy two locations simultaneously. Satisfying the equilibrium equations of each element while simultaneously ensuring compatibility of nodal displacements yields the unique solution required to describe the behavior of a structure due to a given load condition. [Ref. 2]

It is important to keep in mind that the FEM yields an approximate and not an exact solution. This does not mean that the results obtained through its use are inaccurate

by definition. However, it does mean that the way the finite element model has been developed has impact on the accuracy of the results obtained during analysis, and interpretation of results must allow for this.

An analogy is the use of digital methods to approximate the area under a parabolic curve. There is an exact solution easily obtained by taking the integral of the function and evaluating it between the given limits. A computer can approximate the value by summing rectangles or trapezoids or using Simpson's Rule. Generally, the more pieces into which the given range is broken, the greater the accuracy of the approximation. For finite element methods, a finer mesh or more elements used to describe a given structure increases accuracy. More regularity in the shapes of elements chosen increases accuracy also. Triangle shell elements provide best accuracy when they are equilateral. Four-sided elements provide better accuracy for the overall model solution as they approach square in shape. Accuracy is lost when using elements of widely disproportionate sides. These should be avoided. [Ref. 3]

In summary, despite its limitations, finite element analysis provides a powerful analysis tool and is really the only practical method now available to analyze a structure as complex as the Comanche airframe.

C. NASTRAN

The National Aeronautics and Space Administration (NASA) funded initial development of NASTRAN in the 1960s. The word NASTRAN is an acronym for NASA STRuctural ANalysis. Originally written in FORTRAN, it was one of the first programs designed to use the finite element method to analyze structural models. [Ref. 3]

The newest version of the NASTRAN software is now owned and distributed by the MacNeil-Schwendler Corporation (MSC), the contractor NASA selected for early NASTRAN development. It remains industry's leading finite element analysis program. It has done so by continually evolving to take advantage of new analytical capabilities and algorithms. Version 69 is the latest release and is the version used for this research.

Available analysis types include linear statics, normal modes, buckling, heat transfer, dynamics, frequency response and aeroelasticity. Users can model almost any material type: metals, composites, hyperelastic and others. Sparse matrix numerical methods greatly increase solution speed and reduce required disk space, making processing very efficient.

D. PATRAN

MacNeil-Schwendler also produces and markets PATRAN, to provide an integrated computer-aided engineering (CAE) environment for analysis. The PATRAN software is both a preprocessor and postprocessor usable with several finite element analysis codes, including NASTRAN. Its capabilities include geometry modeling, mesh generation, analysis data integration, analysis simulation and results display and evaluation. [Ref. 4]

Most important is PATRAN's capability to allow the user to view any structure or portion of a structure from any angle. A zoom capability allows the user to see the level of detail necessary for the particular task. The menu-driven graphical interface makes model manipulation relatively easy when compared with working directly with a NASTRAN analysis deck, the text data file representing a structure within NASTRAN.

All finite element models and results plots presented in this document were generated using PATRAN Version 6.0. The numerical results reported were calculated using Version 6.2. [Ref. 4]

III. RESEARCH METHODS

A. MODEL DEVELOPMENT

The first step in the process of comparing structural stiffness of various designs is developing the NASTRAN models representing the respective structures. A total of six models are analyzed here. The first is the baseline model as provided by Boeing Helicopter in January of 1997. This model represents the aircraft in its first flight configuration on 4 January 1996. The remaining five models are variations on this baseline structure. Using PATRAN software, model changes were made by changing geometry, material properties, or both.

All changes to the Baseline Model could have been made directly to the original NASTRAN deck. Appendix A is a listing of all changes necessary to produce the new geometries. The data in Appendix A includes a listing of all deleted elements and their associated nodes, all added nodes and their coordinate locations, and all added elements and their associated nodes.

1. Baseline

With only minor differences, the baseline model represents the prototype Comanche helicopter currently undergoing developmental flight testing in West Palm Beach, Florida. One might question why any structural design changes are necessary. The reason is that in order to field a flight-worthy prototype aircraft, a large area of skin in the tail cone region had to have graphite on the outer mold line to achieve needed stiffness. In this configuration, while the aircraft largely meets its structural performance

requirements, it does not meet its radar cross section requirements. Figure 4 shows the baseline tail cone.

This is a "cantilevered" model because displacement boundary conditions are imposed at the forward edge of the tail cone, shown in the foreground of Figure 4. These boundary conditions are represented graphically by arrowheads. The tip of each arrowhead rests on the point or node that is fixed. The direction of the arrowheads indicates the degree of freedom that is constrained, displacement in the x, y, or z directions. The numerals (1, 2, or 3) adjacent to the constrained nodes also indicate the translational constraints in the 1, 2, or 3 (x, y, or z respectively) directions.

Note that some nodes are constrained in motion in all three directions and others in only two, while still others not at all. This configuration of boundary conditions was developed by Boeing to model the effects of aerodynamic forces and moments on the main rotor and forward fuselage as they are transmitted aft to the Boeing-Sikorsky interface, the forward edge of the tail cone. This boundary condition arrangement will be used for analysis of all structural models.

It is important to illustrate the structural impact of other design requirements on the tail cone structure. For example, radar cross section requirements impact not only skin lay-up configuration and materials, but also orientation angles and curvature of structural surfaces.

The infrared signature suppression requirement also has significant impact on this structural design. The exhaust system must substantially cool engine exhaust before it can be discharged overboard. The tailcone structure must accommodate a heat

exchanging apparatus that uses ambient air to absorb heat from the engine exhaust. The resulting mixture of air and exhaust gas leaves the aircraft at a temperature higher than that of the ambient air but much lower than the raw exhaust gas. Reduction in temperature produces a reduction in infrared signature.

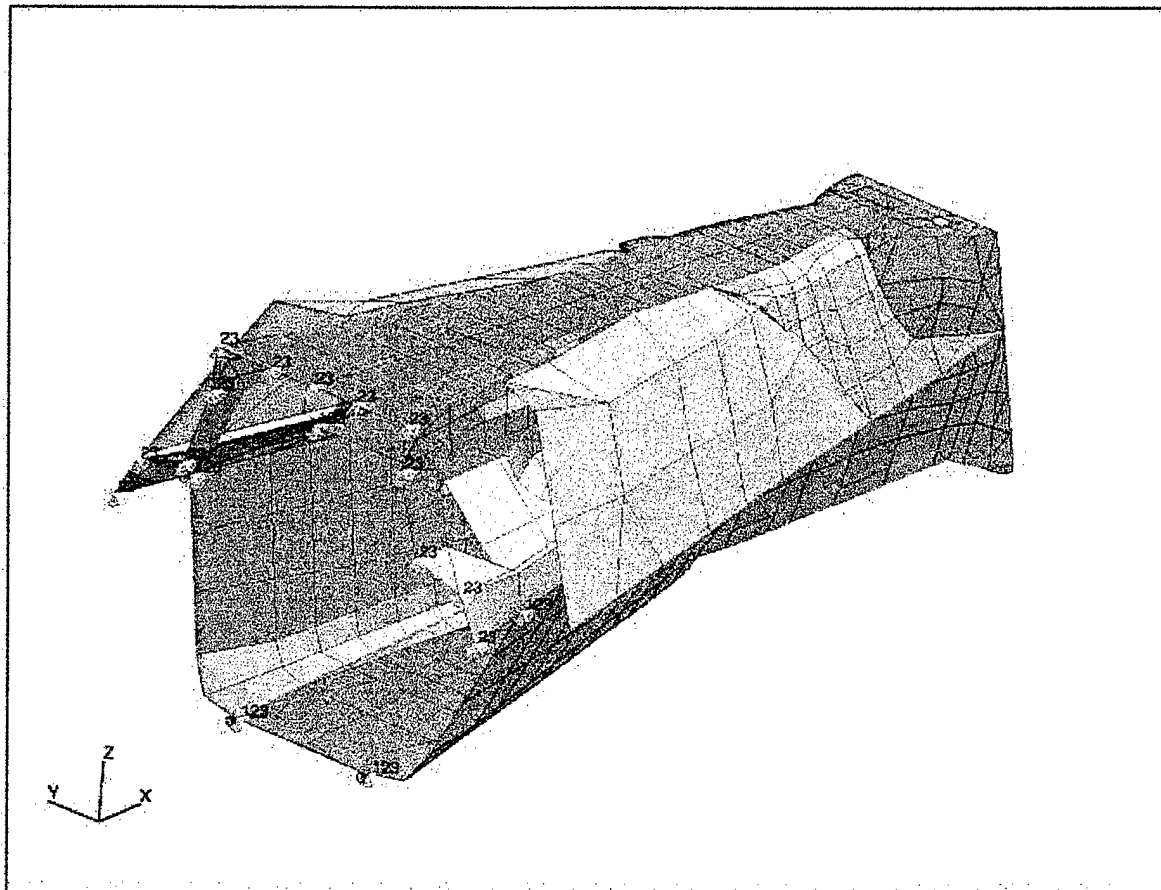


Figure 4: Baseline Tail Cone

The large elements on the upper half and forward two thirds of the tail cone (displayed in blue in Figure 4) are the exhaust covers. The exhaust covers essentially serve as a thermal shield for the hot exhaust gas undergoing the heat exchange process

within the tail cone. These covers are considered non-structural because their load-carrying capability is negligible.

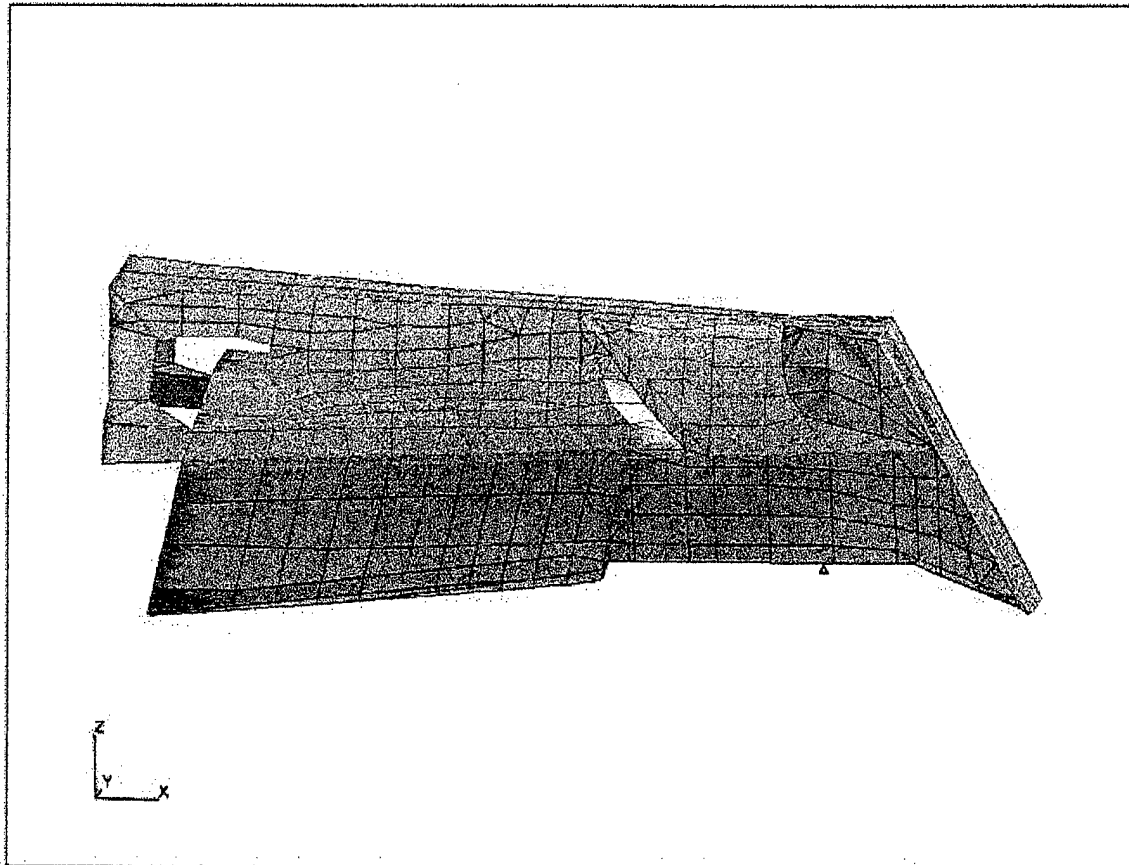


Figure 5: Baseline Tail Cone, Exhaust Covers Not Displayed

The PATRAN software uses color contour plots to show such quantities as displacement, stress, and strain as a function of location in the structure. For this reason, exhaust cover elements will not be displayed for this or any of the other cases in figures illustrating structural modifications or loading analyses. Displaying quantities of the

structural elements under the exhaust covers provides far more useful information. An important note is that although the exhaust covers are not displayed, their small structural influence is being calculated by NASTRAN and is incorporated into the displayed results. Figure 5 shows the tail cone with the exhaust covers not displayed.

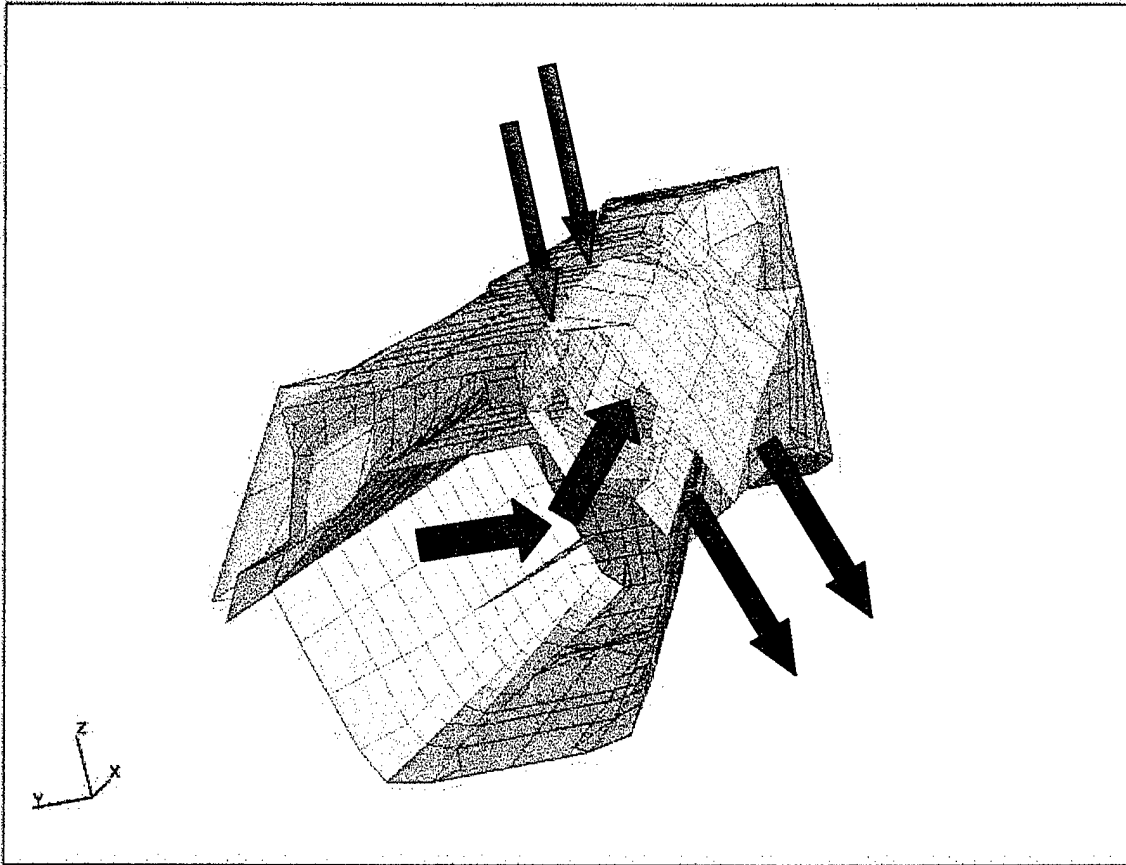


Figure 6: Exhaust Cooling Schematic

Figure 6 illustrates the exhaust cooling process within the tail cone. This portion of the structure is bilaterally symmetric, so the process is illustrated on only one side of the aircraft. Exhaust gas enters the tail cone via a metallic conduit that is not shown. The red

arrow represents the hot exhaust gas path. The blue arrows show the path of ambient-temperature rotor wash forced into the tail cone through space between the upper deck of the tail cone and the exhaust covers. The purple arrows show the intermediate-temperature discharge mixture of exhaust gas and ambient air. All proposed structural modifications must allow for infrared signature suppression by the method discussed.

The heat-exchanging volume within the tail cone extends aft of a major structural entity, the Forward Tail Landing Gear Bay Bulkhead (FTLGBB). The FTLGBB spans

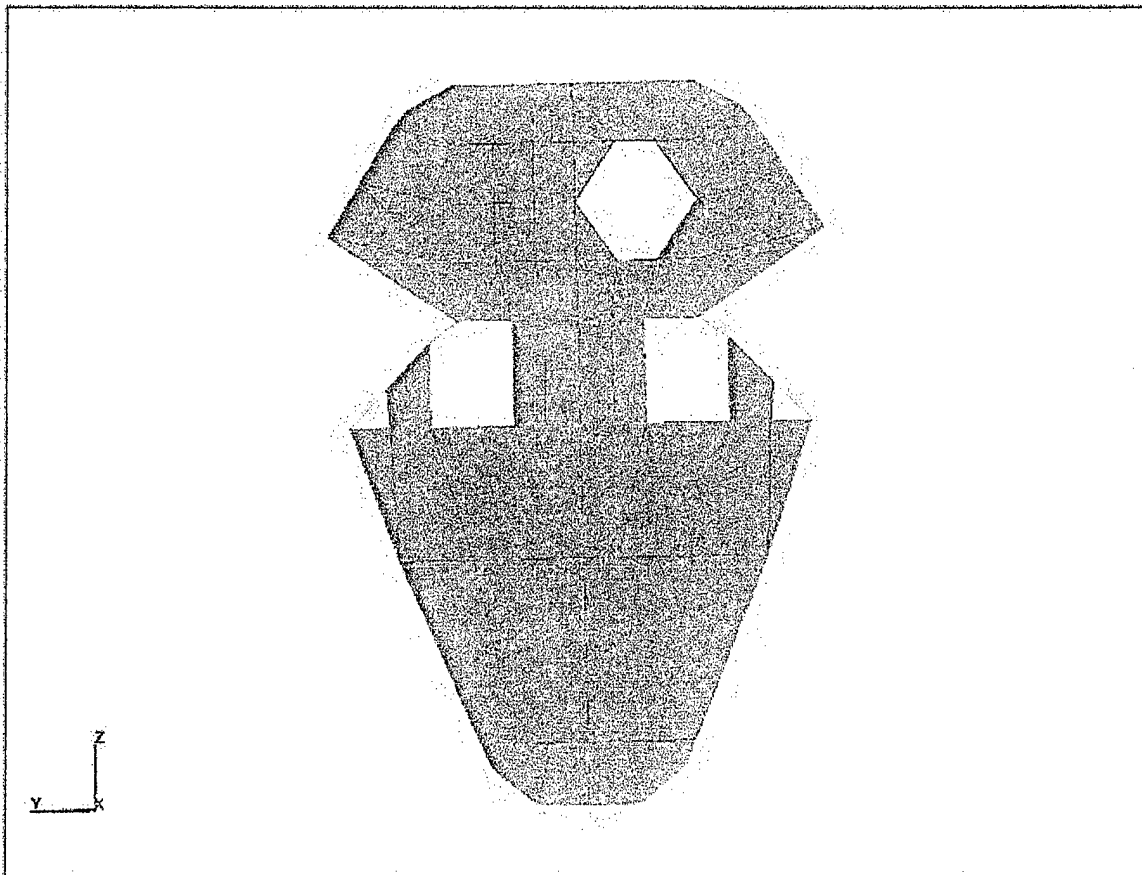


Figure 7: Forward Tail Landing Gear Bay Bulkhead, Baseline Model

most of the tail cone cross-section and is not oriented perpendicular to the aircraft center line. The top of the FTLGBB is canted aft. Figure 7 shows the bulkhead as seen from the front end of the tail cone with the display of all other structure suppressed. The cut-ins that give the bulkhead an hourglass shape are needed to allow the heat-exchanging volume to extend beyond the plane of the bulkhead.

The FTLGBB defines the forward wall of the tail landing gear bay. With the tail landing gear extended and the bay doors open, it is the wall that keeps debris and water out of the hollow tail cone. It serves an important purpose in carrying structural loads. The cross-section of the tail landing gear bay is structurally an open section because the doors are not structural. With the landing gear extended and the doors open, it is physically an open section. Torque loads are typically not carried well by open section structures and this one is no exception.

The "torque box" that sits above the tail landing gear bay must carry torque loads rising from aerodynamic forces on the horizontal and vertical stabilizers and from the thrust of the tail fan. This closed-section torque box is made up of the upper walking deck on top, the port and starboard tail cone skin on the sides and the deck that is the "ceiling" of the tail landing gear bay, the Waterline 3160 Deck, as the bottom.

The main reinforcing beams that run forward from the FTLGBB to the Boeing-Sikorsky Interface are located in the lower portion of the tail cone. The FTLGBB and the structure immediately fore and aft of it serve to transition loads from the upper torque box aft of the FTLGBB to the large closed section that encompasses almost the entire tail cone cross section forward of it. Stiffening of the section of the structure that includes

this bulkhead could have substantial beneficial effects, especially in increasing natural frequencies of vibration.

Figure 8 shows in red the “slice” of the tail cone that defines the FTLGBB Section. In Figure 8 the plane of the FTLGBB is perpendicular to the x-z plane. Figure 9

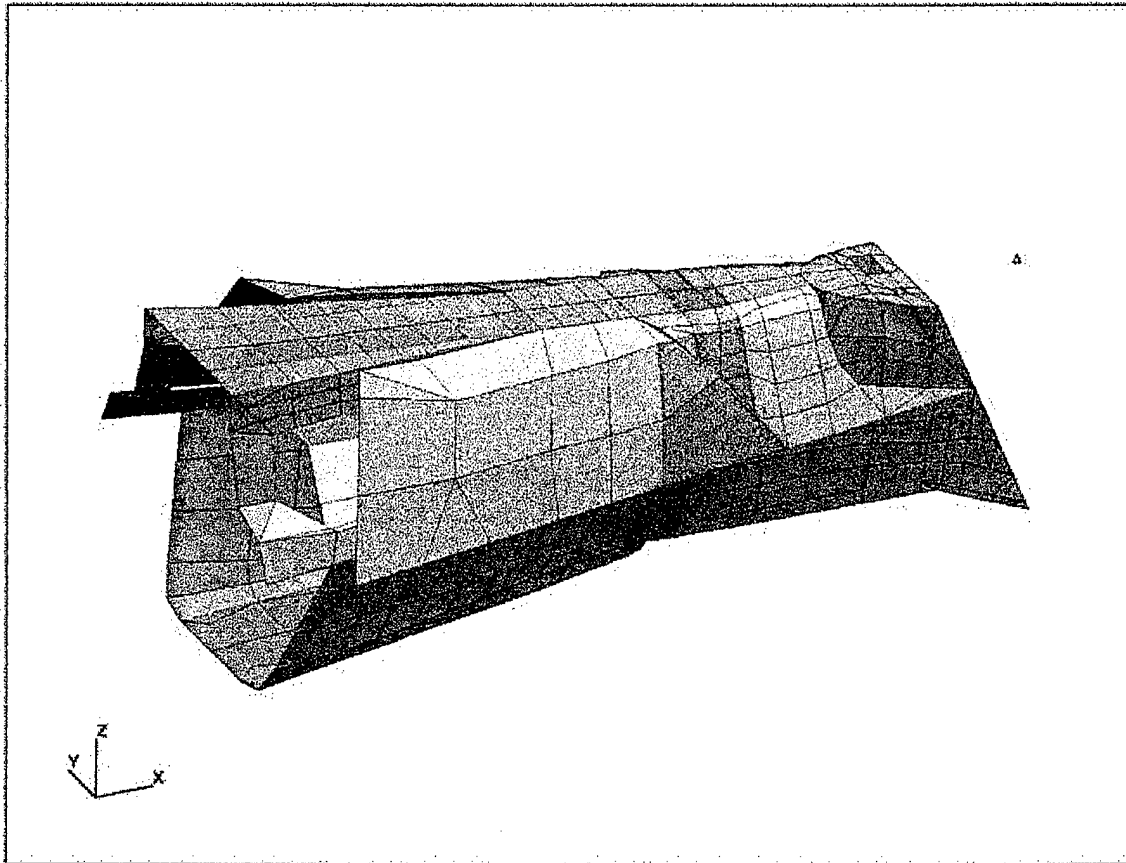


Figure 8: FTLGBB Section in Tail Cone

is the bulkhead section as viewed from the front of the tail cone with the display of all other structure suppressed. Notice the elements that make up the Exhaust Closeouts. The starboard side (left side of Figure 9) elements immediately fore and aft of the bulkhead

are displayed. On the port side, only the Exhaust Closeout elements aft of the bulkhead are shown.

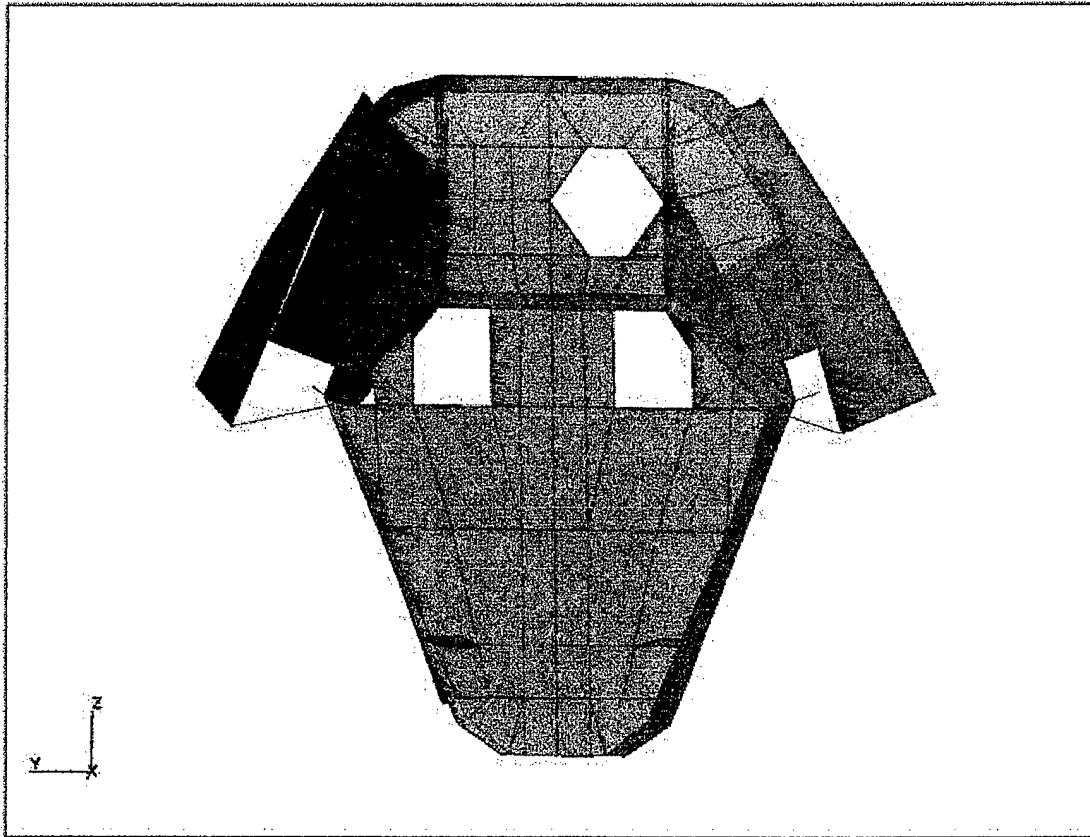


Figure 9: Front View of FTLGBB Section

2. Baseline with Kevlar Exterior Skin (Base-Kevlar)

The first structural modification involved only changes in material properties. That is, the geometry of the Base-Kevlar model is identical to that of the baseline model. (Note that shortened titles that will be used throughout this report to identify modified models appear in parentheses after their respective sub-section headings.)

This model is not investigated as a potential design-improvement modification. In fact, it is known to be unacceptable. It is essentially analyzed only to obtain another baseline set of structural stiffnesses for a structure made of materials likely to meet radar signature requirements. This set of structural stiffnesses will serve as another basis of comparison for models with geometry modifications intended to improve structural performance and made of materials likely to enable the design to meet radar signature requirements.

Appendix B is a spreadsheet printout of the weight and center of gravity changes for each modification. For Base-Kevlar, the gross weight is reduced by 0.43 pounds and the center of gravity shifts forward by 0.025 inches compared to Baseline. The center of gravity shift computation assumes an aircraft gross weight of 10,600 pounds. As is the case for all modifications, weight and center of gravity impact is negligible.

3. Bulkhead Section Modified (Bulk-Mod)

This is the Baseline model with structural modification confined to the FTLGBB and structure in the immediate vicinity. The intent here was to stiffen the structure by fastening all structural skin of the aft, upper tail cone to the FTLGBB. The bulkhead was enlarged to completely span the cross-section of the tail cone in the plane of the bulkhead. This changed the shape of the bulkhead from resembling an "hourglass" to resembling a "mushroom." Figure 7 shows the Baseline FTLGBB. Figure 10 shows the FTLGBB as modified for the Bulk-Mod Model. Elements displayed are also those of the Baseline FTLGBB. Elements in red have been added for the Bulk-Mod Model. The red

elements also serve as the lower exhaust closeout structure as well as part of the FTLGBB for the Bulk-Mod Model.

A major impact of this change is on the exhaust system. In the Baseline model, exhaust gases could pass through the plane of the FTLGBB. In the Bulk-mod model, the FTLGBB spans the entire cross-section so it becomes part of the exhaust closeout structure. This results in a reduction in available heat-exchanging volume of

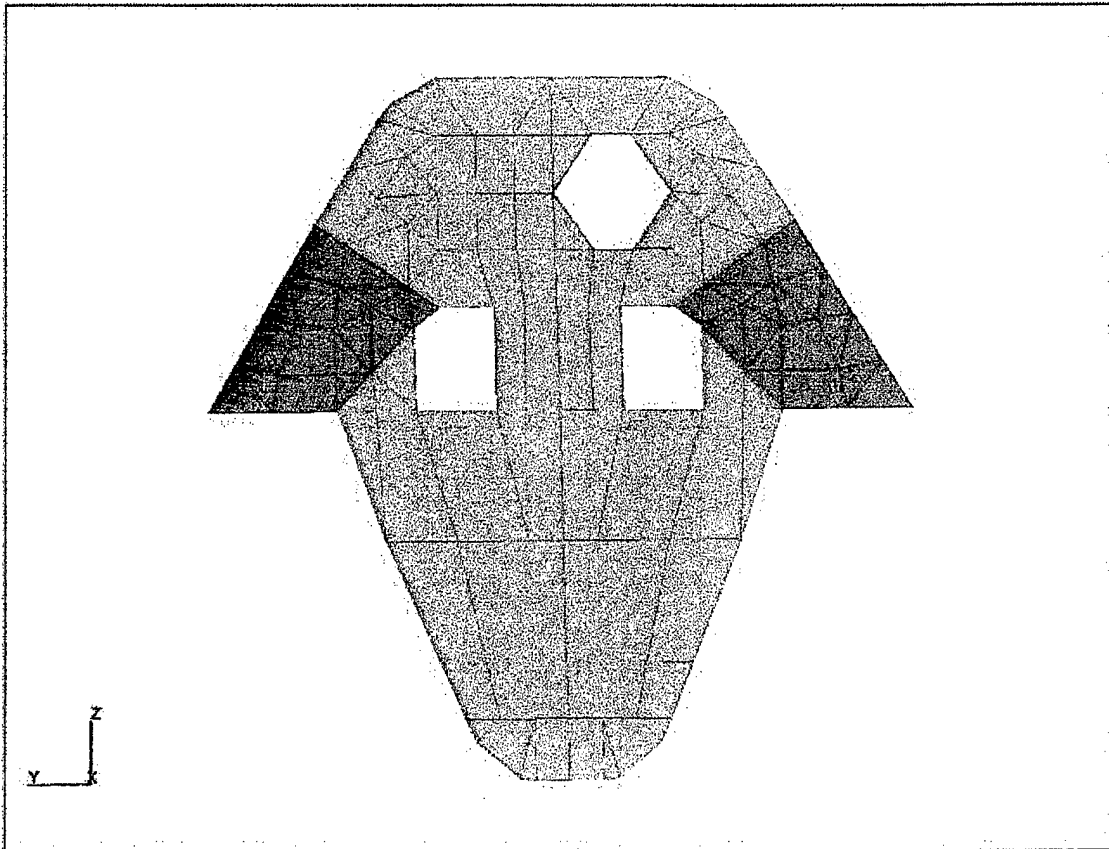


Figure 10: Bulk-Mod FTLGBB

approximately five percent and potential airflow changes that could increase infrared signature.

No quantitative analysis has been done to determine the impact on infrared signature. This type of analysis might be necessary for a trade study to determine

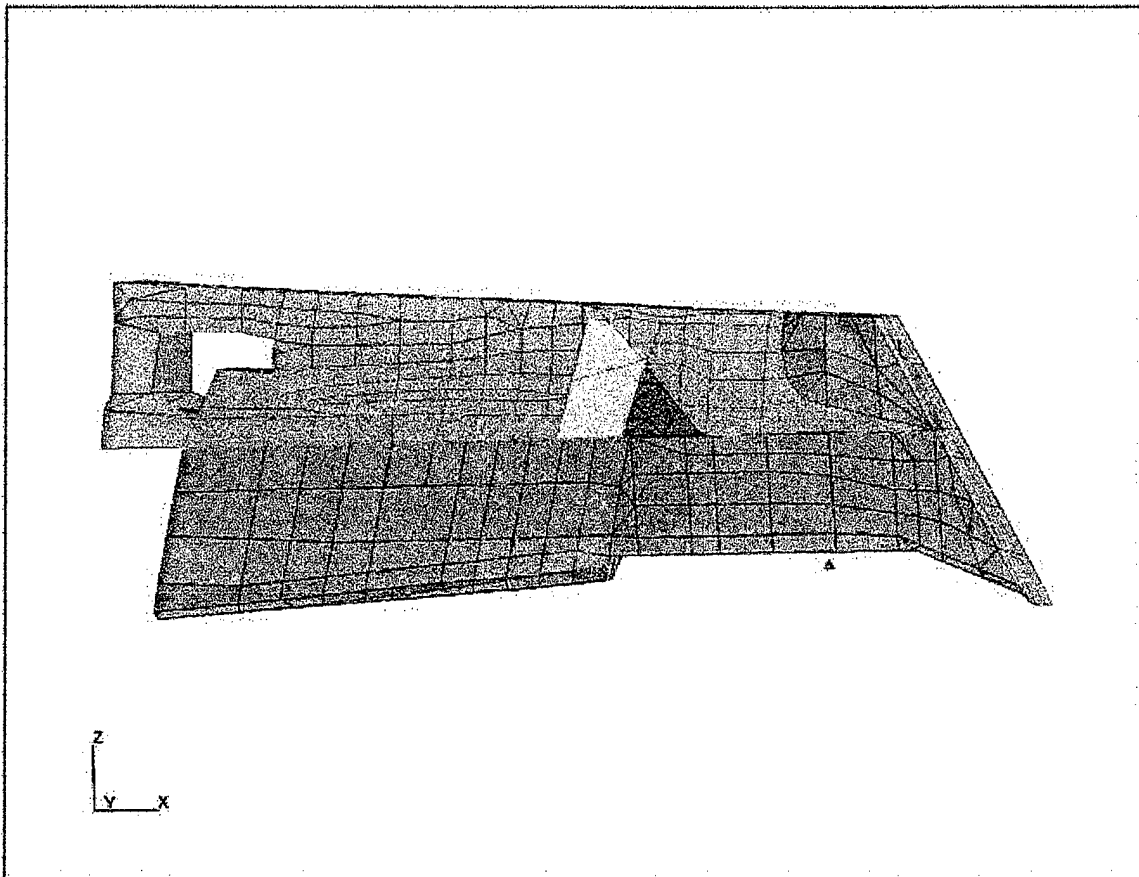


Figure 11: Aircraft Skin Added for FTLGGB Modification

whether structural improvement gained as a result of this modification, if any, justifies the impact on infrared signature. However, the small reduction in volume occurs at the aft end of the chamber. This is the location where the temperature gradient, the driving

force for heat exchange, is at its minimum. This means that heat exchange in this portion of the chamber is also at its minimum. The flow will likely not be significantly altered because the opening through which rotor wash is forced into the heat-exchange volume is unchanged. For these reasons, it was thought that infrared significance was small enough to justify investigating the structural improvement of this model.

The shortened heat-exchange chamber necessitates other structural modifications near the bulkhead. Elements of the exhaust lining, the shell elements visible when the exhaust covers are removed, must be joined to the FTLGGB to prevent exhaust from leaking into the interior tail cone. Exhaust lining structure aft of the FTLGGB plane is no longer necessary. It is therefore removed.

The exhaust cover aft of the bulkhead is also no longer needed. The exhaust covers are clipped along a line lying in the plane of the FTLGGB. The external aircraft surface that had been exhaust cover aft of the bulkhead is replaced by structural aircraft skin with the same material properties as the elements of the upper aft tail cone. Figure 11 shows the added skin elements in red. The remaining aft exhaust cover elements are shown in blue. The exhaust covers of the Baseline Model covered the whole area shaded red and blue in Figure 11.

The Waterline 3160 Deck serves as the "ceiling" of the Tail Landing Gear Bay. The Bulk-Mod model also expands this deck aft of the FTLGGB to cover what was an exhaust port for the Baseline model. This addition ties the deck into the skin of the upper aft tail cone as far forward as the FTLGGB. It also ties the skin into the FTLGGB across the entire y-axis span of the tail cone at its widest point and should add significant

horizontal bending stiffness to the Bulk-Mod structure. Figure 12 is a view from above the tail cone looking down and forward onto the Waterline 3160 Deck. (See Axes in lower left corner of Figure 12 for orientation). Some elements of the upper tail cone are not displayed to expose the deck. The added elements to this deck for the Bulk-Mod model are shown in red and the FTLGBB is shown in blue for orientation.

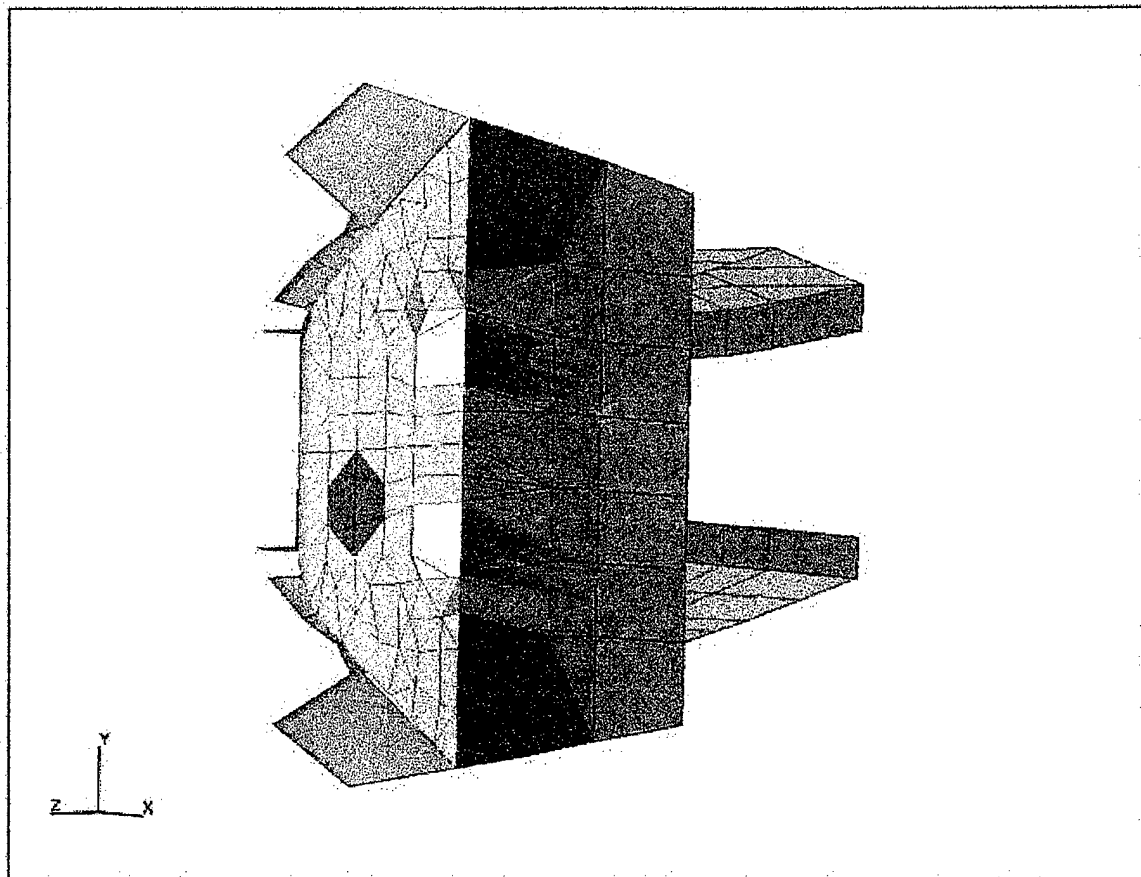


Figure 12: Waterline 3160 Deck

Figure 13 shows a view of the Bulk-Mod structure looking aft and up. The elements in red are those added to the FTLGBB, the Waterline 3160 Deck, and the skin

on the side of the aircraft that replaced a portion of the exhaust cover from the Baseline Model.

The aircraft gross weight for the Bulk-Mod Model actually decreases by 0.48 pounds compared to Baseline. The center of gravity shifts forward by 0.027 inches, again assuming the aircraft gross weight is 10,600 pounds.

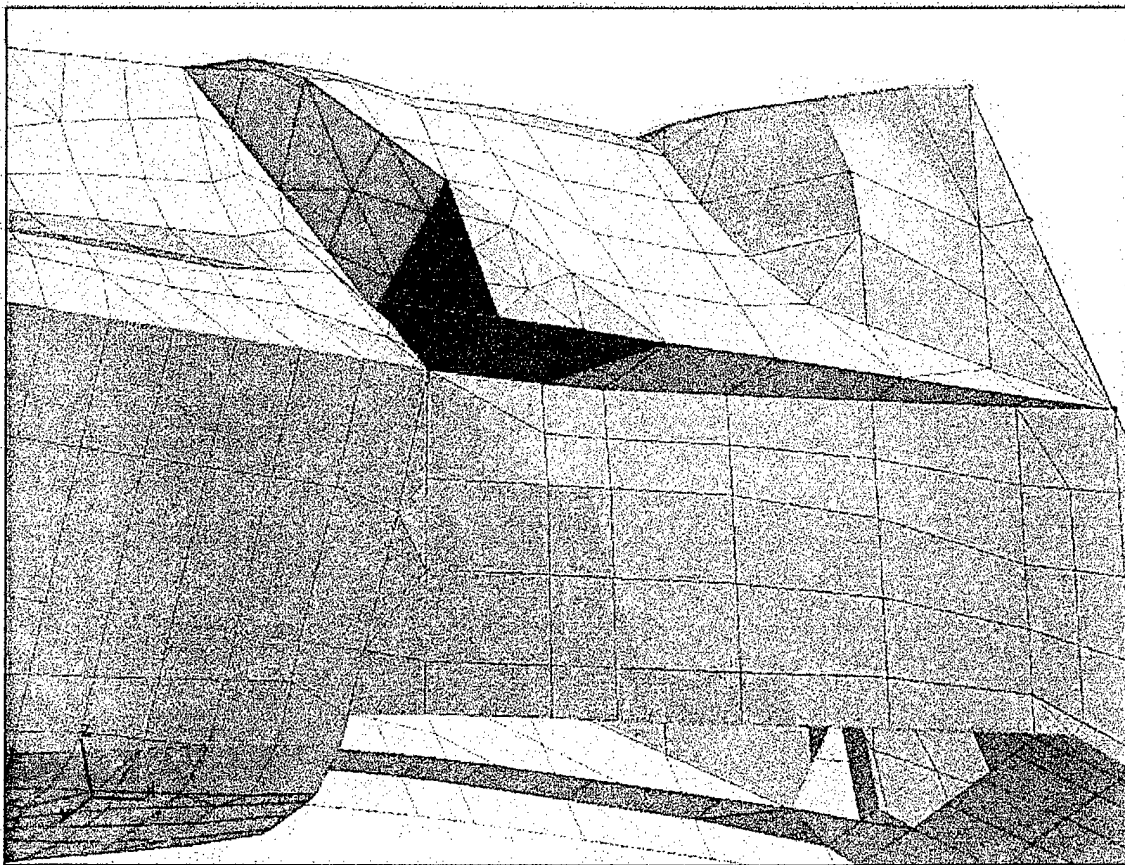


Figure 13: Added Elements, Bulk-Mod

4. Aft Tail Cone Modified (Cone-Mod)

The intent of modifying the aft tail cone was to increase the enclosed cross-sectional area of the upper tail cone. The important structural entity of the aft tail cone is the "torque box" defined by the Upper Walking Deck on top, the Water Line 3160 Deck as its bottom and the aircraft skin on either side. This is the part of the structure that carries most of the loading, primarily because the lower aft tail cone contains the Tail Landing Gear Bay, an open section that does not carry torsion loads well.

To increase the cross-sectional area of this "torque box," the Upper Walking Deck was first enlarged. Figure 14 shows in red the added elements needed to model this new structure. The new dimensions of the Upper Walking Deck were determined by connecting straight lines between the deck edges in the plane of the FTLGBB and the deck edges in the plane of the Aft Tail Cone Bulkhead.

For this research, this Upper Walking Deck expansion was considered to be the largest practical configuration because it represents the largest aft deck possible without changing the shape of either connected bulkhead. The assumption here is that changing the dimensions of either bulkhead would be unacceptable due to the expense and tooling impacts of these changes.

Dropping vertical planes from the new deck edges and joining these vertical planes and the existing skin faces of the upper tail cone created the new skin geometry. For the Cone-Mod model, the added elements were all designated to have the same material properties as the Upper Walking Deck, which has the same material properties as the skin of the upper tail cone for the Baseline model.

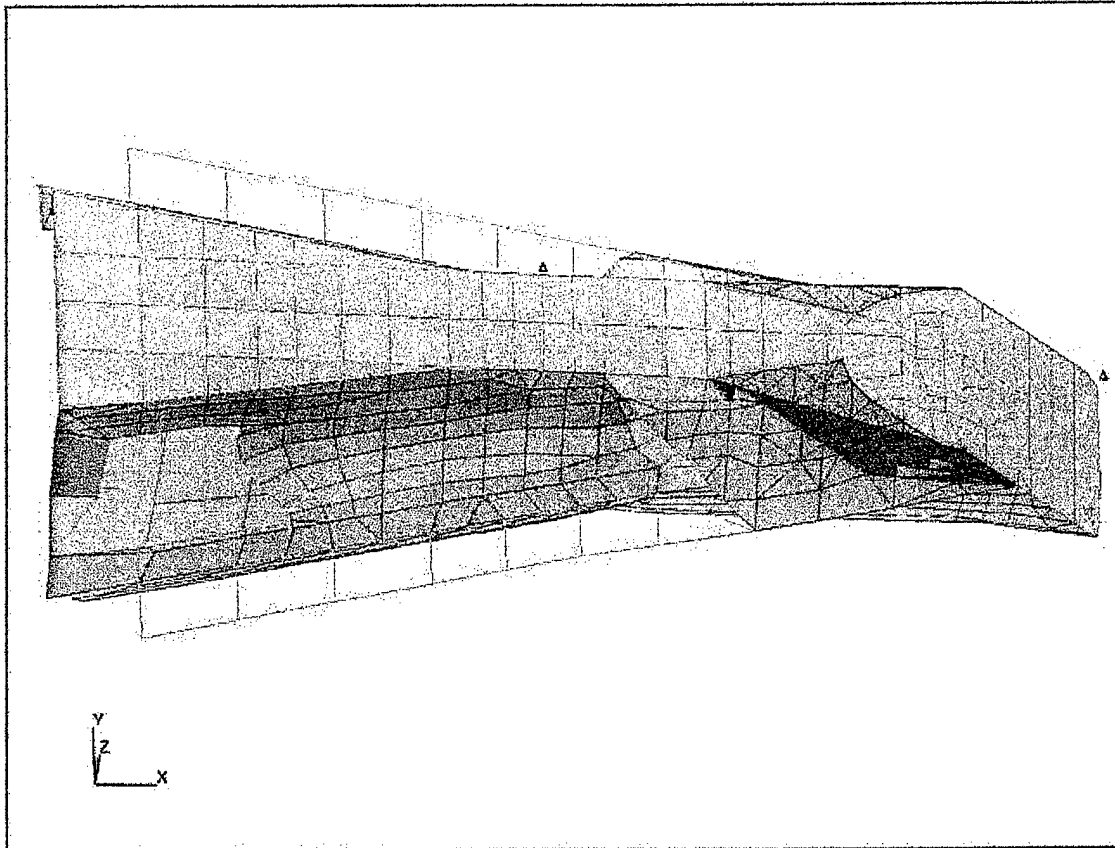


Figure 14: Aft Tail Cone Modification (Cone-Mod)

The gross weight increase from Baseline for the Cone-Mod Model is 0.75 pounds. The center of gravity shifts aft by 0.042 inches.

5. Bulkhead Section and Aft Tail Cone Modified (Full-Mod)

The Full-Mod model is simply the modifications to both the FTLGBB section and the aft tail cone combined into a single model. The material properties used are those of the added elements for the Bulk-Mod and Cone-Mod models.

The gross weight increase from Baseline is 0.26 pounds due to the structural modifications made for the Full-Mod Model. The center of gravity shifts aft by 0.015 inches.

6. Full-Mod with Kevlar Exterior Skin (Full-Kevlar)

The Full-Kevlar model has exactly the same outer mold line geometry as the Full-Mod model. The material properties, however, are different. The aft tail cone skin for this model has material property that is likely to achieve the desired radar signature. This skin configuration has four plies of graphite on the inner mold line, 33 millimeters of core material and two plies of Kevlar on the outer mold line. This compares to the Baseline model where the skin configuration has two plies of graphite on the inner mold line, 12.7 millimeters of core, and six plies of graphite on the outer mold line.

The aircraft gross weight increase from that of Baseline Model is 0.34 pounds. The center of gravity shift from Baseline is 0.019 inches aft.

B. LOAD CASES

The actual aerodynamic forces on the aft fuselage and empennage of the aircraft in flight will produce various combinations of forces and moments in all three axes on the tail cone. However, the assumption here is that sufficient information on tail cone stiffness is available through analysis of only three load cases. The applied load cases for this research are: a negative x-direction moment, a positive y-direction force and a negative z-direction force.

It is expected that in actual flight, loads transmitted to the aft end of the tail cone would be distributed throughout the structure. That is, forces and moments would not be transmitted to the tail cone as point forces or moments. To model distributed loads, a PATRAN capability called a multi-point constraint (MPC) had to be used.

First, through trial and error, a load application node was located within a millimeter of the Baseline tail cone's center of rotation at the aft bulkhead. This node location is the same for all applied loads on all models. Next a rigid MPC was attached to all nodes of the aft bulkhead perimeter and to the load application node. This arrangement models a perfectly rigid test fixture attached to the aft bulkhead. All nodes attached via MPC to the load application node maintain their relative positions to one another after application of loads. The main purpose of the MPC is to allow an applied point force or moment to be distributed across the tail cone cross-section to model, as closely as possible, the actual in-flight load distribution.

1. Long Axis Moment

The x-direction moment on the tail cone occurs in flight due to the aerodynamic force on the vertical stabilizer plus unsymmetrical vertical loading of the horizontal tail due to roll of the aircraft. The vertical stabilizer is designed to generate an aerodynamic force to counter the torque of the main rotor. Due to the presence of the tail fan, the vertical stabilizer is located some distance above the tail cone. The separation of the tail cone and vertical stabilizer center of pressure creates a moment arm. The aerodynamic force on the vertical stabilizer, then, is primarily responsible for the long axis moment in the negative x-direction. The actual aerodynamic loads on the vertical tail are transmitted

to the tail as both a shear force and a rolling moment. Here these load cases are treated separately and only the moment is applied for this load case. The applied load is 10,000 Newton-Meters.

2. Lateral Force

The y-direction force on the aft end of the tail cone is also due to anti-torque forces applied to the vertical tail and transmitted through the structure to the tail cone. This load case is designed to examine the lateral bending stiffness of the tail cone. The applied load selected is 5000 Newtons.

3. Vertical Force

In high-speed forward flight, the tip-path-plane of the main rotor must tilt forward significantly to maintain airspeed. This has a tendency to lower the nose of the fuselage, increasing drag. The z-direction force occurs in high-speed forward flight where downward aerodynamic force is generated on the horizontal tail to level the fuselage attitude and reduce drag. Here, the magnitude of the selected applied load is 5000 Newtons directed in the negative z-direction, downward.

IV. RESULTS AND ANALYSIS

The results of the analyses will be presented in two ways. First, numerical values will be presented in tables below. Second, a total of 36 figures (Figures 15-50) will be presented showing PATRAN contour plots of displacement for each model under each load condition and contour plots of strain energy density for each model under each load condition.

Numerical results are presented in three separate tables. The tables present essentially the same information reported in different units. Reported information is the stiffness of each model in torsion about the longitudinal axis, lateral bending, and vertical bending. For torsion, stiffness is reported as moment per degree of rotation of the input node. For bending, stiffness is the force per unit of displacement of the input node.

The Table 1 results are in SI units: torsional stiffness in Newton-Meters per Degree and bending stiffness in Newtons per Meter.

Model	Torsion (N-m)/degree	Horizontal Bending (N/m)	Vertical Bending (N/m)
Baseline	25,820	2,635,000	1,906,000
Base-Kevlar	19,710	2,580,000	1,840,000
Bulk-Mod	28,130	2,670,000	1,897,000
Cone-Mod	26,080	2,775,000	1,907,000
Full-Mod	28,110	2,728,000	1,910,000
Full-Kevlar	23,180	2,686,000	1,863,000

Table 1: Model Stiffnesses in SI Units

Table 2 presents the same information as Table 1 in English units: torsional stiffness in Foot-Pounds per degree and bending stiffness in Pounds per foot.

Model	Torsion (ft-lbf)/degree	Horizontal Bending (lbf/ft)	Vertical Bending (lbf/ft)
Baseline	19,050	180,500	130,600
Base-Kevlar	14,530	176,800	126,100
Bulk-Mod	20,750	182,900	130,000
Cone-Mod	19,240	190,100	130,700
Full-Mod	20,730	187,000	130,900
Full-Kevlar	17,100	184,000	127,700

Table 2: Model Stiffnesses in English Units

Table 3 presents the same data as the previous tables normalized to Baseline values.

Model	Torsion	Horizontal Bending	Vertical Bending
Baseline	1.000	1.000	1.000
Base-Kevlar	0.763	0.979	0.965
Bulk-Mod	1.089	1.013	0.995
Cone-Mod	1.010	1.053	1.000
Full-Mod	1.089	1.036	1.002
Full-Kevlar	0.897	1.019	0.977

Table 3: Model Stiffnesses Normalized to Baseline Values

As expected, the Baseline geometry with Kevlar on the outer mold line (Baseline Kevlar Model) was shown to be very soft. It was almost 24% less stiff than the Baseline Model in torsion. The Full-Kevlar model, however, was only 10% softer than the Full-Mod Model in torsion. *The most important result is that all of the geometry changes cannot offset material effects. The Full-Kevlar Model is significantly less stiff than the Baseline under all three load conditions.*

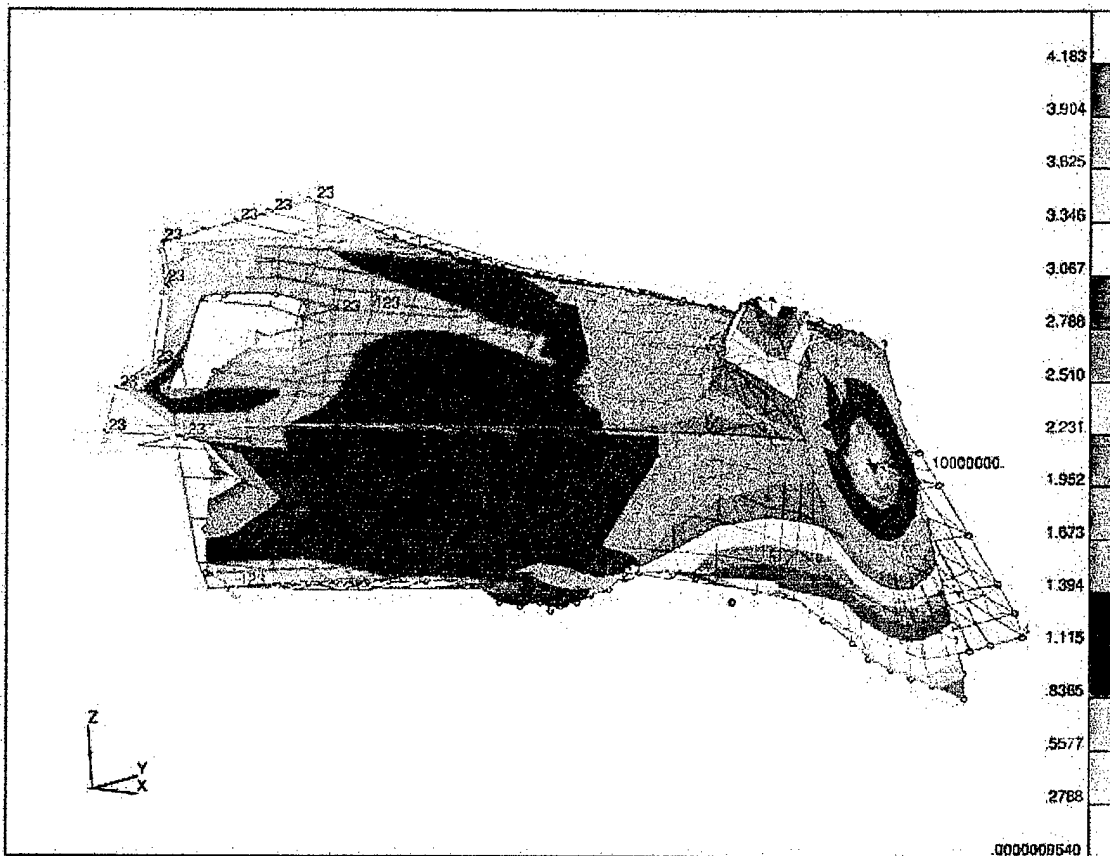


Figure 15: Torsion Displacement of Baseline Model

The values shown on the displacement plots (The odd-numbered figures from Figure 15 to Figure 49 are displacement plots for the 18 load cases.) are magnitudes of the displacement vector at each node of the structural model. The PATRAN software also has the capability to display displacements as x, y, or z components.

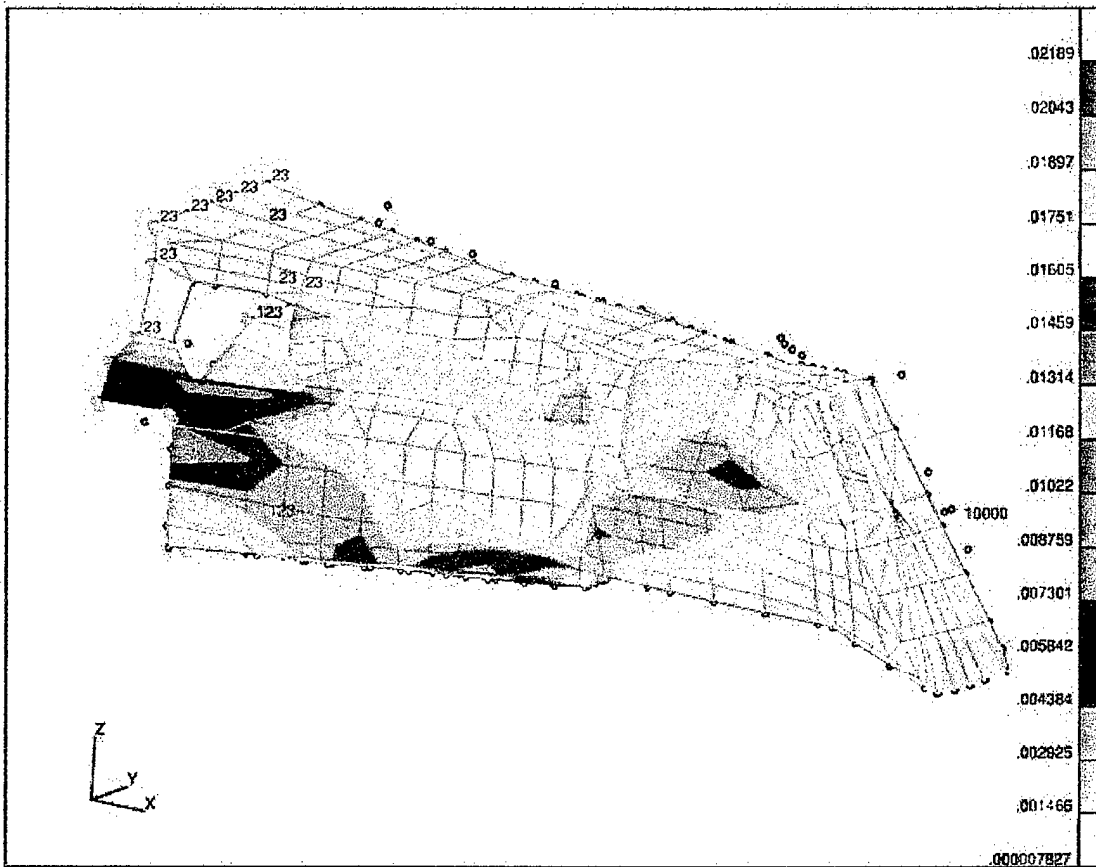


Figure 16: Torsion Strain Energy Density Fringe of Baseline Model

Figure 16 is a fringe, or contour plot of strain energy density (strain energy per unit volume) as a function of position on the structure. (The even-numbered figures from Figure 16 to Figure 50 are strain energy density plots for each of the 18 model load cases.)

The magnitude of the strain energy density is not as important here as the relative values. Higher values on a structure indicate “soft spots,” or the places where adding material may provide the most stiffness increase per pound of added material.

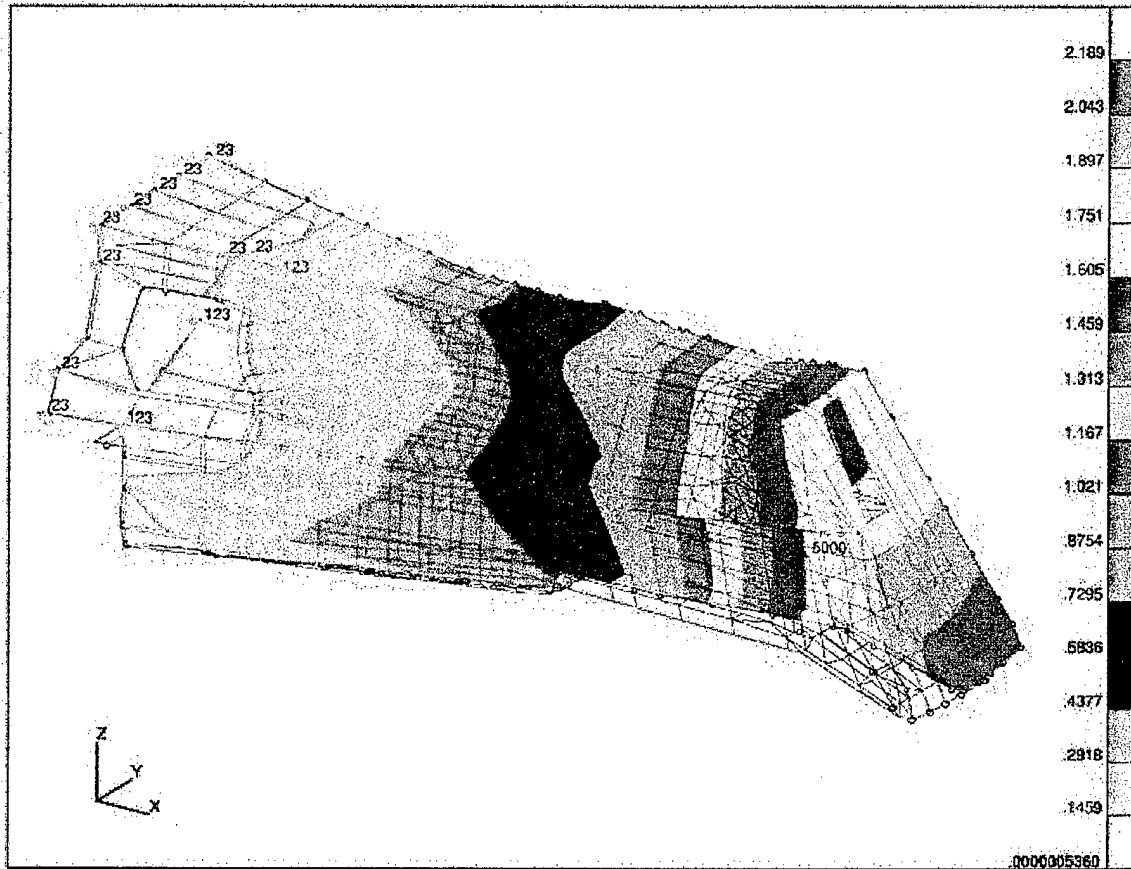


Figure 17: Horizontal Displacement of Baseline Model

Notice that for the torsional displacement plots, displacement occurs primarily in the y and z directions. In none of the torsional load cases does displacement in the x direction exceed four percent of the magnitude of displacement of the load application node. For the lateral and vertical force load cases, displacement occurs primarily in the

direction of the applied force. In all bending cases, the displacement in the direction of the applied force is at least 95 percent of the magnitude of displacement of the load application node.

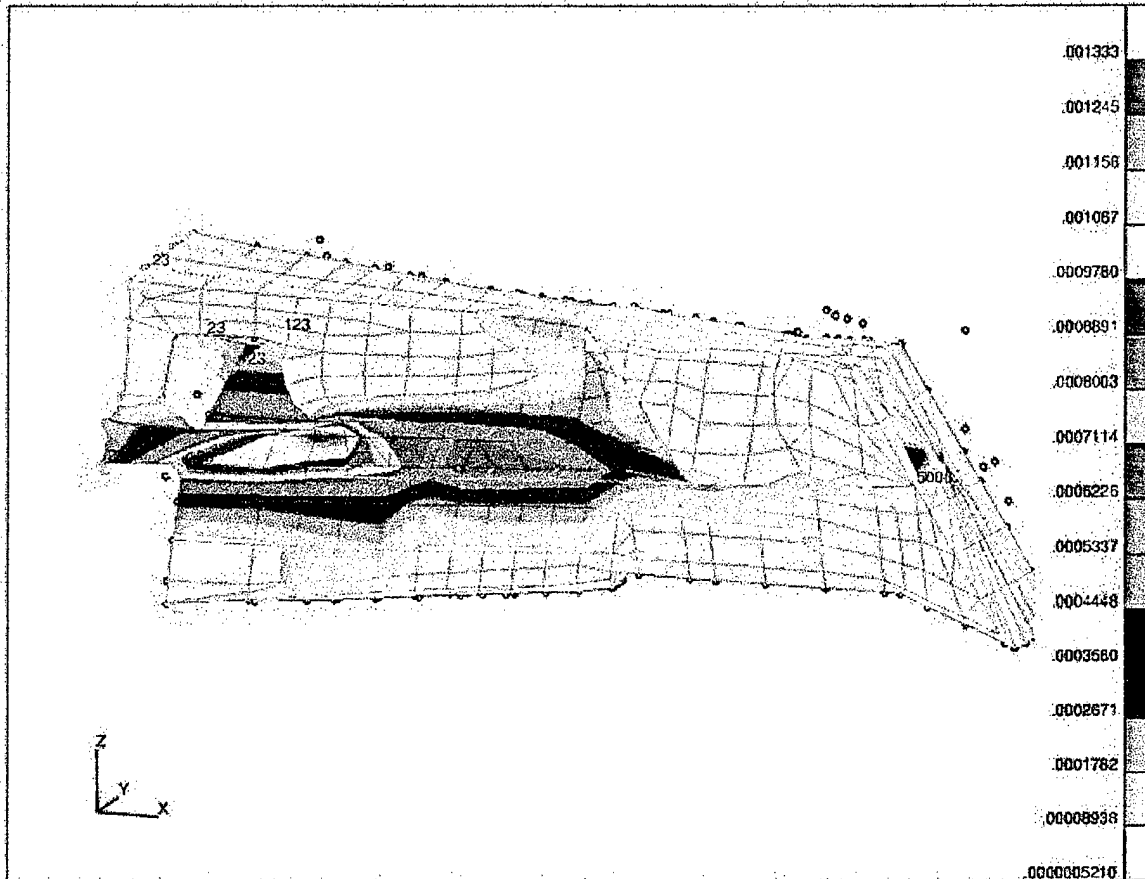


Figure 18: Horizontal Strain Energy Density Fringe of Baseline Model

Notice that on the strain energy density plots, the largest values tend to occur from the forces arising due to the imposition of the cantilevering boundary conditions. For the actual aircraft, or the full aircraft NASTRAN model, these forces would likely not arise. Therefore, high strain energy density areas in the vicinity of the boundary

condition nodes should not be targets, necessarily, for structural stiffening based on these results.

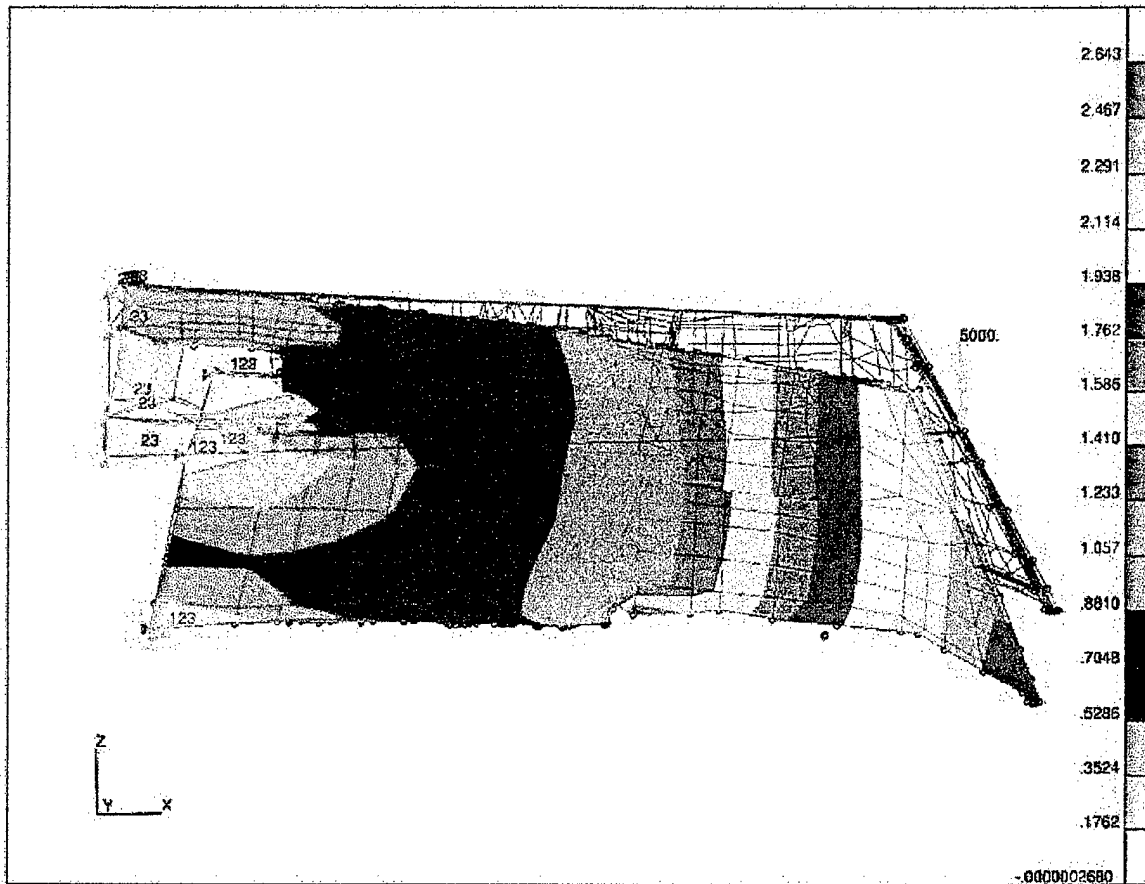


Figure 19: Vertical Displacement of Baseline Model

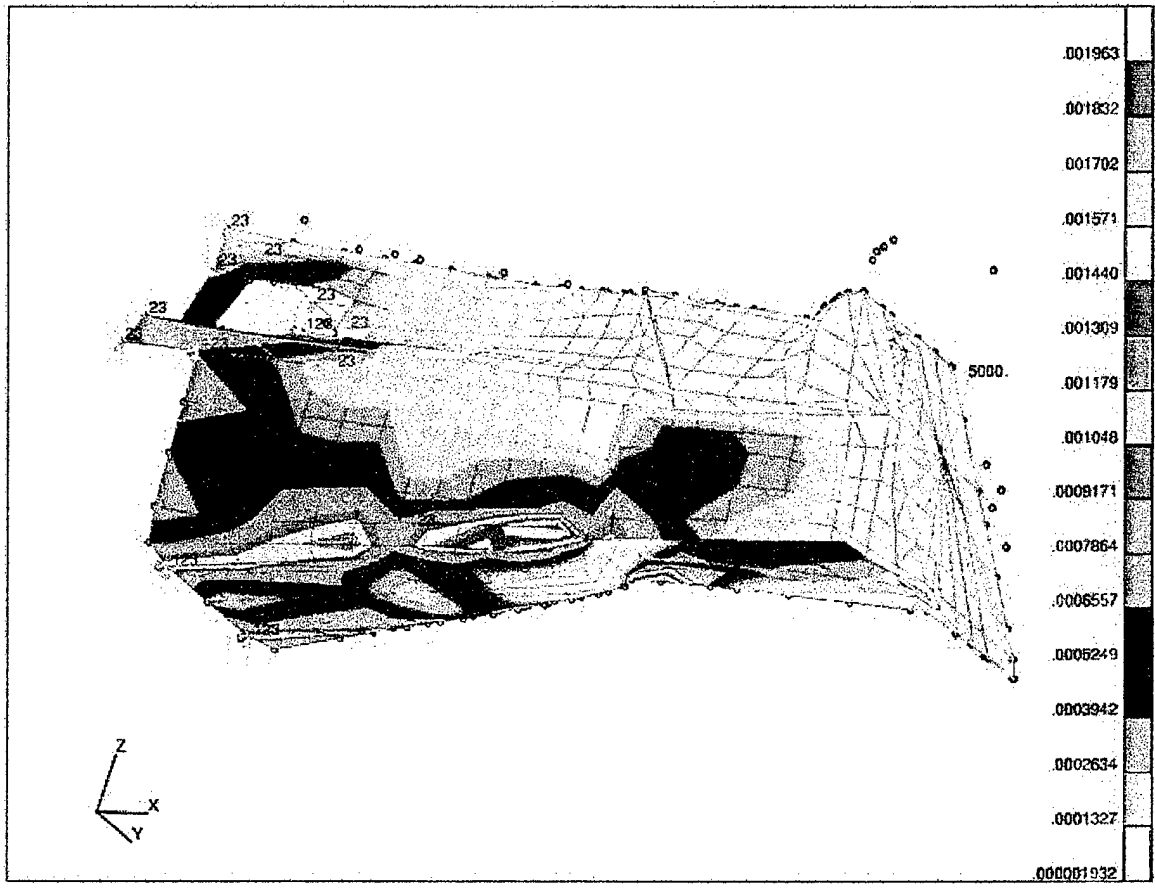


Figure 20: Vertical Strain Energy Density Fringe of Baseline Model

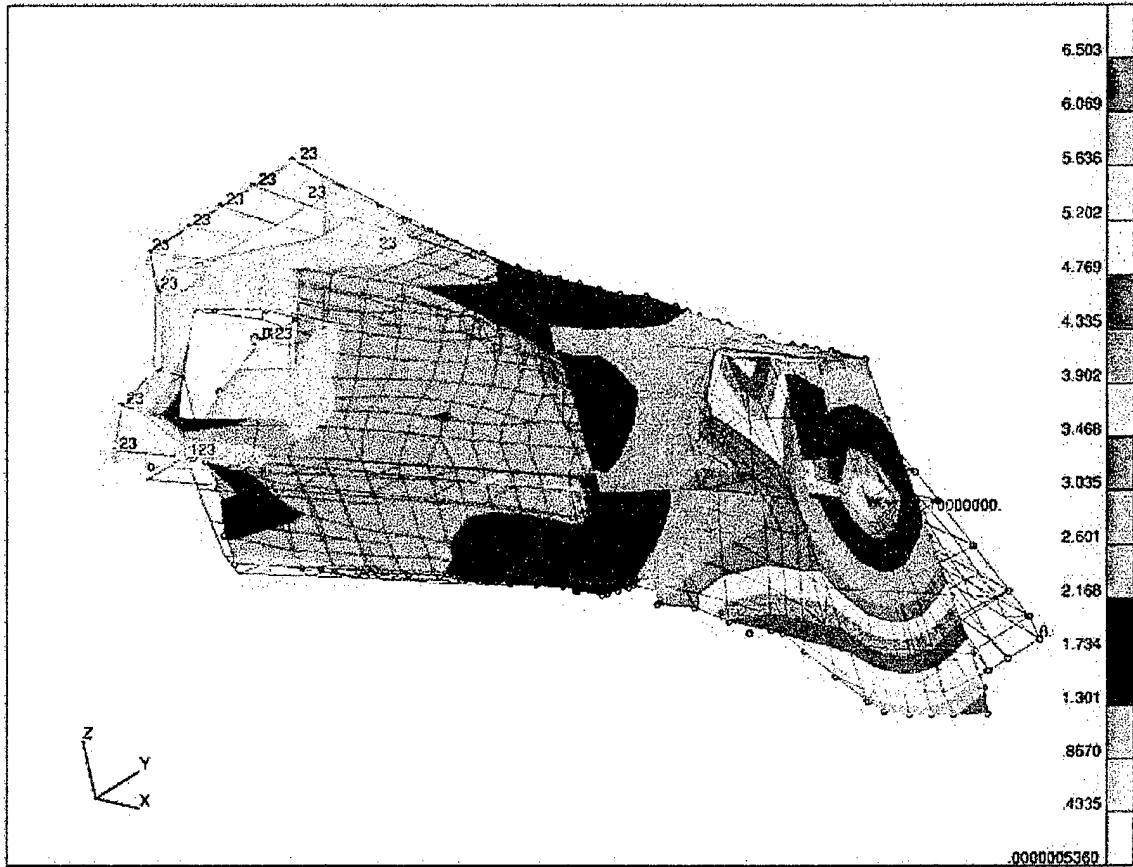


Figure 21: Torsion Displacement of Base-Kevlar Model

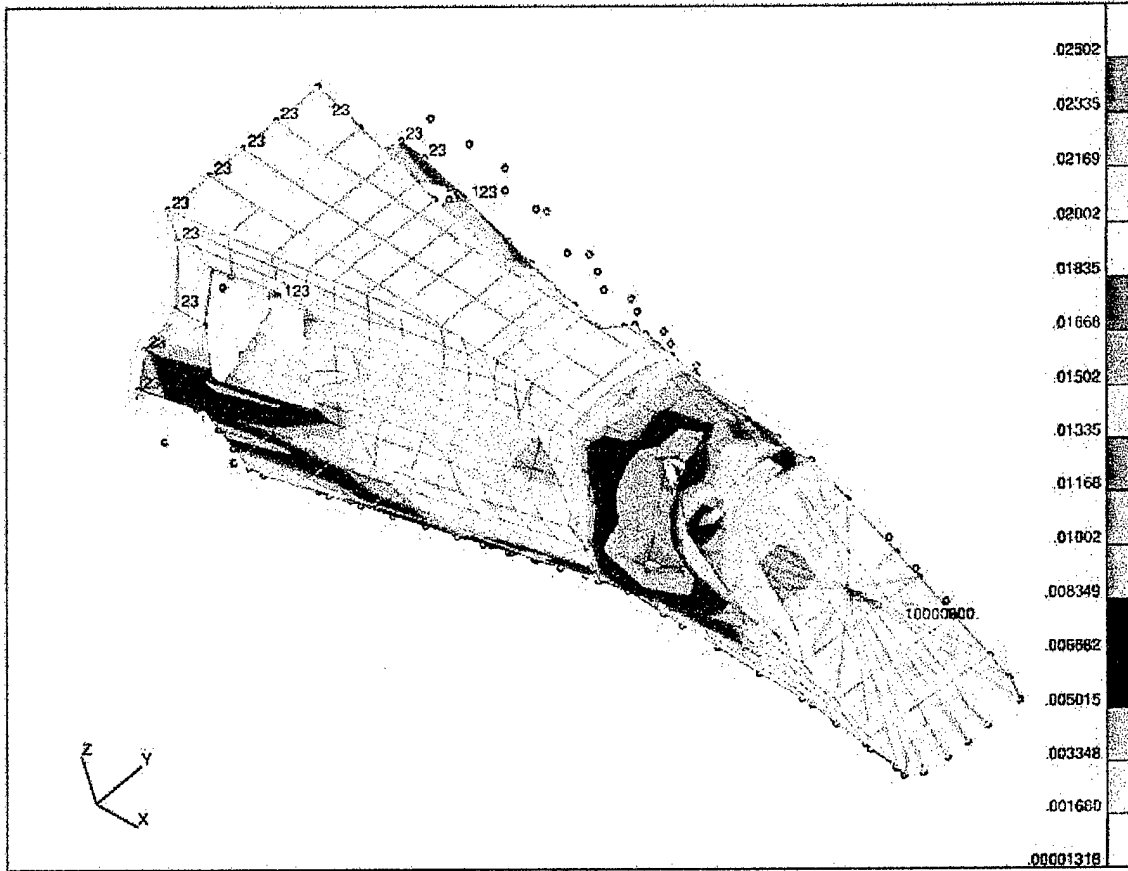


Figure 22: Torsion Strain Energy Density Fringe of Base-Kevlar Model

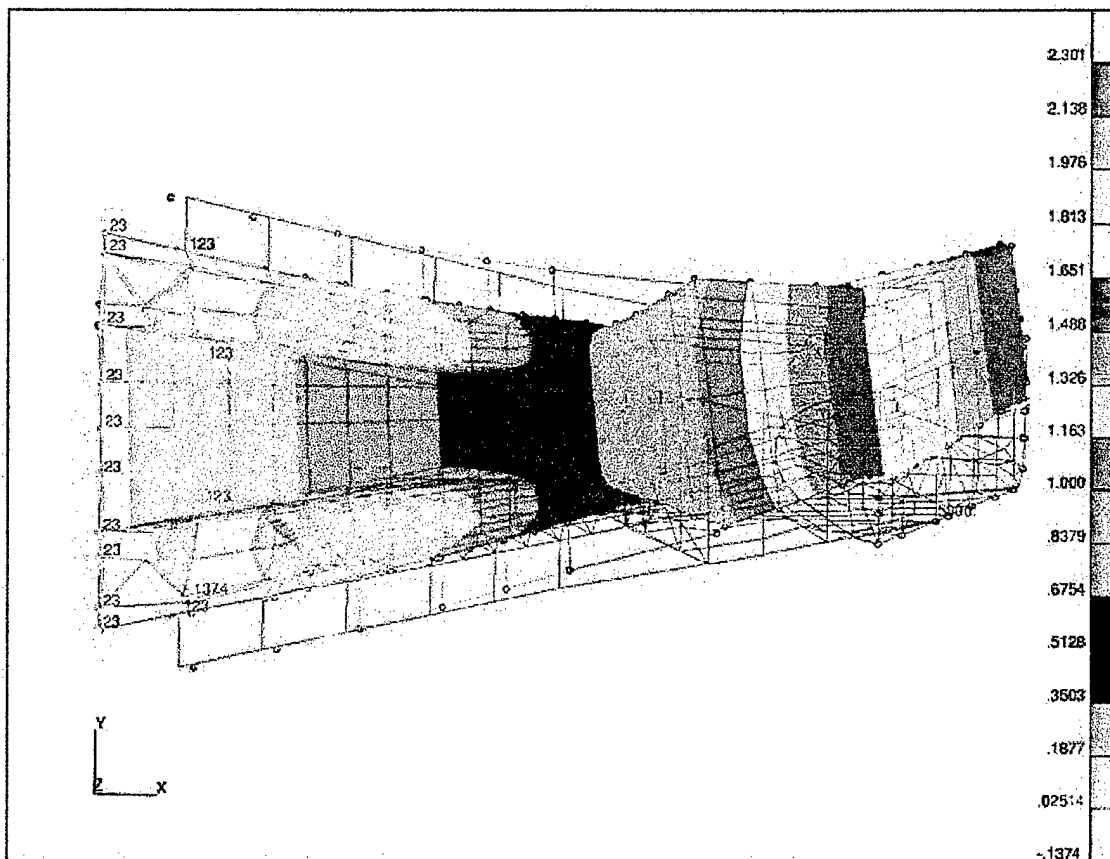


Figure 23: Horizontal Displacement of Base-Kevlar Model

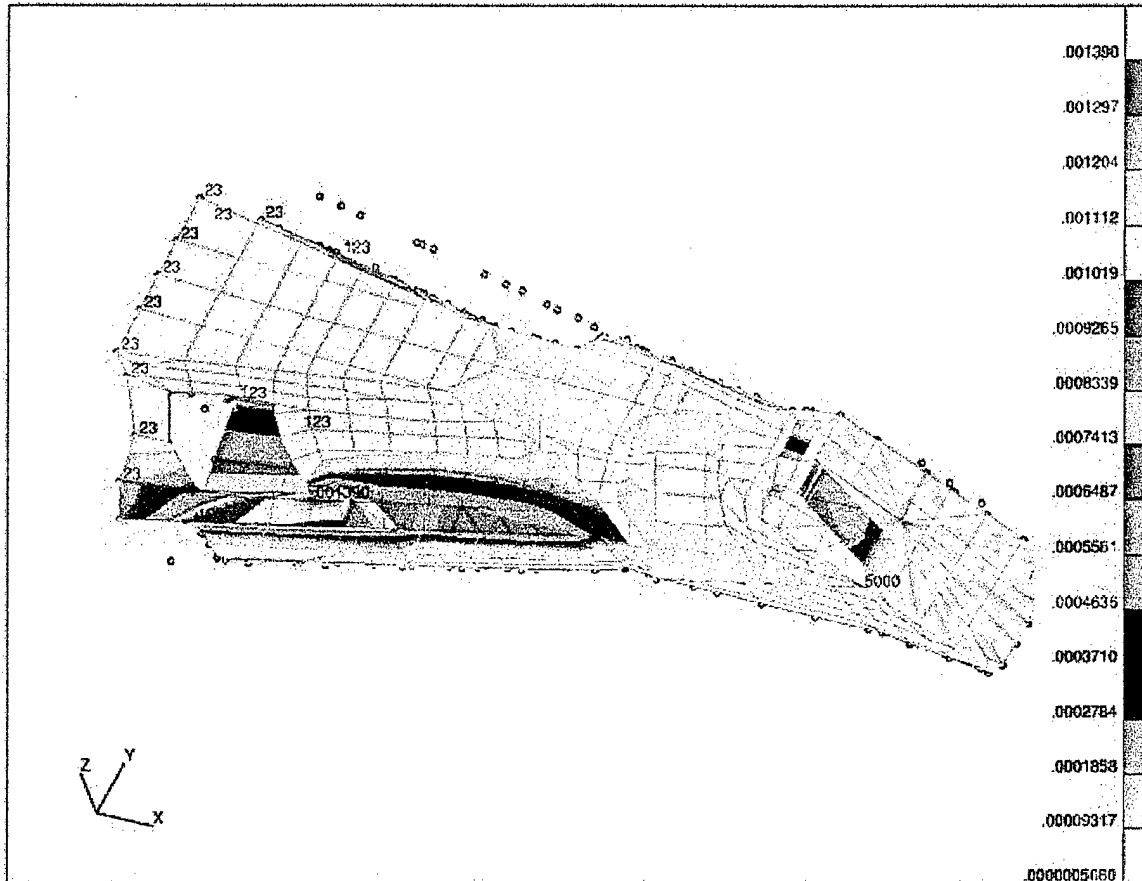


Figure 24: Horizontal Strain Energy Density Fringe of Base-Kevlar Model

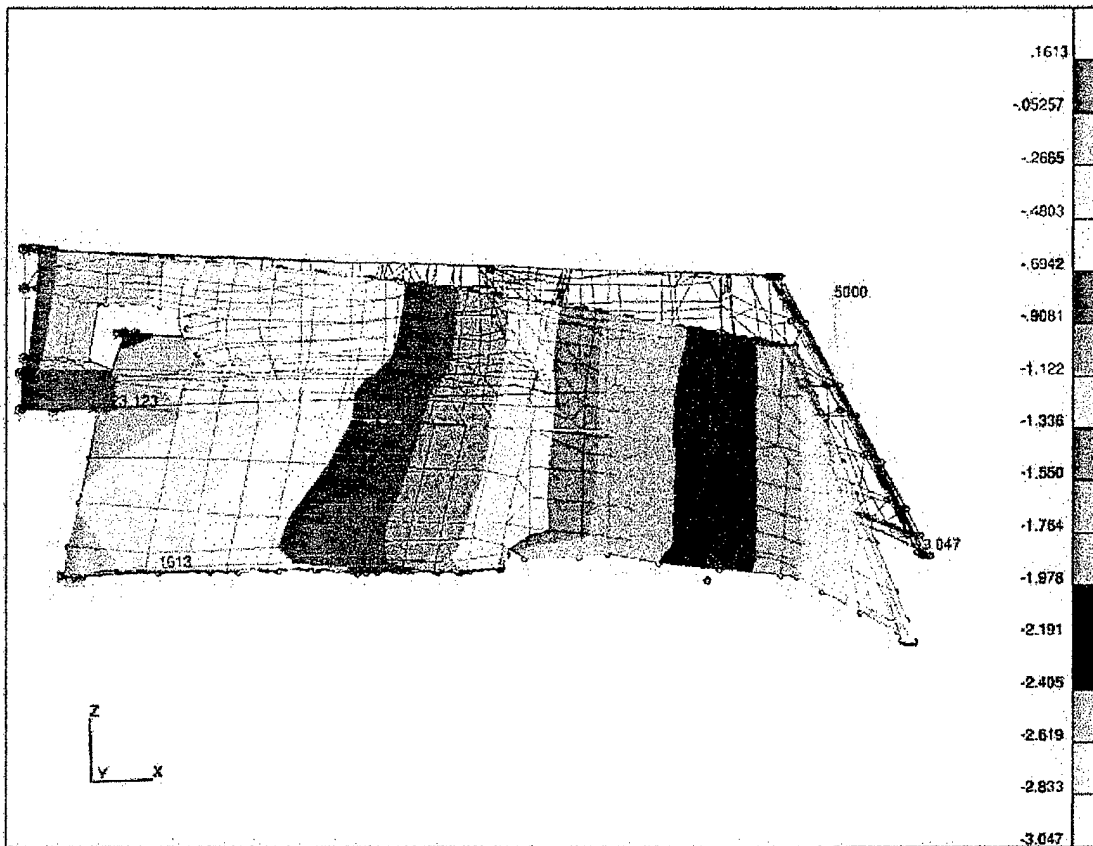


Figure 25: Vertical Displacement of Base-Kevlar Model

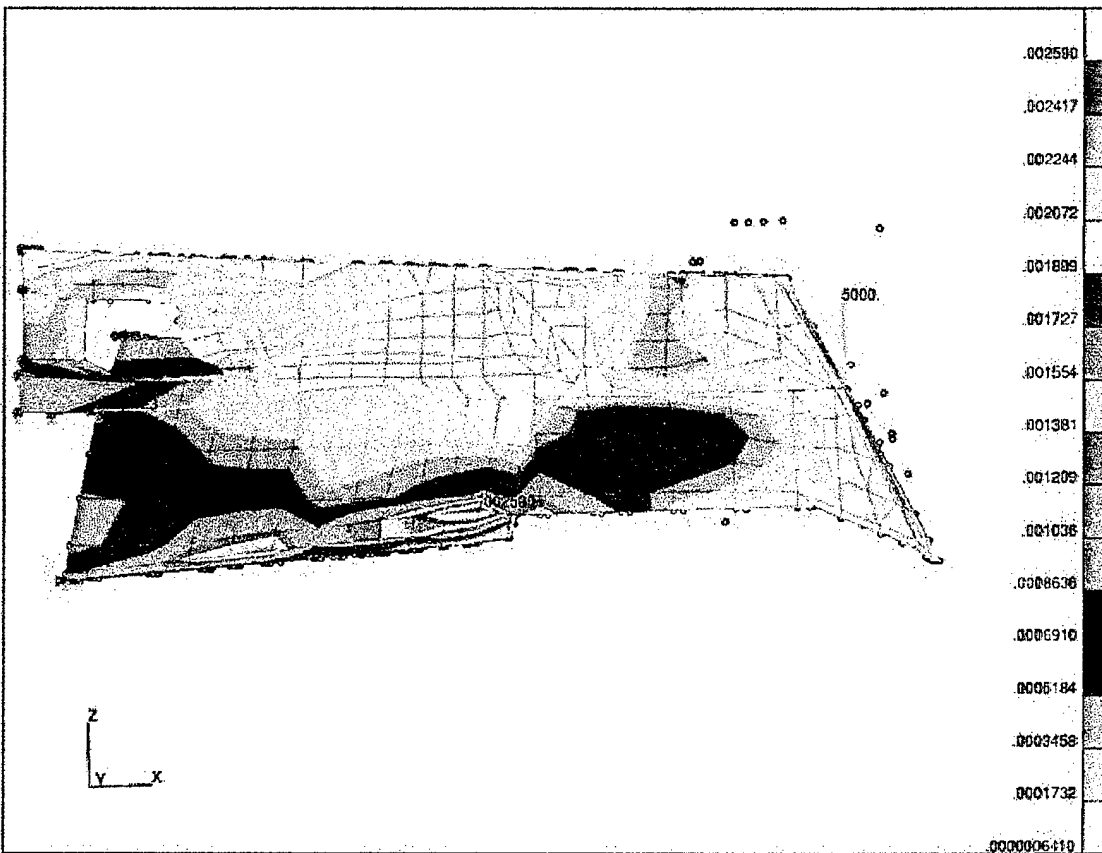


Figure 26: Vertical Strain Energy Density Fringe of Base-Kevlar Model

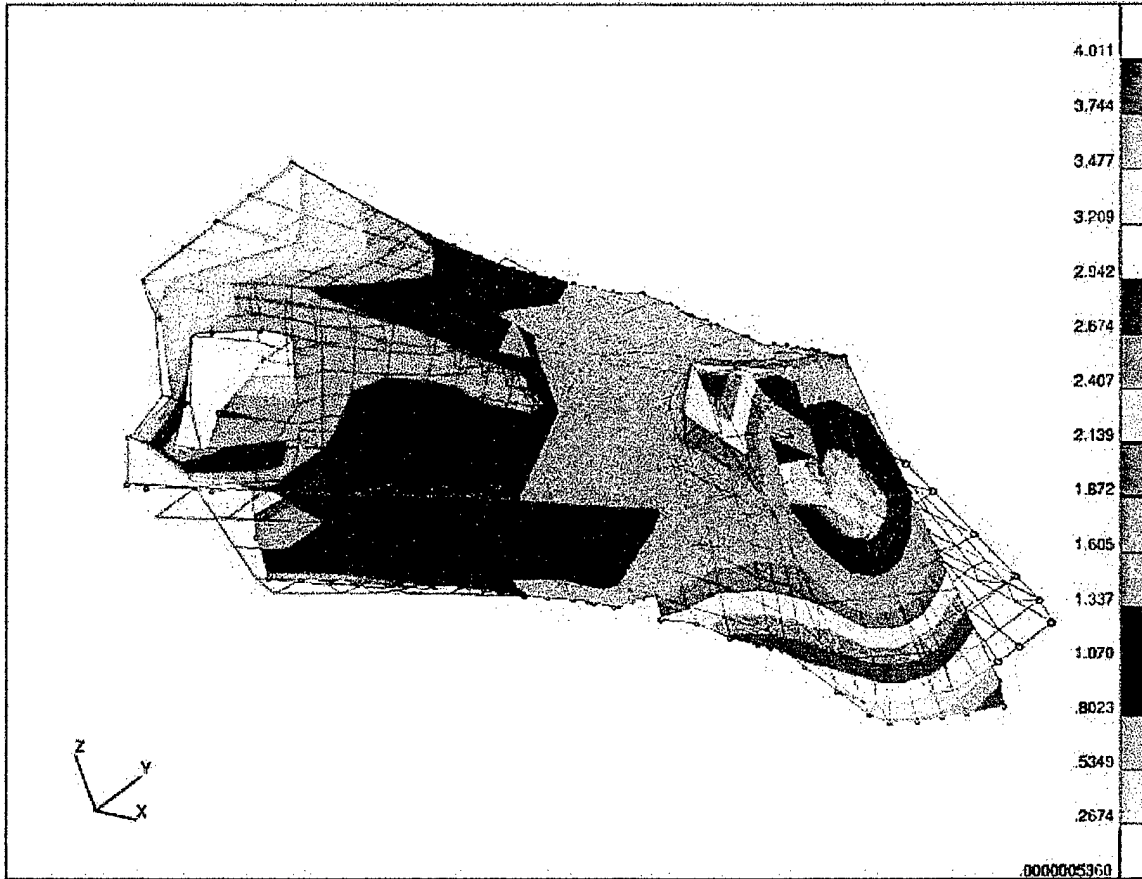


Figure 27: Torsion Displacement of Bulk-Mod Model

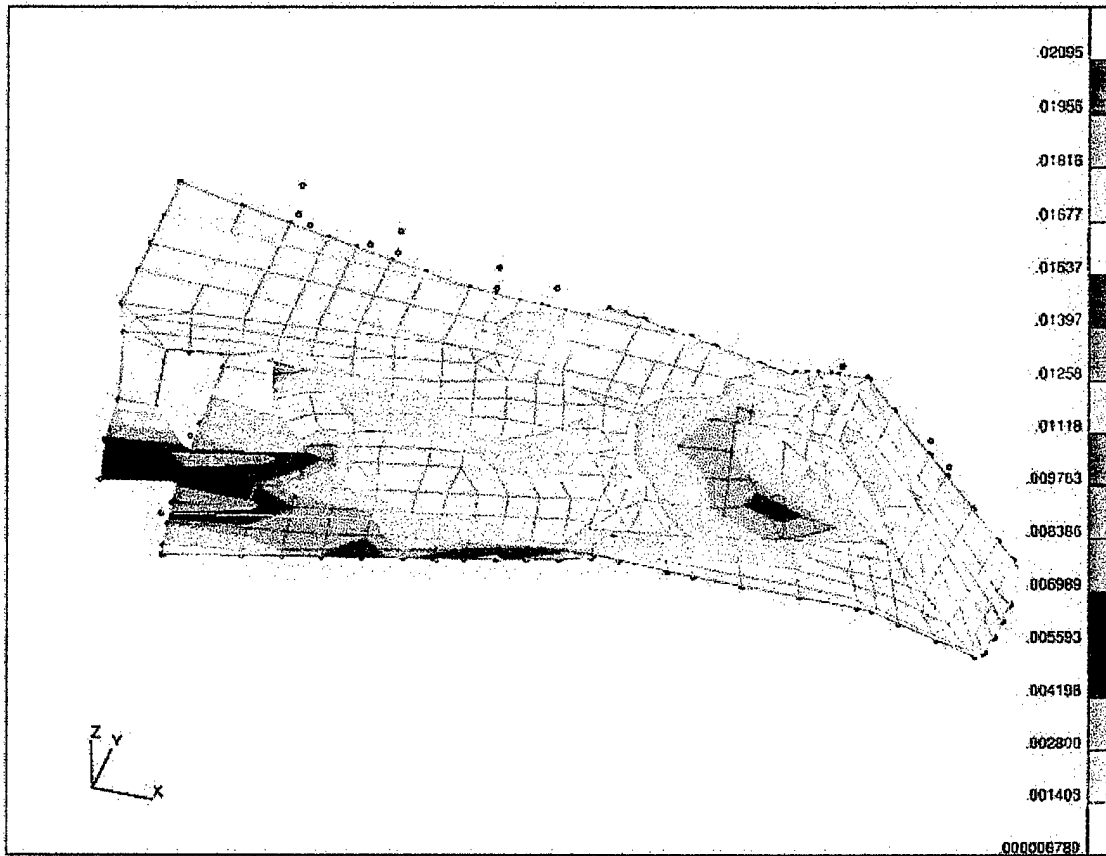


Figure 28: Torsion Strain Energy Density Fringe of Bulk-Mod Model

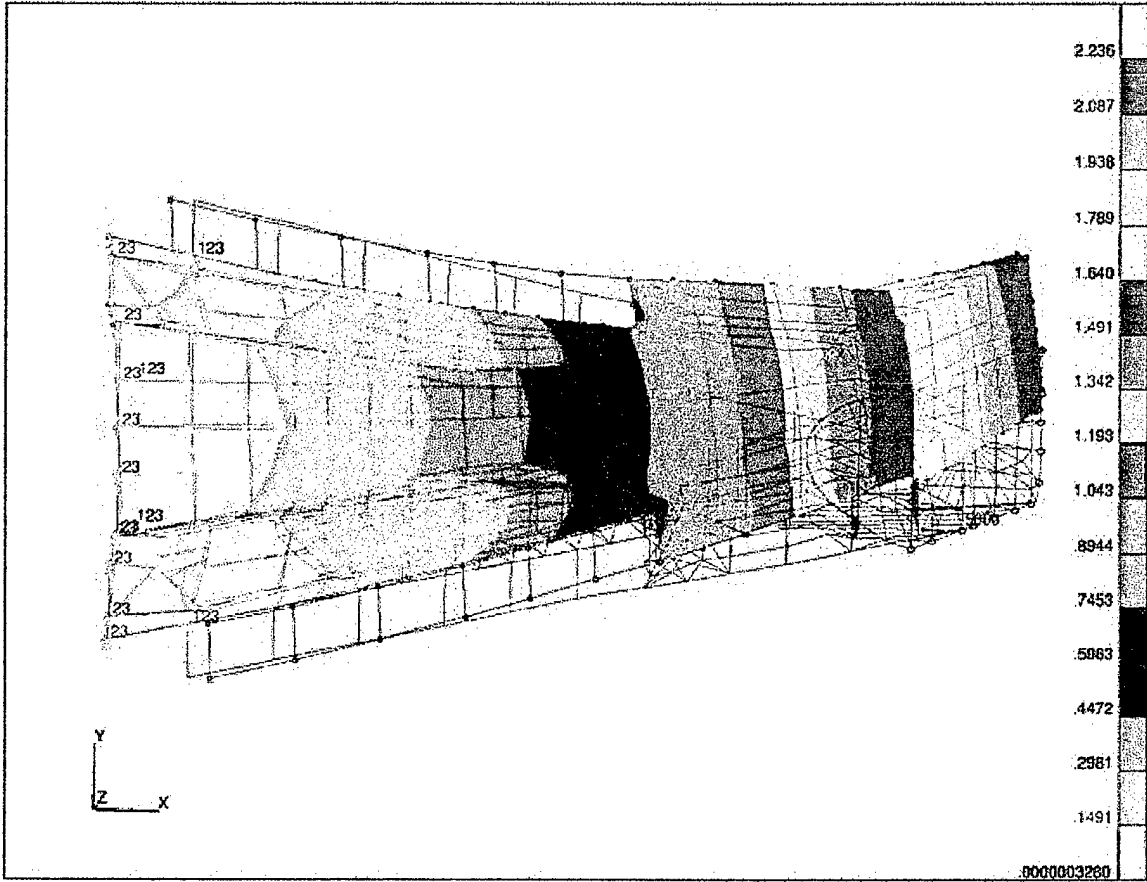


Figure 29: Horizontal Displacement of Bulk-Mod Model

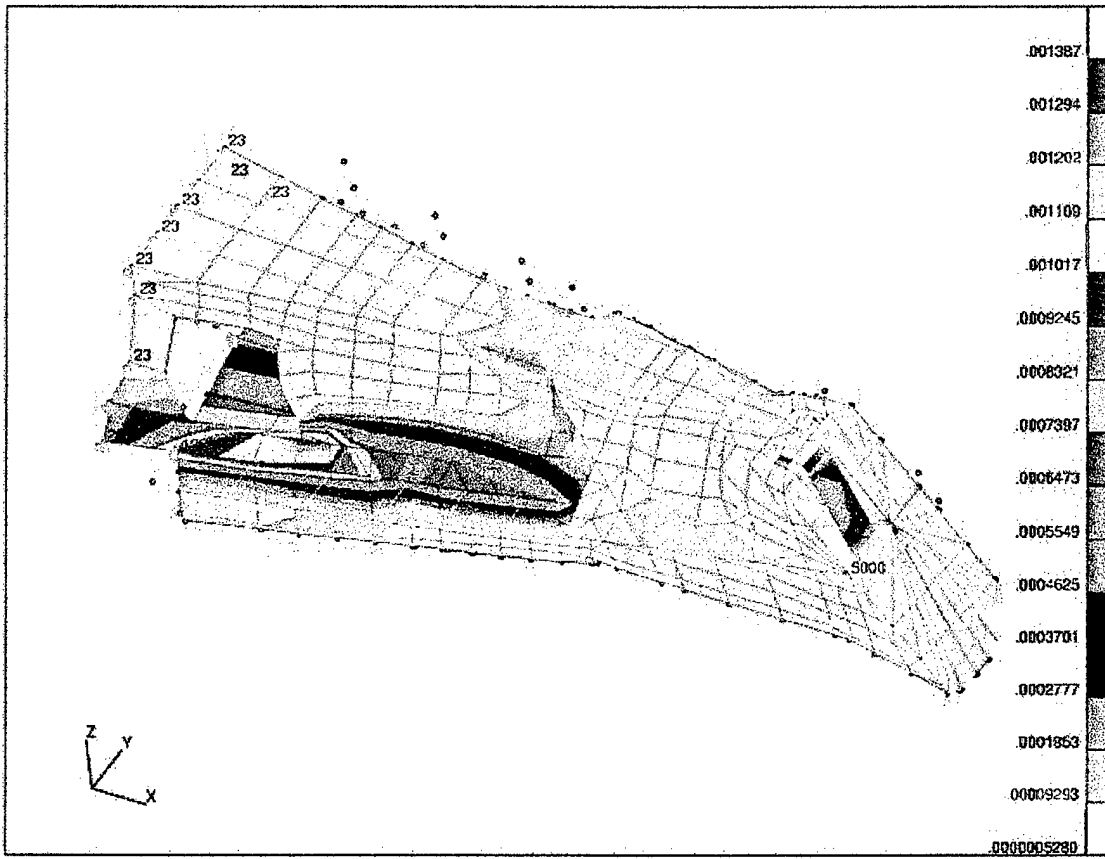


Figure 30: Horizontal Strain Energy Density Fringe of Bulk-Mod Model

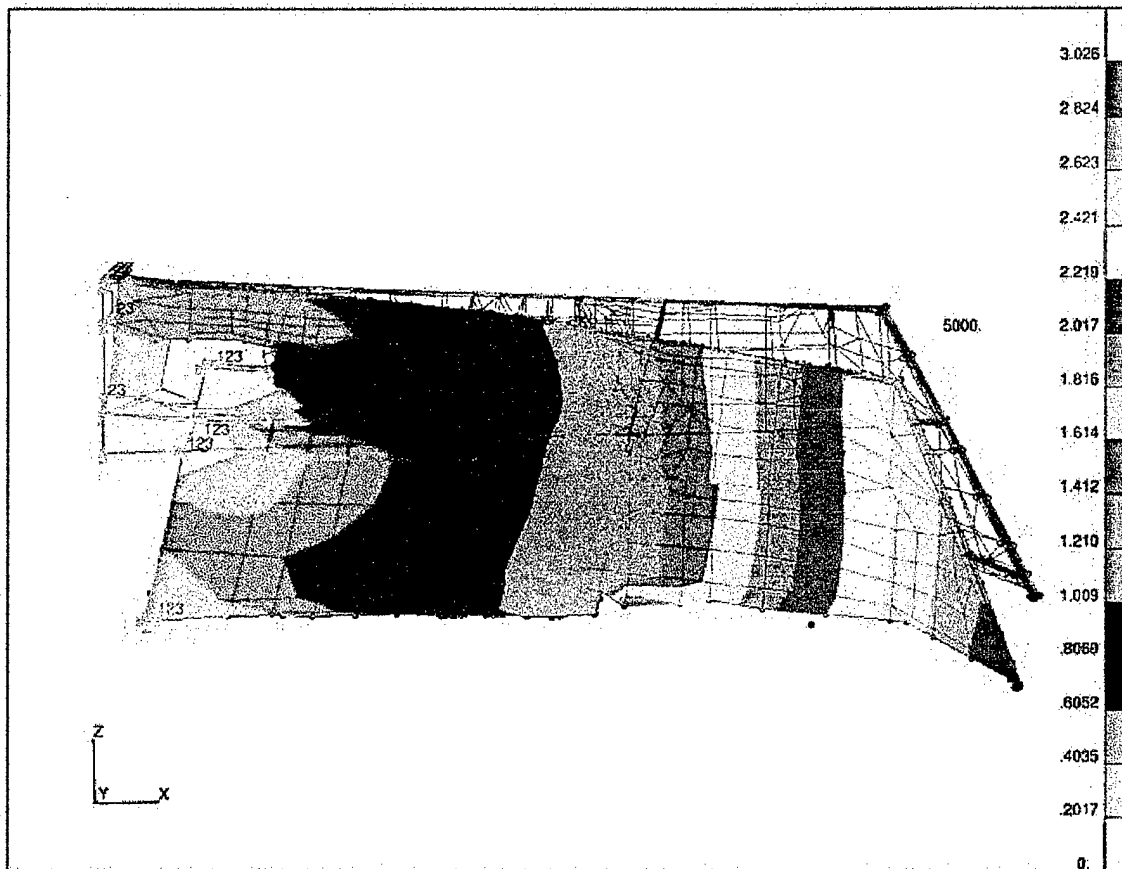


Figure 31: Vertical Displacement of Bulk-Mod Model

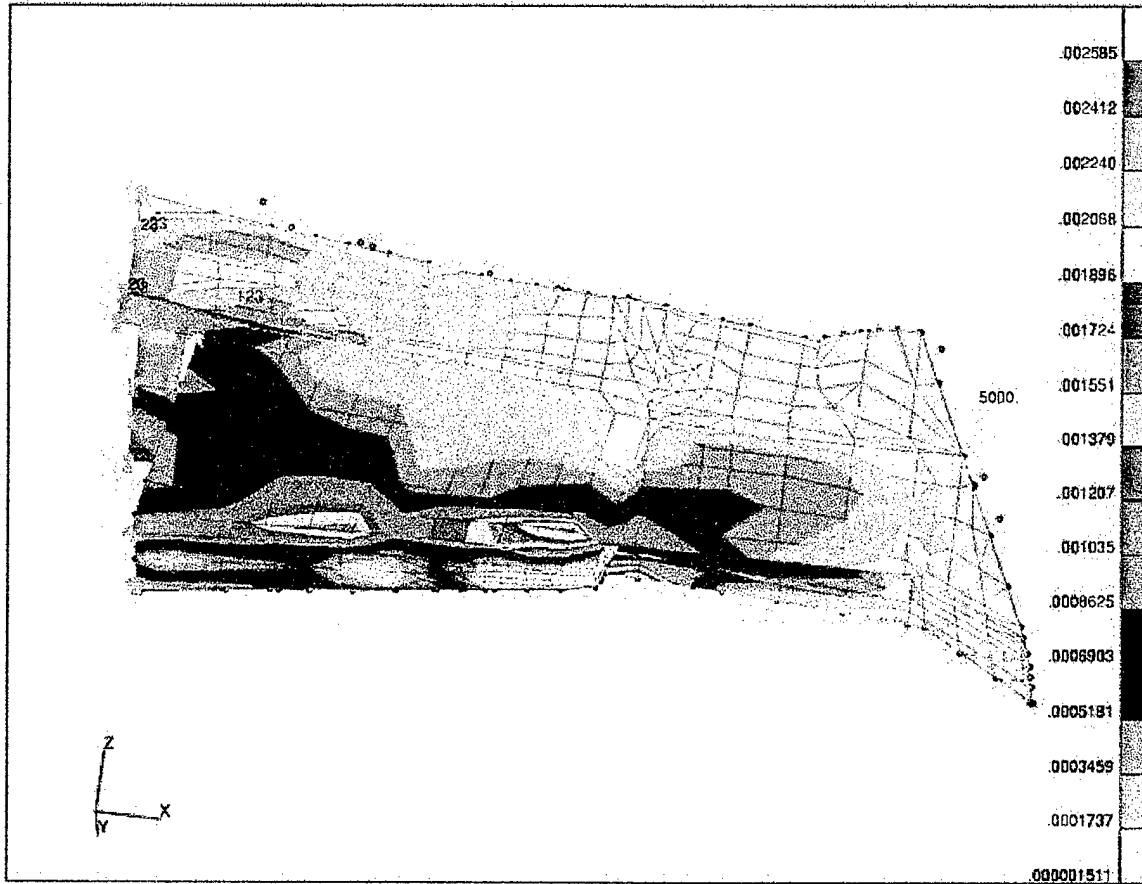


Figure 32: Vertical Strain Energy Density Fringe of Bulk-Mod Model

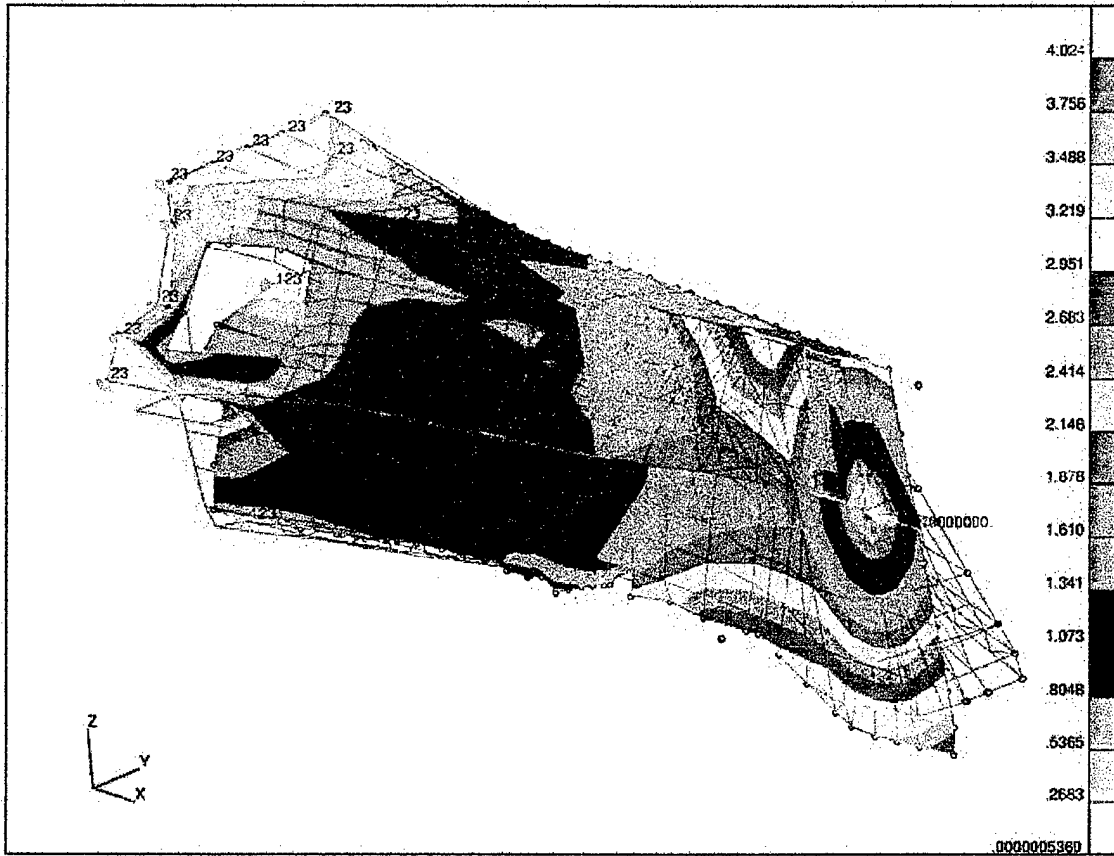


Figure 33: Torsion Displacement of Cone-Mod Model

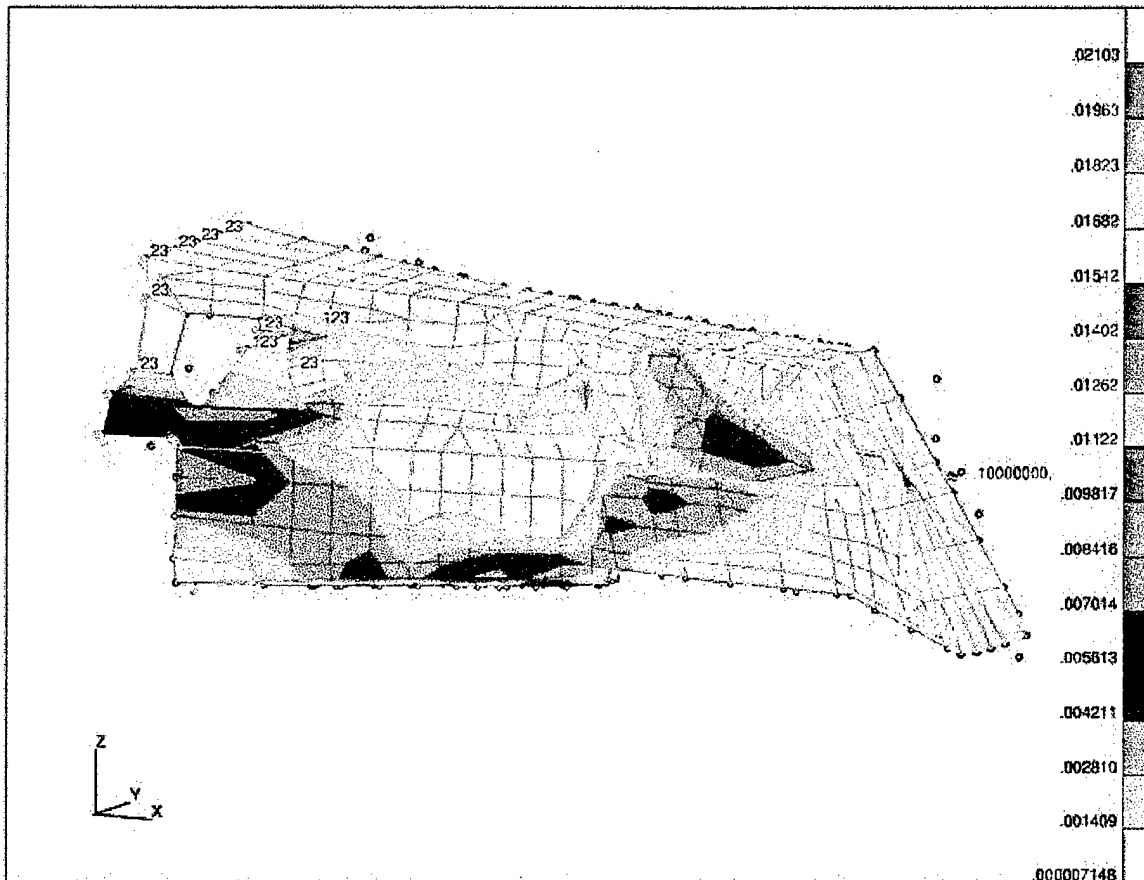


Figure 34: Torsion Strain Energy Density Fringe of Cone-Mod Model

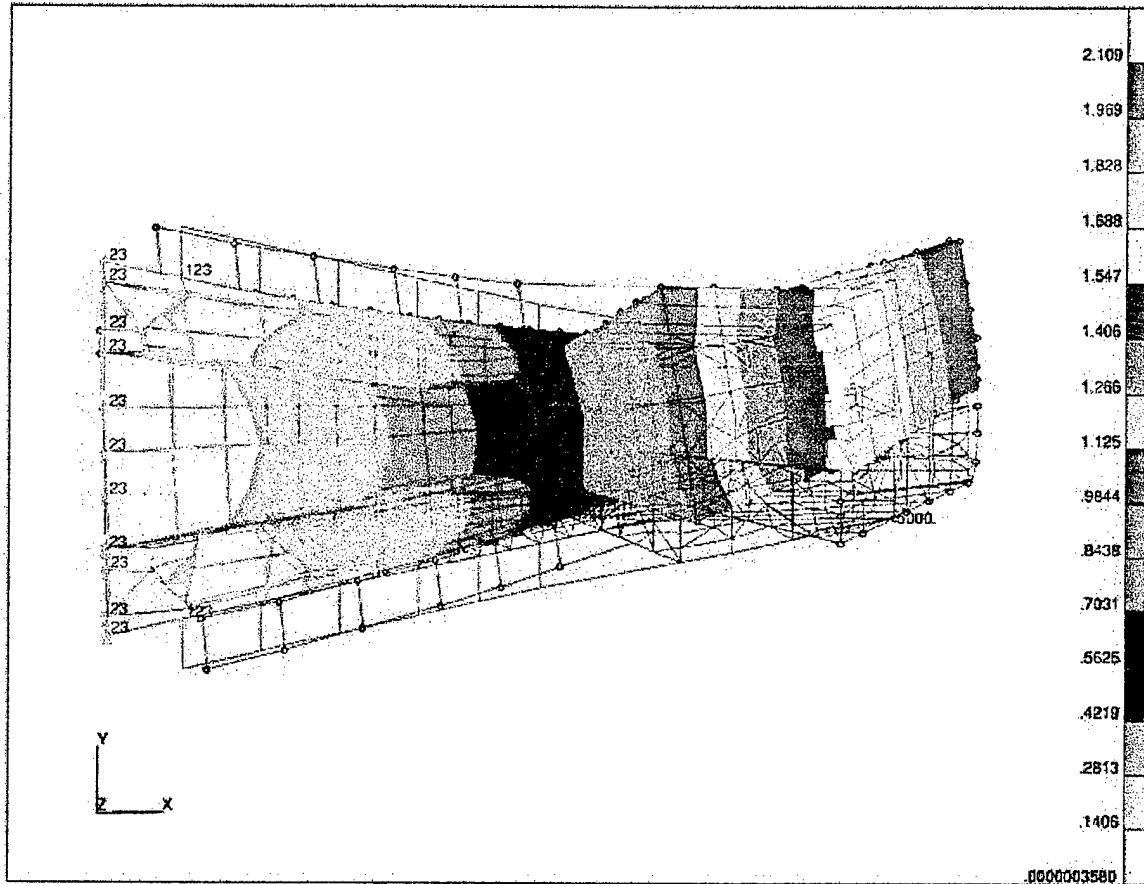


Figure 35: Horizontal Displacement of Cone-Mod Model

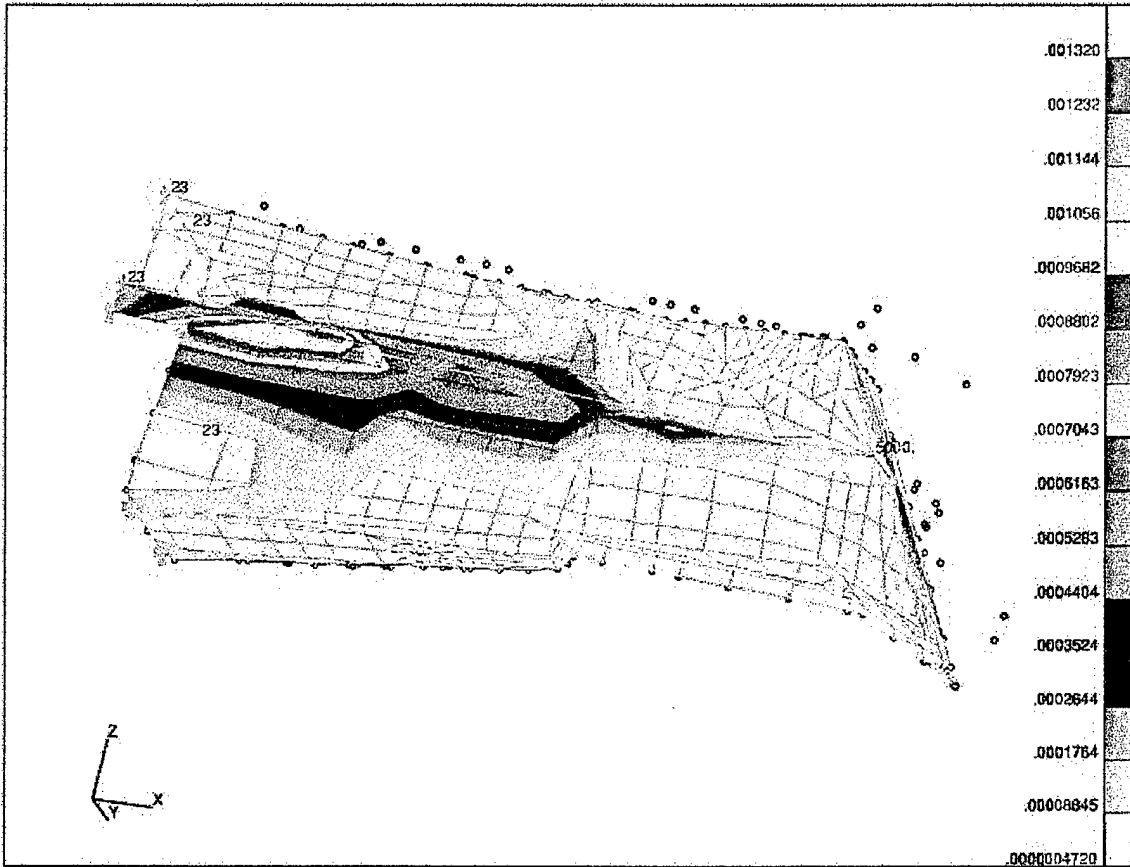


Figure 36: Horizontal Strain Energy Density Fringe of Cone-Mod Model

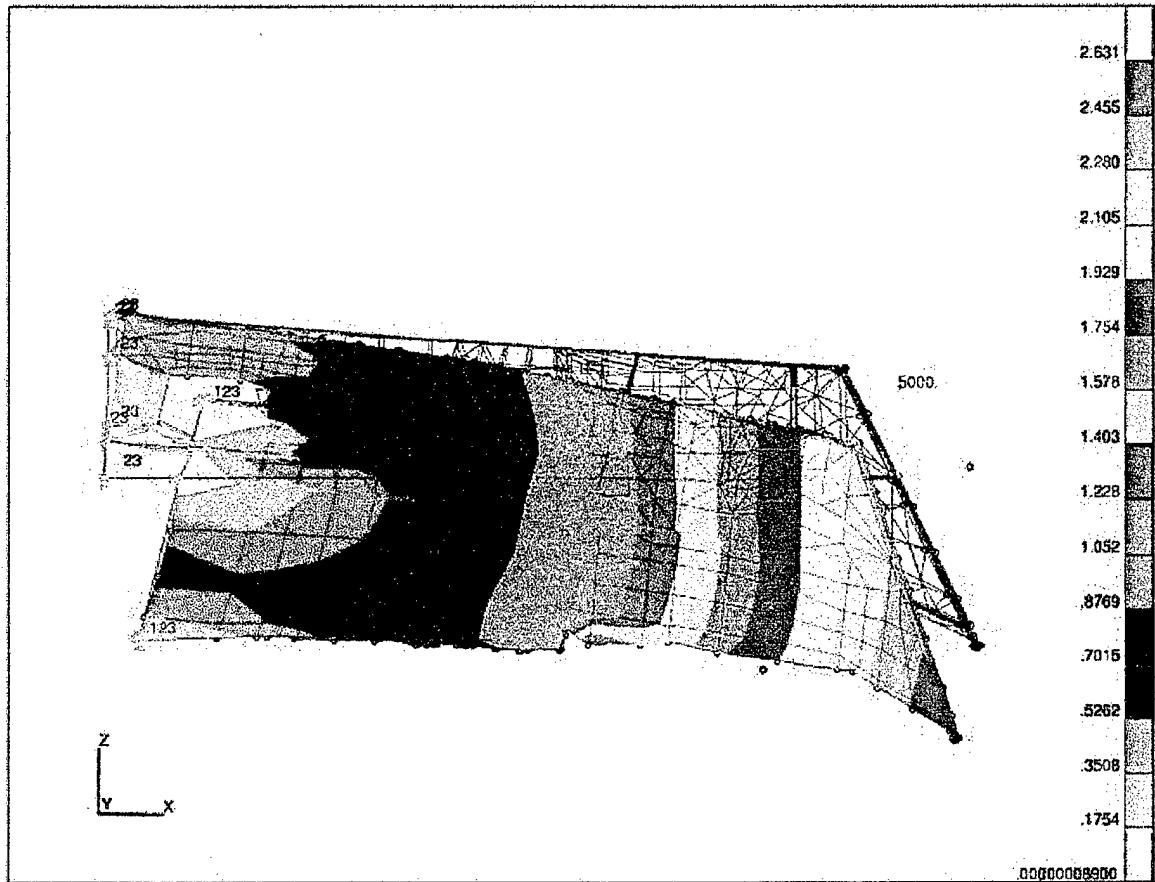


Figure 37: Vertical Displacement of Cone-Mod Model

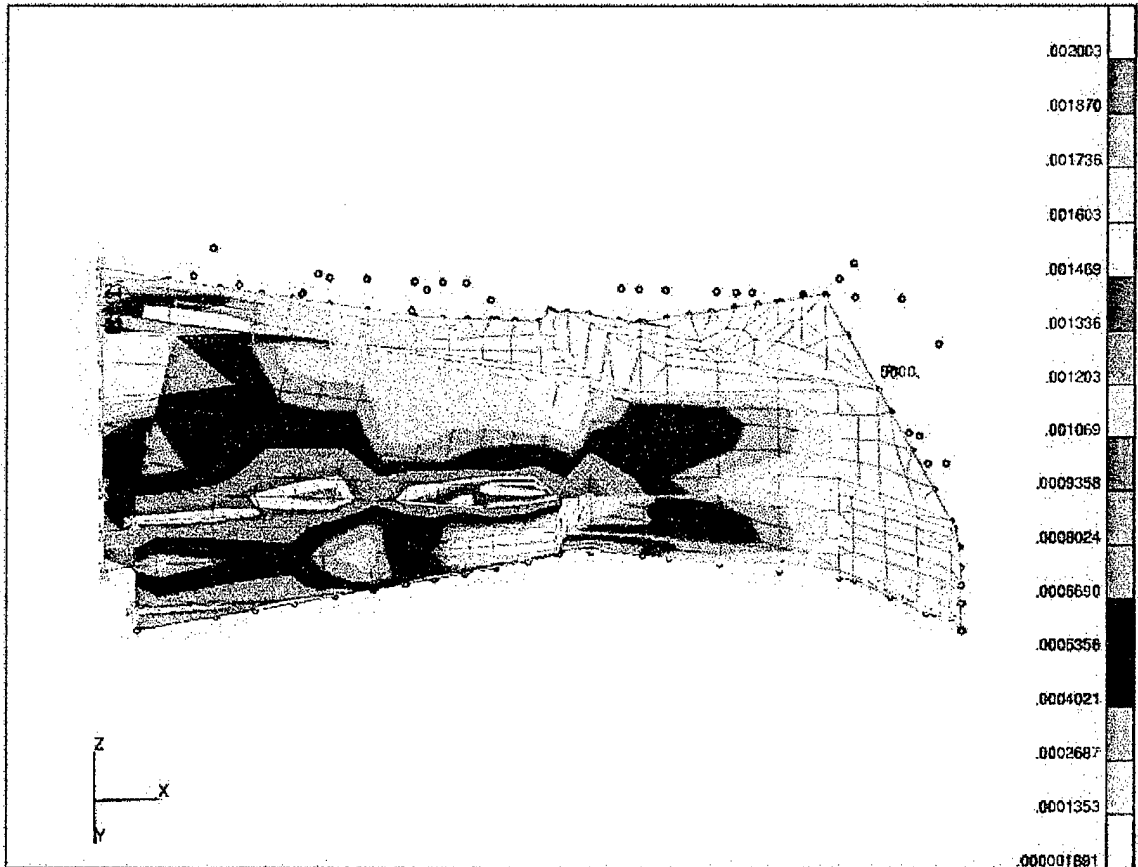


Figure 38: Vertical Strain Energy Density Fringe of Cone-Mod Model

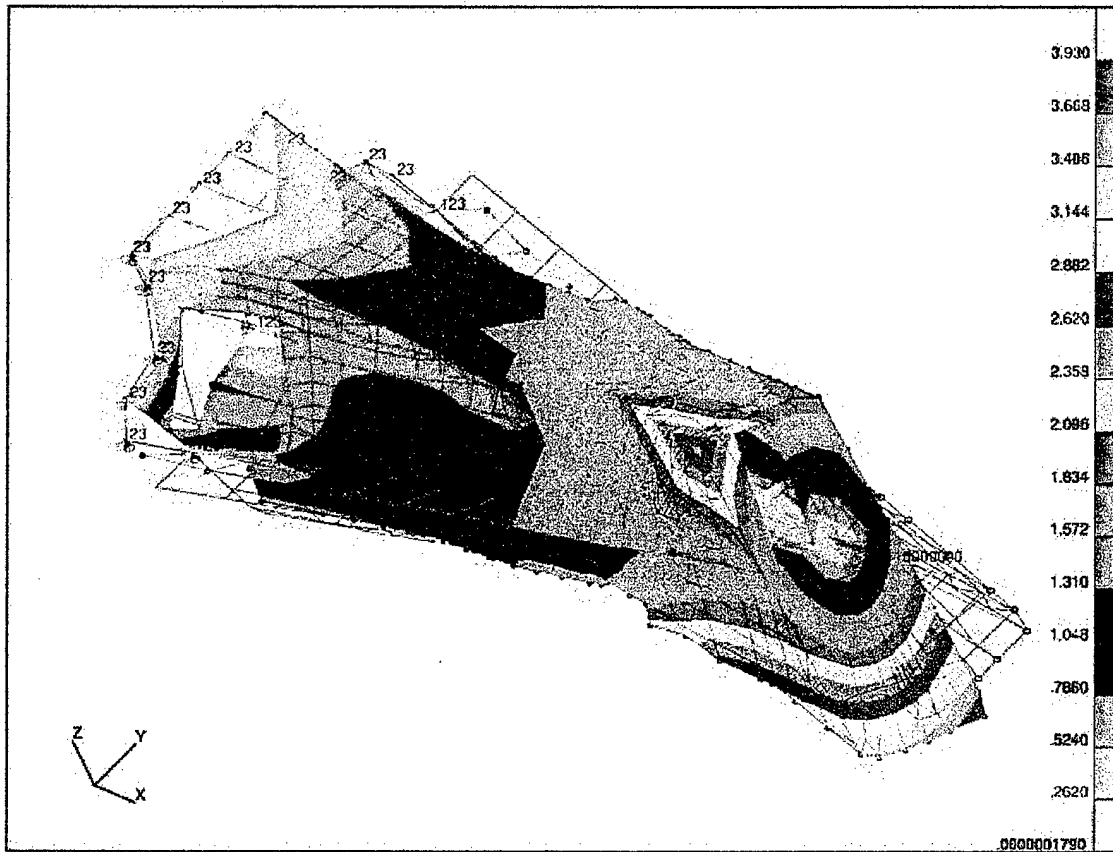


Figure 39: Torsion Displacement of Full-Mod Model

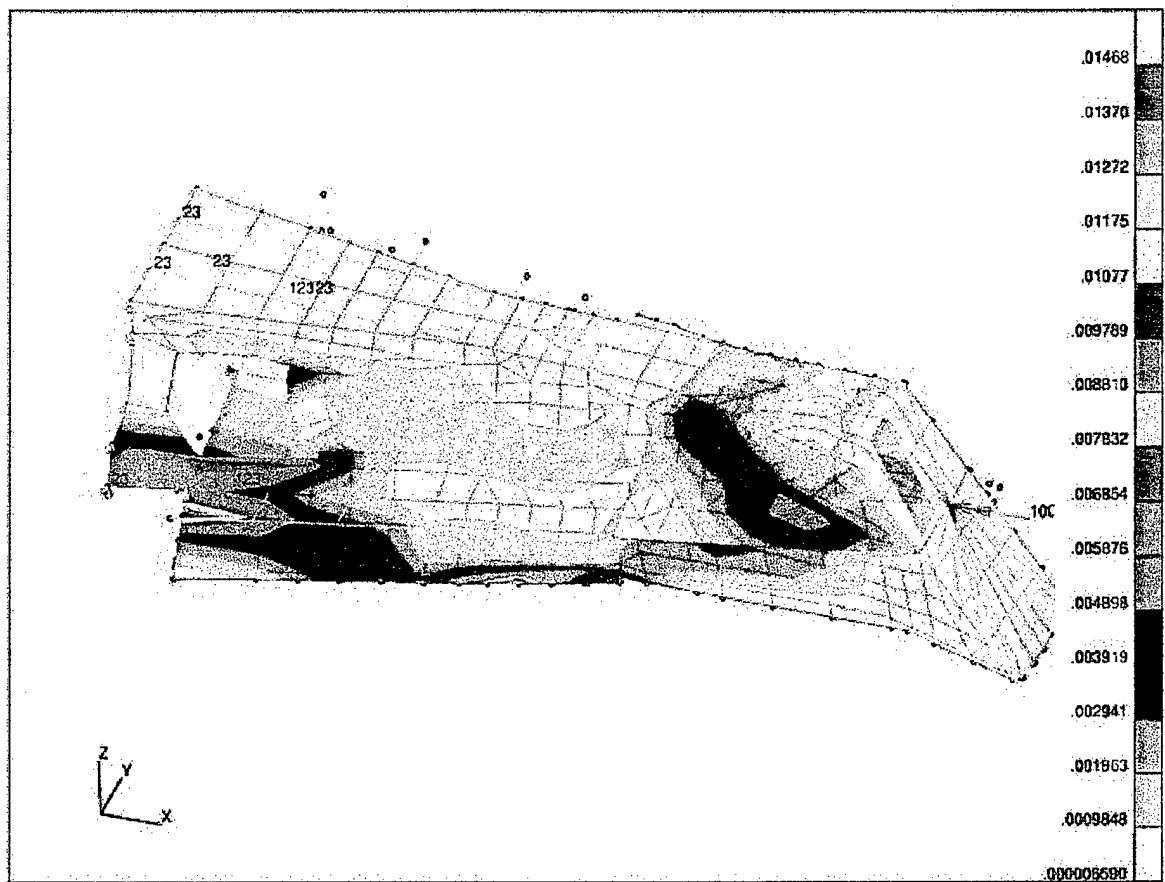


Figure 40: Torsion Strain Energy Density Fringe of Full-Mod Model

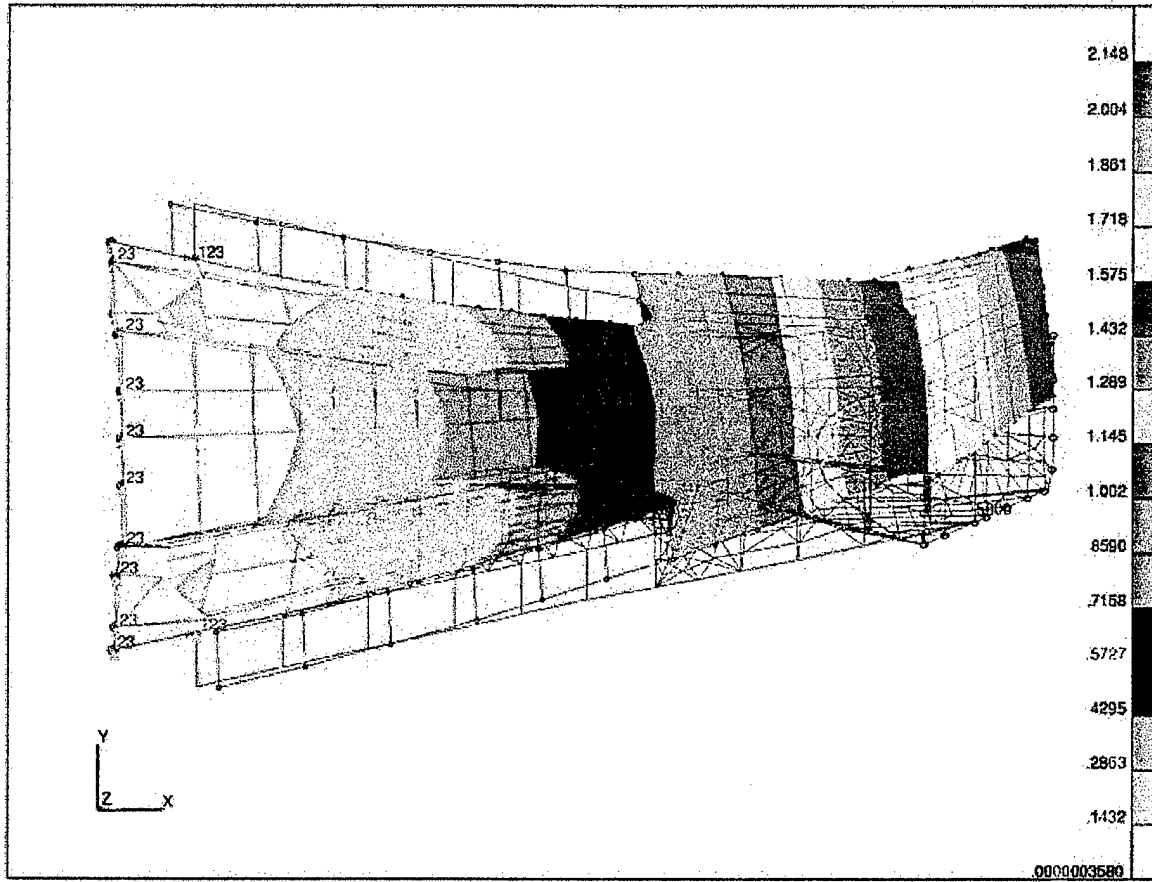


Figure 41: Horizontal Displacement of Full-Mod Model

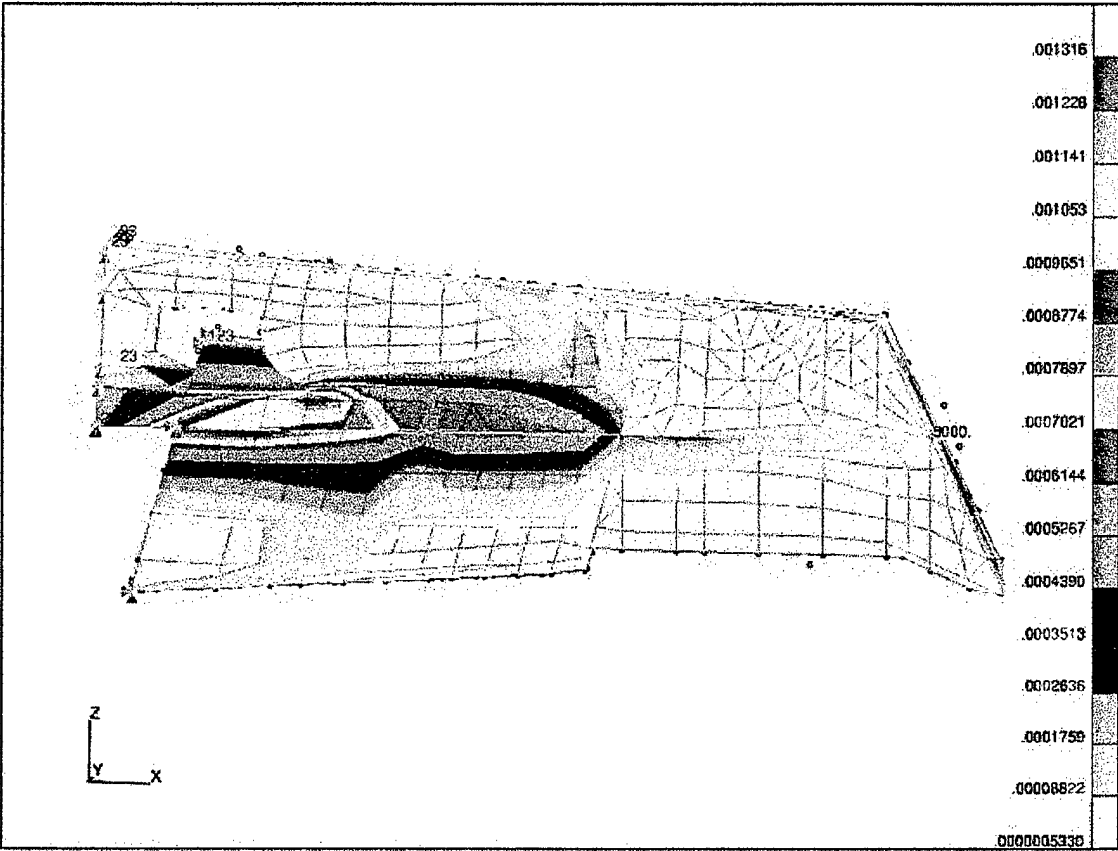


Figure 42: Horizontal Strain Energy Density Fringe of Full-Mod Model

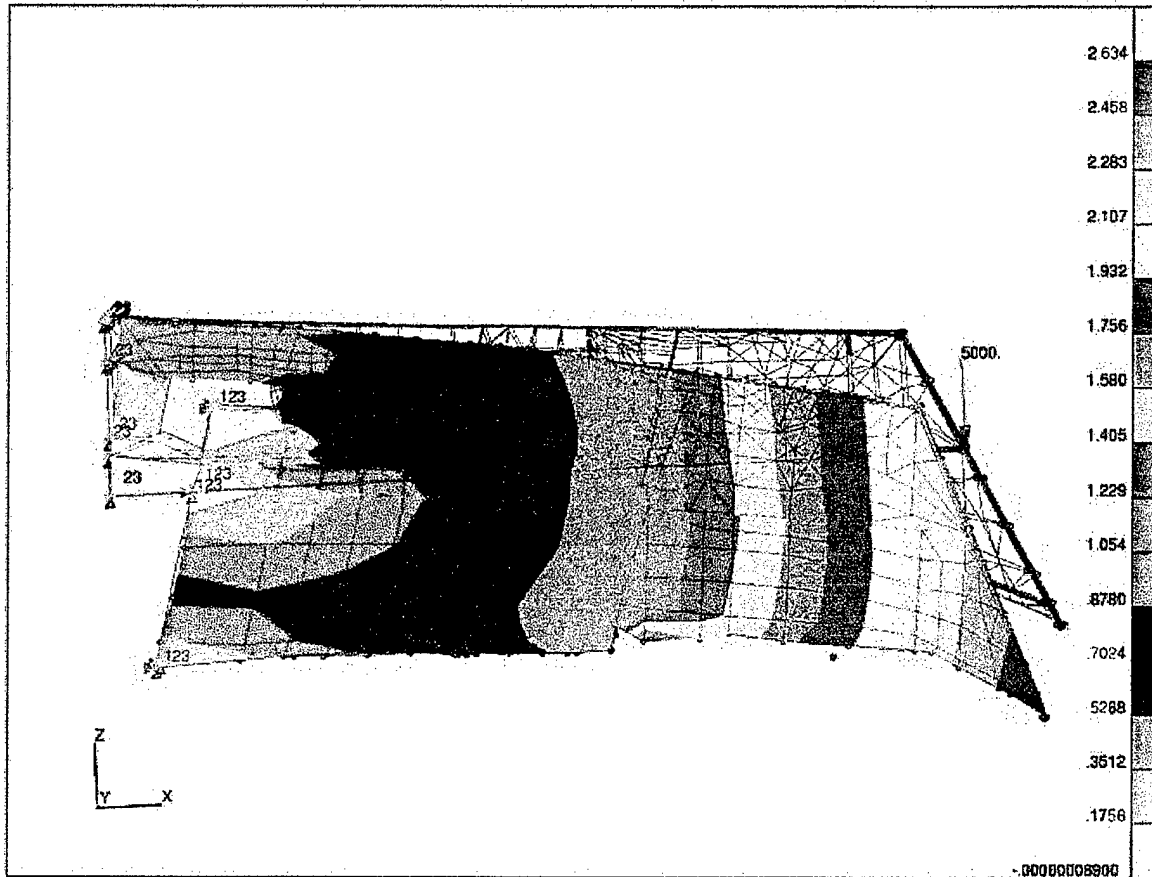


Figure 43: Vertical Displacement of Full-Mod Model

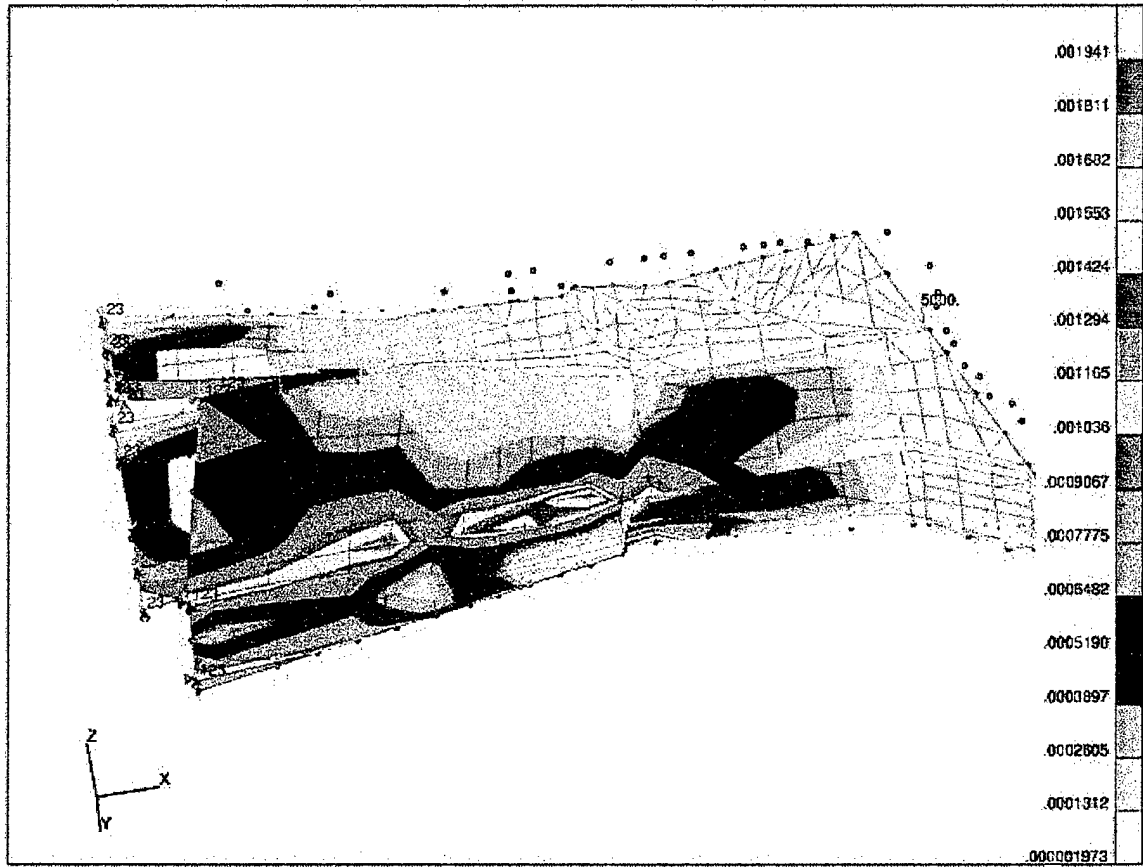


Figure 44: Vertical Strain Energy Density Fringe of Full-Mod Model

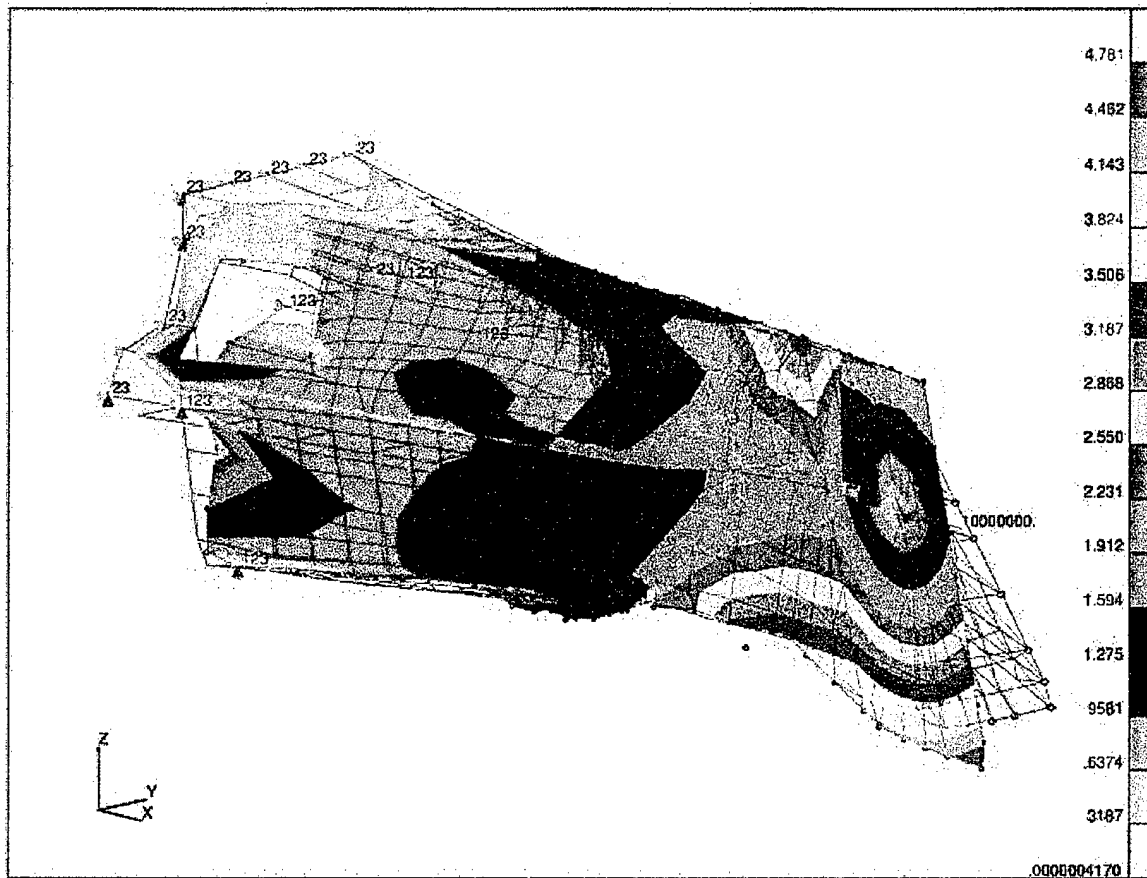


Figure 45: Torsion Displacement of Full-Kevlar Model

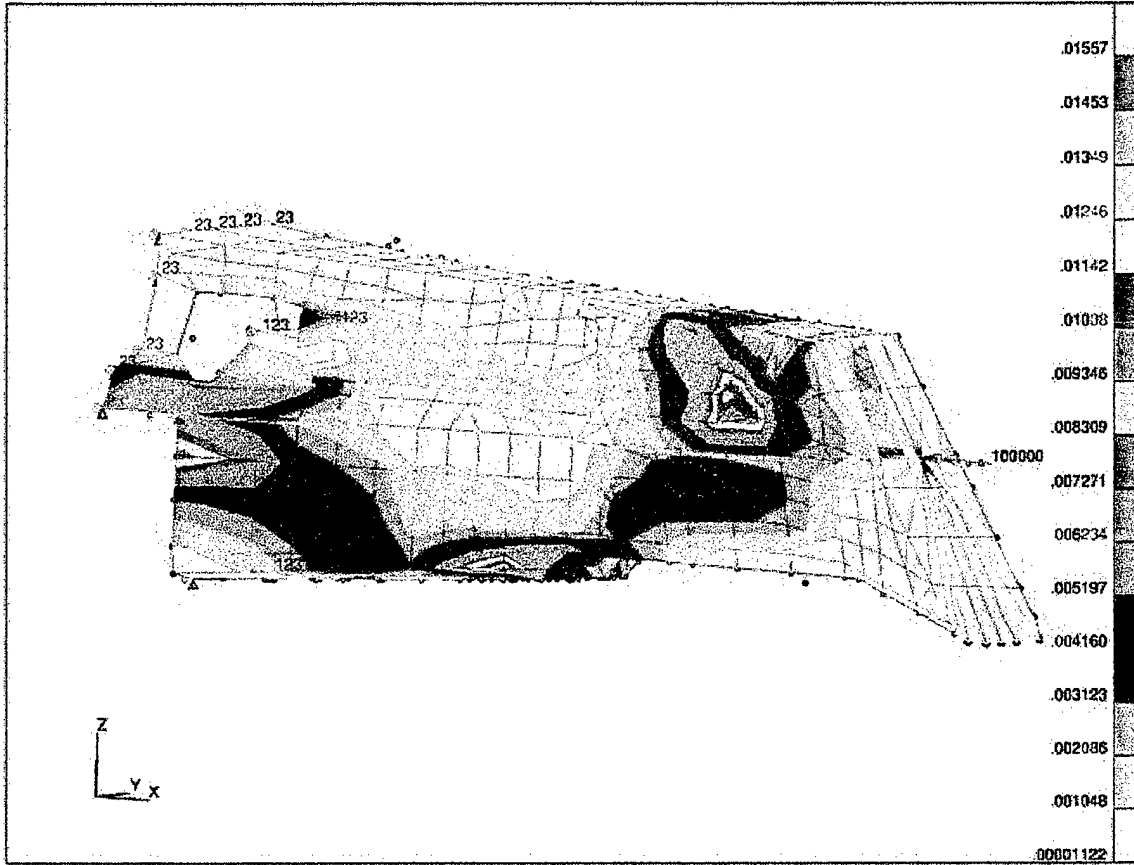


Figure 46: Torsion Strain Energy Density Fringe of Full-Kevlar Model

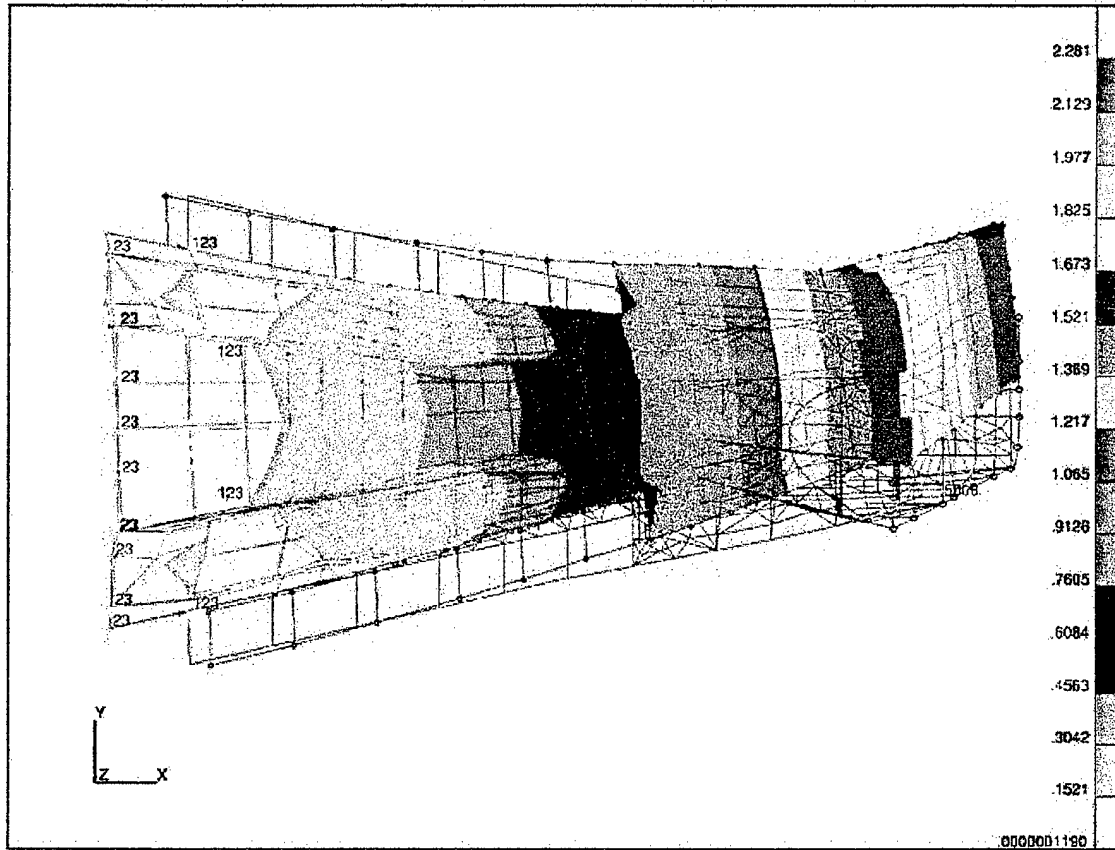


Figure 47: Horizontal Displacement of Full-Kevlar Model

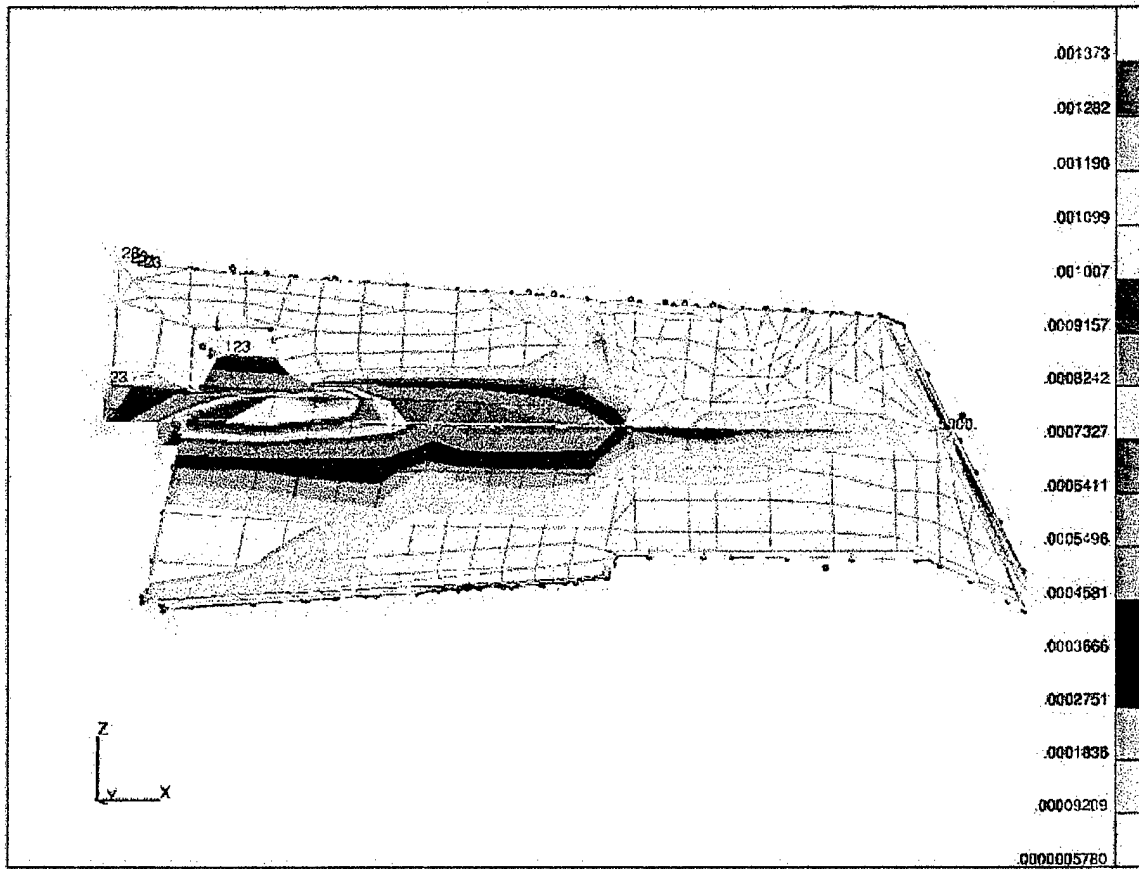


Figure 48: Horizontal Strain Energy Density Fringe of Full-Kevlar Model

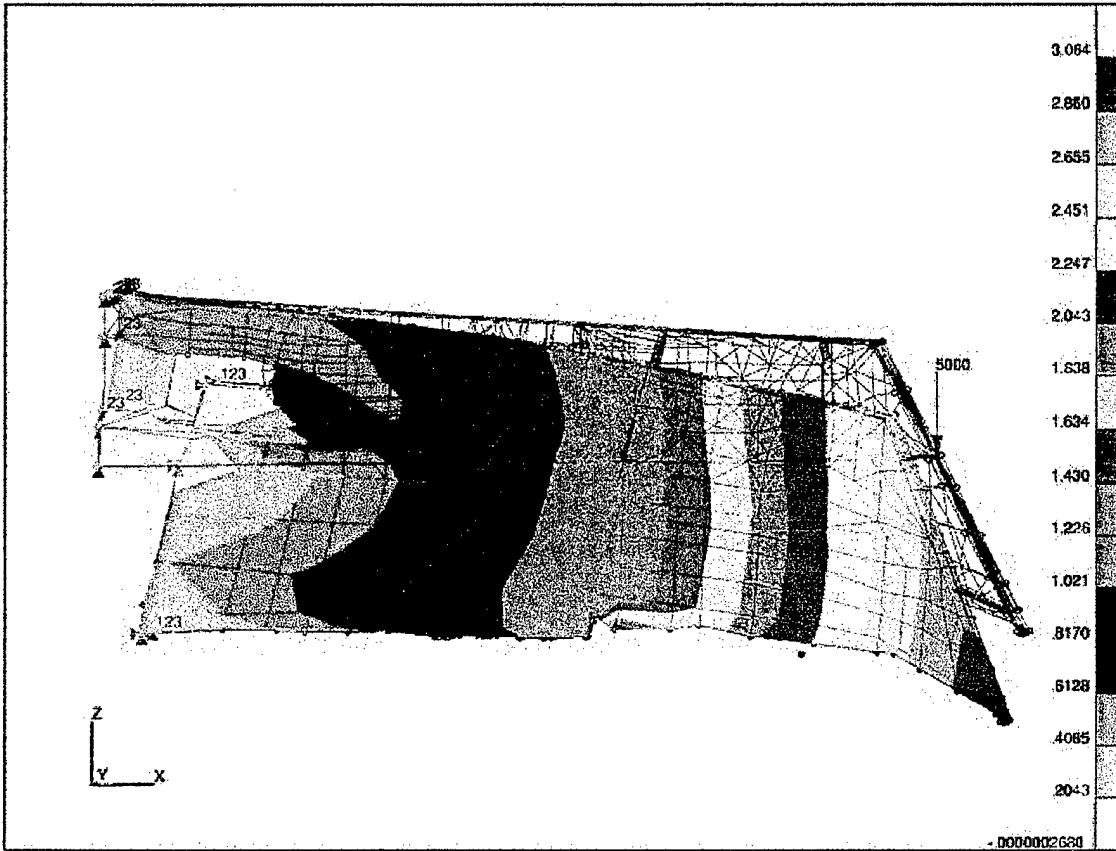


Figure 49: Vertical Displacement of Full-Kevlar Model

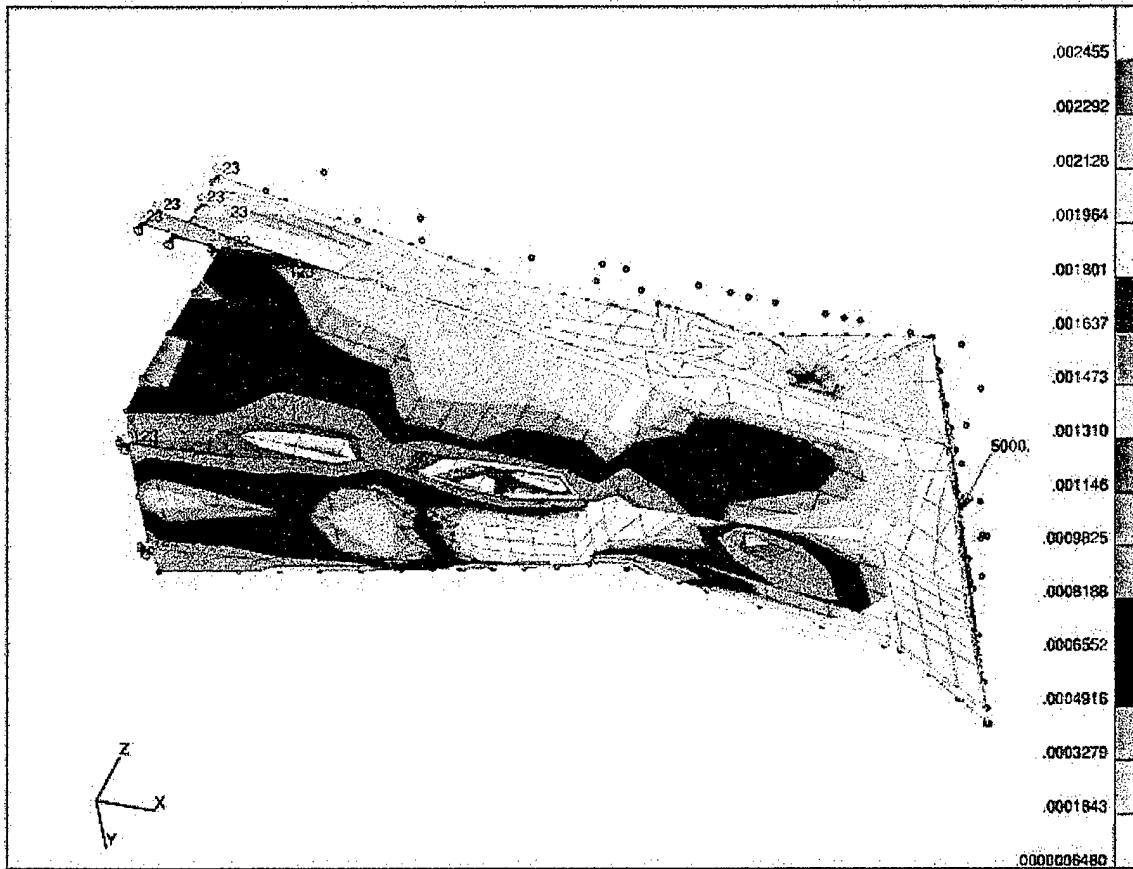


Figure 50: Vertical Strain Energy Density Fringe of Full-Kevlar Model

V. CONCLUSIONS AND RECOMMENDATIONS

A. CONCLUSIONS

The goal of this work was to find a design that would meet both structural stiffness requirements and radar cross section requirements. The Baseline Model was considered the goal for torsional stiffness and horizontal and vertical bending stiffnesses. The geometry changes analyzed here did produce stiffness increases with Baseline Model materials. However, the geometry changes were not sufficient to produce Baseline stiffness values using radar cross section compliant materials.

While there are further minor geometry changes that may increase stiffness values slightly without increasing weight, these increases are likely to be small when compared to what is required to achieve Baseline values with radar cross section compliant materials. The geometry changes necessary to achieve radar cross section requirements and Baseline stiffness may necessitate radical changes to the aircraft outer mold line. It would probably require substantial changes to the shapes of the bulkheads on either side of the Forward Tail Landing Gear Bay.

The geometry modification to the Forward Tail Landing Gear Bay Bulkhead Section (Bulk-Mod) increases torsional and horizontal bending stiffnesses and decreases weight slightly. However, the FTLGBB modification also reduces vertical bending stiffness and reduces the volume of the exhaust cooling space by approximately five percent. Incorporation of this modification depends on whether the added torsional stiffness justifies the bending stiffness and infrared signature impacts.

The geometry modification to the aft tail cone (Cone-Mod) increases all stiffness values while increasing weight by less than one pound. Incorporating the design change required would surely involve tooling changes due to the substantial change to the tail cone above the Forward Tail Landing Gear Bay. The bulkheads on either side of the Forward Tail Landing Gear Bay would not be changed. Again, the benefit of the stiffness increase must be weighed against the costs involved with the design change and potential new tooling.

B. RECOMMENDATIONS

1. Aluminum Forward Tail Landing Gear Bay Bulkhead

Boeing engineers have indicated that machining the FTLGBB from a single piece of aluminum would be about 65% less expensive to produce than the current composite bulkhead. The aluminum version would also weigh slightly less than the current design and would serve well as part of the exhaust closeout structure. If the geometry change of the FTLGBB proposed here were accepted, the required redesign could encompass both the material changes and the geometry change.

2. Vertical Stabilizer Longerons

Investigate the structural improvement of reducing the number of longerons from three to two in the Vertical Stabilizer. In the current configuration, the forward-most of the three longerons attaches to a hard point at the bottom of the vertical stabilizer but not on top. The aft-most longeron attaches to a hard point in the horizontal stabilizer on top but not on the bottom. These "unconnected" longeron ends transmit loads via shear in

the skin. The proposed modification would use two longerons to connect two hard points on top to two hard points on the bottom, potentially reducing weight while improving structural performance.

3. Tail Fan Gear Box Struts

The radar cross-section requirement on the struts that span the circular opening for the Tail Fan is that the struts be oriented at least 23 degrees off of vertical, top-aft or top-forward. In the current design, they are oriented top-forward. Loads would be forced to "zig-zag" to transmit through these struts, and nature resists this occurring. To allow these struts to more efficiently transmit loads to the lower portion of the tail cone, it is recommended to investigate a configuration where the struts maintain their parallel orientation, but are angled 23 degrees top-aft from the vertical.

Another configuration, suggested by Boeing engineers, which could be investigated is a two-strut system where one strut parallels or surrounds the drive shaft and the other is oriented 23 degrees top aft from the vertical. Figure 51 shows a schematic of this configuration.

4. Tail Landing Gear

There is at present a requirement that the helicopter be capable of making a touchdown landing, with a pitch attitude of thirty degrees nose-up. If this thirty-degree nose-up landing requirement could be relaxed to approximately fifteen degrees, the tail landing gear assembly could be shifted forward. In this case, the gear could be anchored at the Forward Tail Landing Gear Bay Bulkhead and not at the aft frame as it currently is. Assuming that this change results in a landing gear design that weighs about the same as

the current one, the change would reduce overall aircraft gross weight due to a reduction in required nose ballast resulting from the forward center of gravity shift..

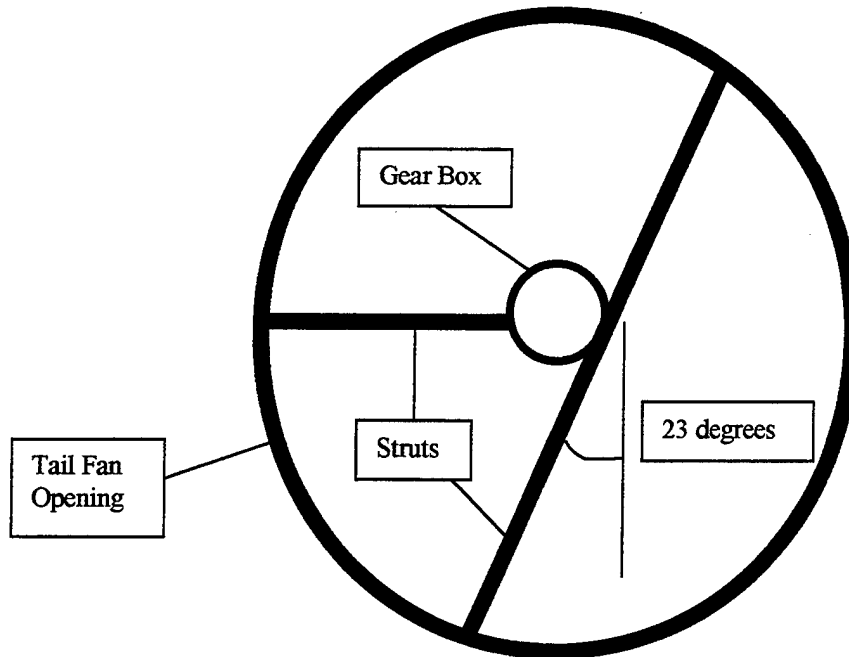


Figure 51: Proposed Strut Configuration Schematic

The Forward Tail Landing Gear Bay Bulkhead is also a more rigid structure than the current aft attachment point. The location change should positively affect natural frequency placement. A forward attachment point could also help the gear meet the four-inch bump requirement with which the current configuration has some difficulty. Finally, the wheel diameter could be increased from eight inches to ten inches, improving ground performance.

5. Tail Configuration for Transportability

For production aircraft, Boeing is exploring the use of an external hinge that would be attached to the vertical tail to allow it to fold so the helicopter could be loaded onto a transport aircraft. Due to space constraints on transport aircraft, the location of the hinge is confined to a very small range on the vertical stabilizer where the folded tail section will fit. An external hinge with a rotation axis outside the surface of the vertical stabilizer requires the two pieces of the vertical stabilizer to separate completely. This separation at the hinge point will have a negative impact on the antennae configuration within the vertical tail.

An alternative to the external hinge would be to have the tail section separate completely from the top of the fan shroud. Instead of an external hinge, this configuration would require a cradle of some sort to hold the tail section during transport. The benefit is that the antennae in the vertical stabilizer could remain in one piece, and structural performance of the vertical tail could be optimized.

6. Dynamic Analysis

The static analysis performed here was done to obtain a better understanding of the aircraft's dynamic structural performance, which is the real concern. Future research will be directed at dynamic analysis of the structural changes proposed here.

Performing dynamic analysis will require achieving an accurate mass model for each of the models analyzed in this research. Currently the mass models are not completely accurate because structural mass has not been included with structural elements. In these models, structural elements have no mass. All mass, structural and

otherwise, is modeled in NASTRAN as a collection of point masses. The best way to ensure accuracy of mass models is to associate structural mass to the actual structural elements by inputting material densities into the models. Point masses would then only be required to model the mass distribution of non-structural components such as drive shafts, gear boxes and computer/black boxes.

7. PATRAN Composite Modeling

The PATRAN software package has an available add-on called the Composite Modeler. It has the capability to model the structural performance of composite layups more accurately than they are in the models used for this research. It also can provide information on manufacturing composite structures as they are modeled. Recommend using PATRAN's Composite Modeler to eliminate the use of "smeared" composite material properties as not only a way of improving model accuracy but also of gaining insight into producibility of proposed design changes.

APPENDIX A: MODIFICATIONS LISTING

Node Changes

Bulkhead Section Modifications

Moved Nodes:

<u>ID</u>	<u>X-Coord</u>	<u>Y-Coord</u>	<u>Z-Coord</u>
14922	14942.00	-260.00	3233.00
14923	14942.00	260.00	3233.00

Added Nodes:

<u>ID</u>	<u>X-Coord</u>	<u>Y-Coord</u>	<u>Z-Coord</u>
92001	14938.60	502.50	3162.02
92002	14956.90	462.55	3228.54
92003	14975.20	422.59	3295.06
92004	14993.50	382.64	3361.58
92005	14938.60	410.00	3162.02
92006	14953.90	400.00	3215.84
92007	14973.65	371.30	3287.37
92008	14987.94	309.38	3338.89
92009	15003.78	298.77	3398.11
92010	14953.90	318.00	3215.84
92011	14972.10	320.00	3279.67
92012	14979.91	265.46	3308.90
92013	14987.73	210.92	3338.12
92014	14938.60	-502.50	3162.02
92015	14956.90	-462.55	3228.54
92016	14975.20	-422.59	3295.06
92017	14993.50	-382.64	3361.58
92018	14938.60	-410.00	3162.02
92019	14953.90	-400.00	3215.84
92020	14973.65	-371.30	3287.37
92021	14987.94	-309.38	3338.89
92022	15003.78	-298.77	3398.11
92023	14987.73	-210.92	3338.12
92024	14979.91	-265.46	3308.90
92025	14972.10	-320.00	3279.67
92026	14953.90	-318.00	3215.84
92027	15021.47	253.10	3464.04
92028	15021.47	-253.10	3464.04
92029	15011.43	210.05	3426.59
92030	15011.43	-210.05	3426.59
92031	15037.10	208.23	3522.48

Node Changes

Bulkhead Section Modifications (Continued)

Added Nodes:

<u>ID</u>	<u>X-Coord</u>	<u>Y-Coord</u>	<u>Z-Coord</u>
92032	15037.10	-208.23	3522.48
92033	15039.55	395.74	3162.02
92034	15091.40	476.70	3161.01
92035	14926.75	239.93	3453.34
92036	15076.20	373.65	3351.51
92037	15033.30	449.65	3228.04
92038	14926.75	-239.93	3453.34
92039	15076.20	-373.65	3351.51
92040	15033.30	-449.65	3228.04
92041	15091.40	-476.70	3161.01
92042	15039.55	-395.74	3162.02

Aft Tail Cone Modifications

Moved Nodes:

<u>ID</u>	<u>X-Coord</u>	<u>Y-Coord</u>	<u>Z-Coord</u>
15213	15250	-215.61	3569.80
15605	15680	-328.98	3470.93
15639	15680	178.80	3510.67

Added Nodes:

<u>ID</u>	<u>X-Coord</u>	<u>Y-Coord</u>	<u>Z-Coord</u>
93001	15784.10	-375.65	3587.28
93002	15680.00	-375.65	3160.00
93003	15584.40	-375.65	3603.39
93004	15521.20	-375.65	3604.53
93005	15444.40	-375.65	3609.23
93006	15244.40	-375.65	3621.42
93007	15140.50	-375.65	3627.69
93008	15066.50	-375.65	3632.15
93009	14938.60	-375.65	3642.34
93010	14742.00	-375.65	3573.43
93011	14647.10	-375.65	3660.55
93012	14552.70	-375.65	3666.45
93013	14458.30	-375.65	3672.34
93014	14363.90	-375.65	3678.24
93015	14256.20	-375.65	3681.81
93016	14067.00	-375.65	3698.42
93017	13919.30	-375.65	3708.46

Node Changes

Aft Tail Cone Modifications (Continued)

Added Nodes:

ID	X-Coord	Y-Coord	Z-Coord
93018	15425.30	-261.34	3609.72
93019	15245.90	-214.17	3620.94
93020	15156.20	-190.59	3626.55
93021	15335.60	-237.76	3615.33
93022	15604.70	-308.51	3598.50
93023	15515.00	-284.93	3604.11
93024	15694.40	-332.09	3592.89
93025	15376.16	-250.60	3461.70
93026	15444.40	-268.55	3406.13
93027	15496.69	-282.82	3362.60
93028	15680.00	-326.52	3594.11
93029	15376.16	-307.82	3361.13
93030	15777.55	-322.08	3343.76
93031	15775.00	-353.17	3483.57
93032	15479.70	-276.74	3505.12
93033	15550.70	-295.67	3480.55
93034	15588.35	-305.90	3416.77
93035	15344.40	-110.43	3615.34
93036	15434.85	-175.85	3609.48
93037	15140.50	168.08	3627.68
93038	15244.40	169.60	3621.39
93039	15444.40	172.53	3609.22
93040	15637.70	175.35	3596.89
93041	15757.50	177.10	3589.03
93042	15534.60	173.84	3603.65
93043	15344.40	171.07	3615.30
93044	15344.40	111.58	3615.30
93045	15757.50	179.12	3539.57
93046	15472.04	174.10	3559.46
93047	15444.40	173.61	3565.23
93048	15284.11	170.81	3606.45
93049	15244.40	170.11	3610.59
93050	15244.40	198.18	3589.01
93051	15344.40	185.35	3599.11
93052	15344.40	195.10	3567.67
93053	15344.40	171.07	3615.31
93054	15680.00	176.19	3594.11
93055	16080.00	44.40	3162.00

Element Changes

Deleted Elements: (For Modification of both Bulkhead Section and Aft Tail Cone)

BAR2s:

<u>ID</u>	<u>Node1</u>	<u>Node2</u>
1115030	15030	15120
1115090	15090	14890
1115099	15099	14899
1115120	15120	15218
1115218	15218	15415
1214936	15009	14936
1215008	15008	14930
1215071	15071	15099
1215072	15072	15090

TRI3s:

<u>ID</u>	<u>Node1</u>	<u>Node2</u>	<u>Node3</u>
3114936	15009	15007	14936
3115008	15008	15001	14930
3214922	14922	15033	15017
3215018	15018	15034	14923
3414924	14924	15017	14928
3414925	14925	14929	15018
3414928	14928	15017	14930
3415008	15008	15112	15103
3415009	15009	15018	14936
3415017	15017	15008	14930
3415018	15018	14929	14936
3415033	15033	15017	14924
3415034	15034	14925	15018
3415101	15101	15202	15103
3415102	15102	15034	15104
3415103	15103	15033	15101
3415131	15131	15104	15009
3415201	15201	15102	15104
3415436	15436	15505	15502
3415437	15437	15502	15434
3415502	15502	15437	15436
3415505	15505	15436	15501
3415506	15506	15603	15601
3415603	15603	15506	15504
3415606	15606	15503	15507
3415637	15637	15639	15602
3415710	15710	24103	15815

Element Changes

Deleted Elements: (Continued)

QUAD4s:

<u>ID</u>	<u>Node1</u>	<u>Node2</u>	<u>Node3</u>	<u>Node4</u>
4115007	15009	15016	15014	15007
4115008	15008	15015	15010	15001
4115014	15016	15027	15025	15014
4115015	15015	15026	15019	15010
4214841	14841	14936	15018	14923
4214890	14890	14891	15091	15090
4214908	14908	15101	15033	14922
4214922	14922	15017	14930	14840
4214923	14923	15034	15102	14918
4414902	14902	14921	14829	14833
4414905	14905	14901	14834	14830
4414908	14908	15101	15033	14922
4414925	14925	15034	15102	14918
4414930	14930	15008	14921	14902
4415009	15009	14936	14901	14905
4415028	15028	15117	15120	15030
4415032	15032	15110	15125	15029
4415033	15033	15103	15008	15017
4415104	15104	15034	15018	15009
4415110	15110	15223	15226	15125
4415115	15115	15213	15215	15117
4415117	15117	15215	15218	15120
4415125	15125	5226	15228	15127
4415207	15207	15402	15403	15208
4415208	15208	15403	15407	15209
4415209	15209	15407	15410	15213
4415213	15213	15410	15413	15215
4415215	15215	15413	15415	15218
4415218	15218	15415	15417	15221
4415223	15223	15419	15420	15226
4415226	15226	15420	15422	15228
4415228	15228	15422	15424	15205
4415402	15402	15507	15503	15403
4415403	15407	15501	15503	15403
4415407	15407	15501	15436	15410
4415410	15410	15436	15437	15413
4415413	15413	15437	15434	15415
4415419	15419	15504	15506	15420
4415420	15420	15506	15601	15422
4415422	15422	15601	15602	15424
4415501	15501	15605	15608	15505
4415503	15503	15606	15605	15501
4415601	15601	15603	15637	15602
4415605	15605	15815	15710	15608

Element Changes

Deleted Elements: (Continued)

QUAD4s:

<u>ID</u>	<u>Node1</u>	<u>Node2</u>	<u>Node3</u>	<u>Node4</u>
4415606	15606	15817	15815	15605
4415637	15637	15705	15708	15639

Element Changes

Bulkhead Section Modifications

Added Elements:

BAR2s:

<u>ID</u>	<u>Node1</u>	<u>Node2</u>
9400020	15009	92009
9400021	92009	92013
9400022	92013	14936
9400036	15009	92004
9400037	92003	92004
9400038	92003	92002
9400039	92002	92001
9400040	92001	92005
9400041	92005	14918
9400050	15090	92034
9400051	92034	92001
9400052	92001	14890
9400106	14908	92018
9400107	92018	92014
9400108	92014	92015
9400109	92015	92016
9400110	92016	92017
9400111	92017	15008
9400112	15008	92022
9400113	92022	92023
9400114	92023	14930
9400127	14899	92014
9400128	92014	15099

TRI3s:

<u>ID</u>	<u>Node1</u>	<u>Node2</u>	<u>Node3</u>
9400002	92004	92003	92007
9400003	92003	92002	92006

Element Changes

Bulkhead Section Modifications

Added Elements: (Continued)

TRI3s:

<u>ID</u>	<u>Node1</u>	<u>Node2</u>	<u>Node3</u>
9400004	92002	92001	92005
9400005	92002	92006	92005
9400006	92003	92007	92006
9400007	92004	92008	92007
9400008	92009	92008	92013
9400009	92008	92012	92013
9400010	92008	92012	92011
9400011	92008	92007	92011
9400012	92013	92012	14929
9400013	92013	14929	14936
9400014	92012	14929	14925
9400015	92012	92011	14925
9400016	92010	92011	14925
9400017	92010	14925	14918
9400024	92009	92027	92029
9400025	92009	92029	92013
9400026	92029	15007	92013
9400027	92013	15007	14936
9400028	14918	14917	14925
9400029	15016	92031	15027
9400030	15025	92031	15027
9400031	15016	92027	92031
9400032	15007	92029	15014
9400033	92027	92029	15014
9400034	92027	15014	92031
9400035	92031	15025	15014
9400042	14918	14925	14923
9400043	14925	14923	14929
9400044	14841	14929	14923
9400045	14936	14929	14841
9400046	15102	15104	15090
9400047	14918	92033	15102
9400048	14918	92033	92005
9400049	92005	92033	92001
9400053	92034	92033	15090
9400054	92033	92034	92001
9400055	15009	92009	14905
9400056	14905	92009	92035
9400057	92009	92013	92035
9400058	92035	14901	92013
9400059	92013	14901	14936
9400060	14830	14905	92035
9400061	92035	14834	14901

Element Changes

Bulkhead Section Modifications

Added Elements: (Continued)

TRI3s:

<u>ID</u>	<u>Node1</u>	<u>Node2</u>	<u>Node3</u>
9400062	14830	14834	92035
9400064	15090	15104	92034
9400065	92002	92001	92037
9400066	92034	92001	92037
9400067	92003	92002	92037
9400068	15104	92034	92037
9400069	15104	92036	92037
9400070	92036	92003	92037
9400071	92036	92003	92004
9400072	15104	92036	15131
9400073	15131	92036	15009
9400074	14909	14908	14924
9400075	92014	92018	92015
9400076	92018	92019	92015
9400077	92019	92015	92016
9400078	92019	92020	92016
9400079	92020	92021	92017
9400080	92020	92016	92017
9400084	92025	92020	92021
9400085	14908	14924	92026
9400086	14924	92026	92025
9400087	14924	92024	92025
9400088	92025	92024	92021
9400089	14928	14924	92024
9400090	14930	14928	92023
9400091	14928	92023	92024
9400092	92024	92023	92021
9400093	92023	92021	92022
9400094	14930	92023	15001
9400095	15001	92030	15010
9400096	15010	92032	15019
9400097	15019	92032	15026
9400098	15010	92030	92028
9400099	15010	92028	92032
9400100	92032	15026	15015
9400101	92032	92028	15015
9400102	92023	15001	92030
9400103	92023	92030	92022
9400104	92030	92028	92022
9400115	14902	92023	14930
9400116	14902	92038	92023
9400117	92023	92038	92022
9400118	92038	14921	92022

Element Changes

Bulkhead Section Modifications

Added Elements: (Continued)

TRI3s:

<u>ID</u>	<u>Node1</u>	<u>Node2</u>	<u>Node3</u>
9400119	14921	92022	15008
9400120	14833	14902	92038
9400121	14833	92038	14829
9400122	14829	92038	14921
9400123	14908	14922	14924
9400124	14922	14924	14928
9400125	14922	14840	14928
9400126	14840	14930	14928
9400129	15103	92041	15099
9400130	92040	15103	92041
9400131	92039	92040	15103
9400132	92014	92040	92041
9400133	92014	92015	92040
9400134	92016	92015	92040
9400135	92016	92039	92040
9400136	92017	92016	92039
9400137	15008	92017	92039
9400138	15008	92039	15112
9400139	15112	92039	15103
9400140	15009	92004	92036
9400141	15101	92042	15099
9400142	15101	92042	14908
9400143	92018	92042	14908
9400144	92042	92018	92014
9400145	15099	92042	92041
9400146	92041	92042	92014

QUAD4s:

<u>ID</u>	<u>Node1</u>	<u>Node2</u>	<u>Node3</u>	<u>Node4</u>
9400001	92004	15009	92009	92008
9400018	92006	92007	92011	92010
9400019	92005	92006	92010	14918
9400023	15009	15016	92027	92009
9400063	15091	14891	14890	92001
9400081	14908	92026	92019	92018
9400082	92026	92025	92020	92019
9400083	92021	92022	15008	92017
9400105	92022	92028	15015	15008

Element Changes

Aft Tail Cone Modification

Modified Element:

QUAD4:

<u>ID</u>	<u>Node1</u>	<u>Node2</u>	<u>Node3</u>	<u>Node4</u>
4214898	14899	92014	15098	14898

Added Elements:

BAR2s:

<u>ID</u>	<u>Node1</u>	<u>Node2</u>
9600062	15415	93035
9600063	15218	93035
9600064	15218	15120
9600065	15120	15030
9600066	15030	93020
9600067	93020	93019
9600068	93019	93021
9600069	93021	93018
9600070	93018	93023
9600071	93023	93022
9600072	93022	93028
9600073	93028	15710
9600074	15608	93028
9600120	24108	93041
9600121	93041	93054
9600122	93054	93040
9600123	93040	93042
9600124	93042	93039
9600125	93039	93043
9600126	93043	93038
9600127	93038	93037
9600128	93037	15032
9600129	15637	93054

Element Changes

Aft Tail Cone Modification

Added Elements (Continued)

TRI3s:

<u>ID</u>	<u>Node1</u>	<u>Node2</u>	<u>Node3</u>
9600001	15030	93020	15117
9600002	15030	15028	15117
9600003	15117	15115	15213
9600004	93020	15117	15213
9600005	93020	93019	15213
9600006	15213	15209	93025
9600007	93026	93027	15403
9600008	93025	93029	93026
9600009	93031	93030	15815
9600010	93028	15710	15605
9600011	93018	93023	93032
9600012	93031	24103	15815
9600013	93030	15815	15817
9600014	93027	15402	15507
9600015	93019	15213	93021
9600016	93022	93033	93028
9600017	93027	93034	15507
9600018	15213	93021	93025
9600019	15606	93031	93030
9600020	93032	93033	93026
9600021	93021	93018	93025
9600022	15208	93029	15207
9600023	15209	15208	93029
9600024	15209	93025	93029
9600025	93029	93026	15403
9600026	15403	93027	15402
9600027	93029	93026	15403
9600028	15207	93029	15402
9600029	93018	93025	93032
9600030	93025	93032	93026
9600031	93032	93033	93022
9600032	93023	93022	93032
9600033	93033	93026	93027
9600034	93033	93027	93034
9600035	15507	93034	15606
9600036	93033	93034	93028
9600037	93028	15605	93034
9600038	93034	15605	93034
9600039	15605	15606	93031
9600040	15605	15710	93031
9600041	15710	93031	26001
9600042	93035	15415	93036

Element Changes

Aft Tail Cone Modification

Added Elements (Continued)

TRI3s:

<u>ID</u>	<u>Node1</u>	<u>Node2</u>	<u>Node3</u>
9600043	15030	15120	93020
9600044	15120	93020	15218
9600045	93020	15218	93019
9600046	15218	93035	93021
9600047	93019	93035	93021
9600048	93035	93036	93021
9600049	15415	15417	93035
9600050	15417	15221	93035
9600051	15221	15218	93035
9600052	93021	93036	93018
9600053	15434	15415	93036
9600054	15502	15434	93036
9600055	93036	93018	93023
9600056	15502	93036	93023
9600057	15505	15502	93023
9600058	15505	93023	93022
9600059	15505	93022	15608
9600060	15608	93022	93028
9600061	15608	93028	15710
9600075	15228	93052	93050
9600076	93050	93051	93052
9600077	93047	93051	93052
9600078	93043	93051	93038
9600079	93051	93038	93050
9600080	93037	93038	93050
9600081	93043	93051	93047
9600082	93050	15125	93037
9600083	93037	15125	15032
9600084	15125	15029	15032
9600085	93050	15125	15127
9600086	93050	15228	15127
9600087	93047	15424	93052
9600088	15424	93052	15205
9600089	93052	15228	15205
9600090	93039	93047	93043
9600091	93042	93039	93046
9600092	93039	93046	93047
9600093	93046	93047	15424
9600094	93046	15424	15602
9600095	93042	93046	15602
9600096	93040	93042	15602
9600097	15639	93040	15602
9600098	93054	93040	15639

Element Changes

Aft Tail Cone Modification

Added Elements (Continued)

TRI3s:

<u>ID</u>	<u>Node1</u>	<u>Node2</u>	<u>Node3</u>
9600099	93045	93054	15639
9600100	93041	93045	93054
9600101	24108	93041	93045
9600102	24108	15816	15708
9600103	93045	15639	15708
9600104	24108	93045	15708
9600105	24108	15705	93041
9600106	15705	93041	93054
9600107	15705	93054	15637
9600108	15637	93054	93040
9600109	15637	15603	93040
9600110	15603	93040	93042
9600111	15603	93042	15504
9600112	15504	93042	93039
9600113	15504	15419	93039
9600114	15419	93039	93043
9600115	15419	93043	15223
9600116	93043	15223	93038
9600117	15223	93038	15110
9600118	93038	15110	93037
9600119	15110	93037	15032
9600130	93028	15608	15605
9600131	15637	93054	15639

APPENDIX B: MASS ANDS CENTER OF GRAVITY CHANGES

Comanche Gross Mass: (Kg) 4808

Material	mat2.41150071	mat2.42130151
Mass/Area (Kg/square mm)	2.39E-06	2.11E-06
Material	mat2.42148301	mat2.42149251
Mass/Area (Kg/square mm)	2.40E-06	2.10E-06
Material	mat2.42150091	mat2.43149091
Mass/Area (Kg/square mm)	2.70E-06	2.70E-06
Material	mat2.44147101	mat2.44149411
Mass/Area (Kg/square mm)	3.00E-06	3.04E-06
Material	mat2.44156011	
Mass/Area (Kg/square mm)	3.90E-06	

Base-Kevlar Structural Changes

Structure Removed From Original Model
(Baseline)

Group	Material	X-CG (mm)	Area (mm ²)	Mass/Area (Kg/mm ²)	Mass (Kg)	X-Moment
side skin	mat2.44147101	15370	731500	3.002E-06	2.196E+00	3.375E+04
aft skin	mat2.44145601	15770	259800	3.900E-06	1.013E+00	1.598E+04
Totals:					3.209E+00	4.973E+04

Structure Added

Group	Material	X-CG (mm)	Area (mm ²)	Mass/Area (Kg/mm ²)	Mass (Kg)	X-Moment
cone skin	mat2.44149411	15470	991600	3.039E-06	3.014E+00	4.662E+04
Totals:					3.014E+00	4.662E+04
Mass Change (Kg):					-1.952E-01	
CG Shift (mm)						-6.457E-01

Bulk-Mod Structural Changes

Structure Removed From Original Model
(Baseline)

Group	Material	X-CG (mm)	Area (mm ²)	Mass/Area (Kg/mm ²)	Mass (Kg)	X-Moment
blkhd	mat2.41150071	15020	59020	2.391E-06	1.411E-01	2.120E+03
dome	mat2.42149251	15020	41680	2.097E-06	8.738E-02	1.312E+03
ex closeout	mat2.42150091	15020	188300	2.696E-06	5.076E-01	7.624E+03
ex cov	mat2.42130151	14940	237900	2.114E-06	5.028E-01	7.512E+03
ex lining	mat2.42130151	15000	60670	2.114E-06	1.282E-01	1.923E+03
Totals:					1.367E+00	2.049E+04

Structure Added

Group	Material	X-CG (mm)	Area (mm ²)	Mass/Area (Kg/mm ²)	Mass (Kg)	X-Moment
blkhd	mat2.41150071	14990	157100	2.391E-06	3.757E-01	5.631E+03
ex closeout	mat2.42148301	14930	78400	2.396E-06	1.878E-01	2.805E+03
ex covers	mat2.42130151	14860	137700	2.114E-06	2.910E-01	4.325E+03
ex lining	mat2.42130151	14930	21110	2.114E-06	4.462E-02	6.661E+02
mid deck	mat2.43149091	15070	91990	2.696E-06	2.480E-01	3.737E+03
Totals:					1.147E+00	1.716E+04
Mass Change (Kg):					-2.200E-01	
CG Shift (mm)						-6.922E-01

Cone-Mod Structural Changes

Structure Removed From Original Model
(Baseline)

Group	Material	X-CG (mm)	Area (mm ²)	Mass/Area (Kg/mm ²)	Mass (Kg)	X-Moment
aft cone	mat2.44156011	15680	123000	3.900E-06	4.797E-01	7.522E+03
up deck	mat2.44147101	15330	266100	3.002E-06	7.987E-01	1.224E+04
Totals:					1.278E+00	1.977E+04

Structure Added

Group	Material	X-CG (mm)	Area (mm ²)	Mass/Area (Kg/mm ²)	Mass (Kg)	X-Moment
side skin	mat2.44147101	15380	420600	3.002E-06	1.262E+00	1.942E+04
walk deck	mat2.44147101	15420	118200	3.002E-06	3.548E-01	5.471E+03
Totals:					1.617E+00	2.489E+04
Mass Change (Kg):					3.388E-01	
CG Shift (mm)						1.065E+00

Full-Mod Structural Changes

Structure Removed From Original Model
(Baseline)

Group	Material	X-CG (mm)	Area (mm ²)	Mass/Area (Kg/mm ²)	Mass (Kg)	X-Moment
aft cone	mat2.44156011	15680	123000	3.900E-06	4.797E-01	7.522E+03
blkhd	mat2.41150071	15020	59020	2.391E-06	1.411E-01	2.120E+03
dome	mat2.42149251	15020	41680	2.097E-06	8.738E-02	1.312E+03
ex closeout	mat2.42150091	15020	188300	2.696E-06	5.076E-01	7.624E+03
ex cov	mat2.42130151	14940	237900	2.114E-06	5.028E-01	7.512E+03
ex lining	mat2.42130151	15000	60670	2.114E-06	1.282E-01	1.923E+03
up deck	mat2.44147101	15330	266100	3.002E-06	7.987E-01	1.224E+04
Totals:					2.646E+00	4.026E+04

Structure Added

Group	Material	X-CG (mm)	Area (mm ²)	Mass/Area (Kg/mm ²)	Mass (Kg)	X-Moment
blkhd	mat2.41150071	14990	157100	2.391E-06	3.757E-01	5.631E+03
ex closeout	mat2.42148301	14930	78400	2.396E-06	1.878E-01	2.805E+03
ex covers	mat2.42130151	14860	137700	2.114E-06	2.910E-01	4.325E+03
ex lining	mat2.42130151	14930	21110	2.114E-06	4.462E-02	6.661E+02
mid deck	mat2.43149091	15070	91990	2.696E-06	2.480E-01	3.737E+03
side skin	mat2.44147101	15380	420600	3.002E-06	1.262E+00	1.942E+04
walk deck	mat2.44147101	15420	118200	3.002E-06	3.548E-01	5.471E+03
Totals:					2.764E+00	4.205E+04
Mass Change (Kg):					1.188E-01	
CG Shift (mm)						3.728E-01

Full-Kevlar Structural Changes

Structure Removed

Group	Material	X-CG (mm)	Area (mm ²)	Mass/Area (Kg/mm ²)	Mass (Kg)	X-Moment
aft cone	mat2.44156011	15680	123000	3.900E-06	4.797E-01	7.522E+03
blkhd	mat2.41150071	15020	59020	2.391E-06	1.411E-01	2.120E+03
dome	mat2.42149251	15020	41680	2.097E-06	8.738E-02	1.312E+03
ex closeout	mat2.42150091	15020	188300	2.696E-06	5.076E-01	7.624E+03
ex cov	mat2.42130151	14940	237900	2.114E-06	5.028E-01	7.512E+03
ex lining	mat2.42130151	15000	60670	2.114E-06	1.282E-01	1.923E+03
up deck	mat2.44147101	15330	266100	3.002E-06	7.987E-01	1.224E+04
side skin 2	mat2.44147101	15470	976200	3.002E-06	2.930E+00	4.533E+04
Totals:					5.576E+00	8.559E+04

Structure Added

Group	Material	X-CG (mm)	Area (mm ²)	Mass/Area (Kg/mm ²)	Mass (Kg)	X-Moment
blkhd	mat2.41150071	14990	157100	2.391E-06	3.757E-01	5.631E+03
ex closeout	mat2.42148301	14930	78400	2.396E-06	1.878E-01	2.805E+03
ex covers	mat2.42130151	14860	137700	2.114E-06	2.910E-01	4.325E+03
ex lining	mat2.42130151	14930	21110	2.114E-06	4.462E-02	6.661E+02
mid deck	mat2.43149091	15070	91990	2.696E-06	2.480E-01	3.737E+03
side skin	mat2.44147101	15380	420600	3.002E-06	1.262E+00	1.942E+04
walk deck	mat2.44147101	15420	118200	3.002E-06	3.548E-01	5.471E+03
side skin 2	mat2.44149411	15470	976200	3.039E-06	2.967E+00	4.590E+04
Totals:					5.731E+00	8.795E+04
Mass Change (Kg):					1.556E-01	
CG Shift (mm)						4.912E-01

APPENDIX C: LIST OF PATRAN DATABASE FILES

<u>File Name</u>	<u>Description</u>
base_red_1.db	Baseline Model with applied moment
base_red_2.db	Baseline Model with applied horizontal force
base_red_3.db	Baseline Model with applied vertical force
base_kev_red_1.db	Baseline geometry, Kevlar OML, applied moment
base_kev_red_2.db	Baseline geometry, Kevlar OML, horizontal force
base_kev_red_3.db	Baseline geometry, Kevlar OML, vertical force
blkhdmod_red_1.db	FTLGGB Section modification, Baseline materials, applied moment
blkhdmod_red_2.db	FTLGGB Section modification, Baseline materials, horizontal force
blkhdmod_red_3.db	FTLGGB Section modification, Baseline materials, vertical force
conemod_red_1.db	Aft cone modification, Baseline materials, applied moment
conemod_red_2.db	Aft cone modification, Baseline materials, horizontal force
conemod_red_3.db	Aft cone modification, Baseline materials, vertical force
tailmod_red_1.db	Both FTLGGB Section and aft cone modifications, Baseline materials, applied moment
tailmod_red_2.db	Both FTLGGB Section and aft cone modifications, Baseline materials, horizontal force
tailmod_red_3.db	Both FTLGGB Section and aft cone modifications, Baseline materials, vertical force
tailkev_red_1.db	Both FTLGGB Section and aft cone modifications, Kevlar OML, applied moment
tailkev_red_2.db	Both FTLGGB Section and aft cone modifications, Kevlar OML, horizontal force
tailkev_red_3.db	Both FTLGGB Section and aft cone modifications, Kevlar OML, vertical force

LIST OF REFERENCES

1. Inman, Daniel J., *Engineering Vibration*, Prentice-Hall Inc., Englewood Cliffs, New Jersey, 1994.
2. Allen, David H. and Haisler, Walter E., *Introduction to Aerospace Structural Analysis*, John Wiley and Sons Inc., New York, New York, 1985.
3. Brauer, John R., *What Every Engineer Should Know about Finite Element Analysis*, Marcel Dekker, Inc., New York, New York, 1988.
4. MSC/PATRAN Installation and Operations Manual, The MacNeal-Schwendler Corporation, Los Angeles, California, 1996.

INITIAL DISTRIBUTION LIST

	No. Copies
1. Defense Technical Information Center.....2 8725 John J. Kingman Rd., STE 0944 Fort Belvoir, VA 22060-6218	
2. Dudley Knox Library.....2 Naval Postgraduate School 411 Dyer Rd. Monterey, CA 93943-5101	
3. Department of Aeronautics and Astronautics, Code AA.....2 Naval Postgraduate School Monterey, CA 93943-5000	
4. BG James Snider.....1 Program Manager, Comanche 4300 Goodfellow Blvd. Saint Louis, MO 63120-1798	
5. Professor E. Roberts Wood, Code AA/Wd.....3 Department of Aeronautics and Astronautics Naval Postgraduate School Monterey, CA 93943-5000	
6. Professor Donald A. Danielson, Code MA/Dd.....1 Department of Mathematics Naval Postgraduate School Monterey, CA 93943-5000	
7. Professor Joshua H. Gordis, Code ME/Go.....1 Department of Mechanical Engineering Naval Postgraduate School Monterey, CA 93943-5000	
8. Robert L. Tomaine.....1 436 Mason Ridge Drive Saint Charles, MO 63304	

9. David L. Peakes..... 1
RAH-66 Program
Boeing Defense & Space Group, Helicopters Division
P.O. Box 16858, #MS P10-74
Philadelphia, PA 19142-0858
10. MAJ Vincent M. Tobin..... 1
13 Mancini Drive
Yorktown Heights, NY 10598